2-2

UNCLASSIFIED

FINAL REPORT

WIDE BAND FREQUENCY TRACKER PERFORMANCE AND DESIGN OF AN ALL ANGLE LASER DOPPLER OPTICAL HOMODYNE RECEIVER

GROUND WIND AND WIND TUNNEL MEASUREMENTS PROGRAM

VOLUME II

J. D. Fridman
K. Meister
J. C. L. Shabeck, Jr.
R. Young

ER70-4286 16 December 1970

RAYTHEON

RAYTHEON COMPANY
EQUIPMENT DIVISION

RAYTHEON COMPANY
EQUIPMENT DIVISION

FINAL REPORT

WIDE BAND FREQUENCY TRACKER PERFORMANCE AND DESIGN OF AN ALL ANGLE LASER DOPPLER OPTICAL HOMODYNE RECEIVER

GROUND WIND AND WIND TUNNEL MEASUREMENTS PROGRAM

VOLUME II

ER70-4286

16 December 1970

Prepared for

GEORGE C. MARSHALL SPACE FLIGHT CENTER

NASA

Huntsville, Alabama 35812

Under

CONTRACT NO. NAS8-21293

Prepared by
J. D. Fridman, Project Engineer
K. Meister
J. C. L. Shabeck, Jr.
R. Young

RAYTHEON COMPANY

EQUIPMENT DIVISION

EQUIPMENT DEVELOPMENT LABORATORIES

Sudbury, Massachusetts 01776

CONTENTS

CONTENTS (Continued)

ILLUSTRATIONS

ILLUSTRATIONS (Continued)

ILLUSTRATIONS (Continued)

TABLES

SECTION 1

INTRODUCTION

The Ground Wind and Wind Tunnel Measurements Program, Contract No. NAS8-21293, can be divided into two distinct phases. Phase I on the Ground Winds work performed has been reported in Raytheon Report No. SR70-4145, Volume I. This report, Volume II, discusses the work performed under the Wind Tunnel Measurements phase of the contract.

On a previous contract, NAS8-22971, two wide band frequency trackers have been designed, fabricated, and delivered to the NASA Marshall Space Flight Center. The purpose of phase II of this contract has been to analyze and measure in detail the characteristics of the wide band frequency trackers in order to determine their performance under flow and turbulence conditions extending from the subsonic to the supersonic. Thus all combinations of FM signals have been simulated across a very wide range of operating conditions to create typical Doppler shifted signals that can be generated in a Laser Doppler Velocimeter Flow and Turbulence Measurement System. Both static and dynamic configurations have been studied and the results interpreted via appropriate theoretical models. Section 2.0 of this report addresses itself to that phase of the work performed.

The second phase of the Wind Tunnel Program required the design and fabrication of an All Angle Laser Doppler Velocimeter. The All Angle LDV may be used for performing one-, two-, or three-dimensional flow measurements and for turbulence cross-correlation studies when used in conjunction with the 3-dimensional laser Doppler velocimeter, also designed and fabricated by Raytheon under Contract No. NAS8-21293. The instrument as designed

and fabricated has some very novel and interesting features. Section 3.0 of this report describes the All Angle LDV and, in addition, addresses itself to some specific design problems of interest.

SECTION 2

WIDE BAND FREQUENCY TRACKER MEASUREMENTS

2.1 INTRODUCTION

The Frequency Tracker, Model 200B, shown in Figure 2-1 provides equivalent flow and turbulence information from frequency modulated (FM) signals derived from a Laser Doppler Velocity Instrument System. The Frequency Tracker is a component of that system, but can also be used in other applications as a frequency demodulator of wide dynamic range. The input to the Tracker is a wideband FM signal. When used as part of the Laser Doppler Velocity System the FM input signals are derived from Doppler shifted and optically heterodyned laser beams detected at a photomultiplier.

The Frequency Tracker is basically a FM demodulator with negative feedback. Compared with a conventional FM demodulator the principal advantage derived from the system is its ability to improve the threshold, resulting from excessive noise, by compressing the bandwidth of the demodulator. It is essentially a tracking filter with variable center frequency whose bandwidth is substantially narrower than that of a frequency modulated signal. The FM signal, in turn, can vary in carrier frequency over the tracking range of the receiver. At any such carrier frequency the frequency deviation and signal frequencies can vary randomly within the specified limits. Depending on the degree of turbulence, the frequency tracker can be used in two modes; i.e., "narrow" for low turbulence, and "wide" for high turbulence. Detailed descriptions of the Wide Band Frequency Tracker, its network configuration and

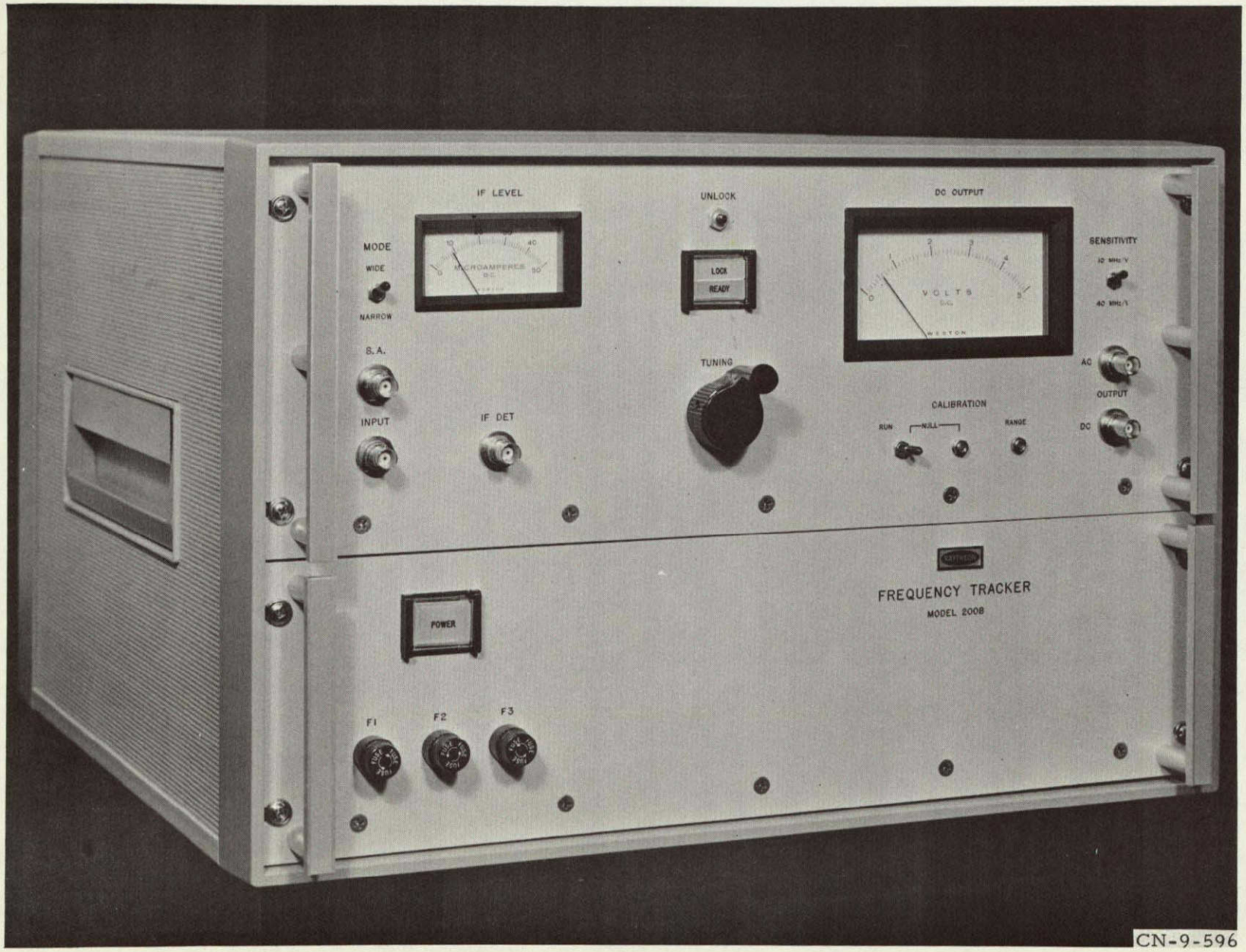

Figure 2-1 Frequency Tracker, Model 200B

electronic circuit schematics will be found in the "Frequency Tracker Model 200B Instruction Manual", delivered to NASA Marshall Space Flight Center, by the Raytheon Company under Contract No. NAS8-22971 and dated September 1969.

A test measurements program has been initiated in order to investigate the detailed characteristics of the Raytheon Model 200B Wide Band Frequency Trackers. The purpose of these measurements is twofold:

a. To establish the accuracy of the Tracker AC and DC performance over the complete range of their FM characteristics.

b. To establish the characteristics of the Tracker when subject to statistical signals similar to those obtained in laser Doppler velocimeter turbulence experiments. In the sections that follow we first briefly summarize the basic theory of the Tracker and then describe the experimental measurements and results obtained in this investigation.

2.2 THEORY OF THE FREQUENCY TRACKER OPERATION

The Frequency Tracker is a frequency compressive feedback FM receiver which can be represented in its basic configuration by the block diagram of Figure 2-2. It fulfills the function of tracking a FM input signal over its bandwidth at a rate defined by the modulating signal frequency. The bandwidth of the FM signal is centered at a given carrier frequency and is given by the following expression:

$$B = 2 f_m(1 + m) \qquad (1)$$

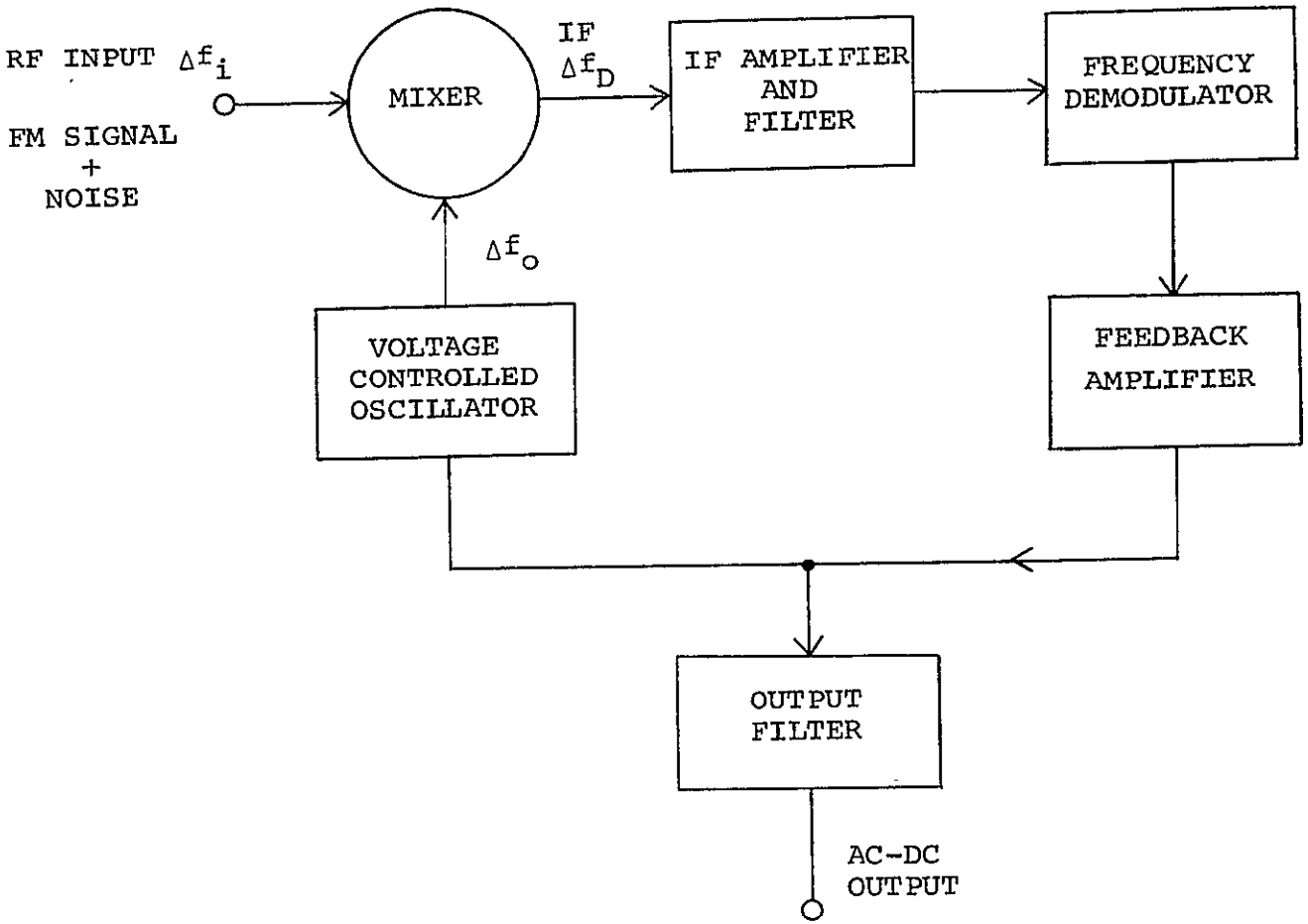

Figure 2-2. Basic Block Diagram of Frequency Tracker

where: f_m = modulating signal frequency
m = modulation index
= $\Delta f/f_m$
Δf = frequency deviation

Thus for large frequency deviations where $\Delta f >> f_m$ the bandwidth is approximately equal to twice the frequency deviation.

As shown in Figure 2-2 the incoming FM signal is heterodyned in a mixer with the output of a voltage controlled oscillator (VCO). Of the resulting sum and difference frequency signals, only the difference is passed by the IF amplifier, and is then frequency demodulated by a limiter/discriminator whose voltage output is proportional to any deviation of the frequency from the IF. The recovered baseband signals are then amplified and fed back to the VCO in such a way as to reduce the instantaneous frequency difference between the FM signal and the instantaneous VCO output frequency. This process reduces the modulation index of the IF signal. The resulting FM signal in the IF portion of the loop occupies a much narrower band than the incoming RF signal. The bandwidth in the IF is given by:

$$B_{IF} = 2f_m\left(1 + \frac{m}{F}\right) \qquad (2)$$

where: F = feedback factor
= $1 + K$
K = open loop gain

For best performance the bandwidth of the IF amplifier has to be matched to the IF signal bandwidth.

From the wideband input noise only a small portion corresponding to the bandwidth B_{IF} is reaching the discriminator, while the signal power is preserved. Therefore it is possible to demodulate properly an FM signal at a much lower input signal to noise ratio than with a conventional open loop discriminator.

The relation of input carrier to noise ratio (CNR) to output signal to noise ratio (SNR) of a FM discriminator is:

$$SNR = \frac{3}{2} m^2 \frac{B}{f_m} CNR \tag{3}$$

For a regular discriminator, the threshold above, which equation 3 is valid, is approximately at:

$$CNR = 10 \text{ dB} \tag{4}$$

In the tracking loop, where the IF signal has been compressed, the threshold is still 10 dB, but measured in the considerably narrower IF bandwidth. The threshold is therefore improved by the ratio of the two bandwidths:

$$\frac{B_{IF}}{B} = \frac{2f_m \left(1 + \frac{m}{F}\right)}{2 f_m (1 + m)} \tag{5}$$

For $m >> 1$:

$$\frac{B_{IF}}{B} = \frac{1}{m} + \frac{1}{F} \tag{6}$$

The spectrum compression, which is proportional to the feedback factor, cannot be made arbitrarily high since an increase of the feedback factor will also cause additional regenerative loop noise. The optimum feedback factor, and therefore the IF bandwidth, are determined by a trade-off between conventional threshold given by the frequency discriminator and the feedback threshold. The best loop performance can be expected if the feedback threshold is equal to the conventional threshold.

The feedback threshold is caused by input FM noise which is detected by the discriminator and results in phase noise at the VCO. It has been shown that the threshold occurs where the variance of the VCO phase noise is 0.1. The phase noise can be related

to the input noise by the closed loop transfer function. For the feedback filters selected for this tracker, the feedback threshold is:

$$\rho_a = 10\pi \frac{(F-1)^2}{\sqrt{F^3 + F} + \sqrt{2F^2}} \tag{7}$$

The IF discriminator threshold is:

$$r_{a,T} = 20\ (1 + \frac{m}{F}) \tag{8}$$

where: ρ_a = feedback threshold carrier to noise ratio, referred to a bandwidth of f_m
f_m = modulation frequency (maximum)
$r_{a,T}$ = discriminator threshold carrier to noise ratio, referred to a bandwidth of f_m
F = feedback factor = 1 + open loop gain
m = modulation index = $\Delta f/f_m$
Δf = frequency deviation (maximum)

ρ_a and $r_{a,T}$ as functions of F are shown in Figure 2-3. In the wide mode, m = 300 and in the narrow mode, m = 100. The optimum feedback factors and the corresponding IF bandwidths (equation 2) are therefore:

narrow: $F = 45$, $B_{IF} = 1.5$ MHz
wide: $F = 25$, $B_{IF} = 1.0$ MHz

Although the noise threshold optimization was based on a feedback filter resulting in a stable loop, additional effects of the circuits (e.g., residual phase shift of operational amplifiers at high frequencies, time delays in the IF, etc.) have to be considered to determine the actual stability of the system. The stability considerations create another trade-off for the feedback

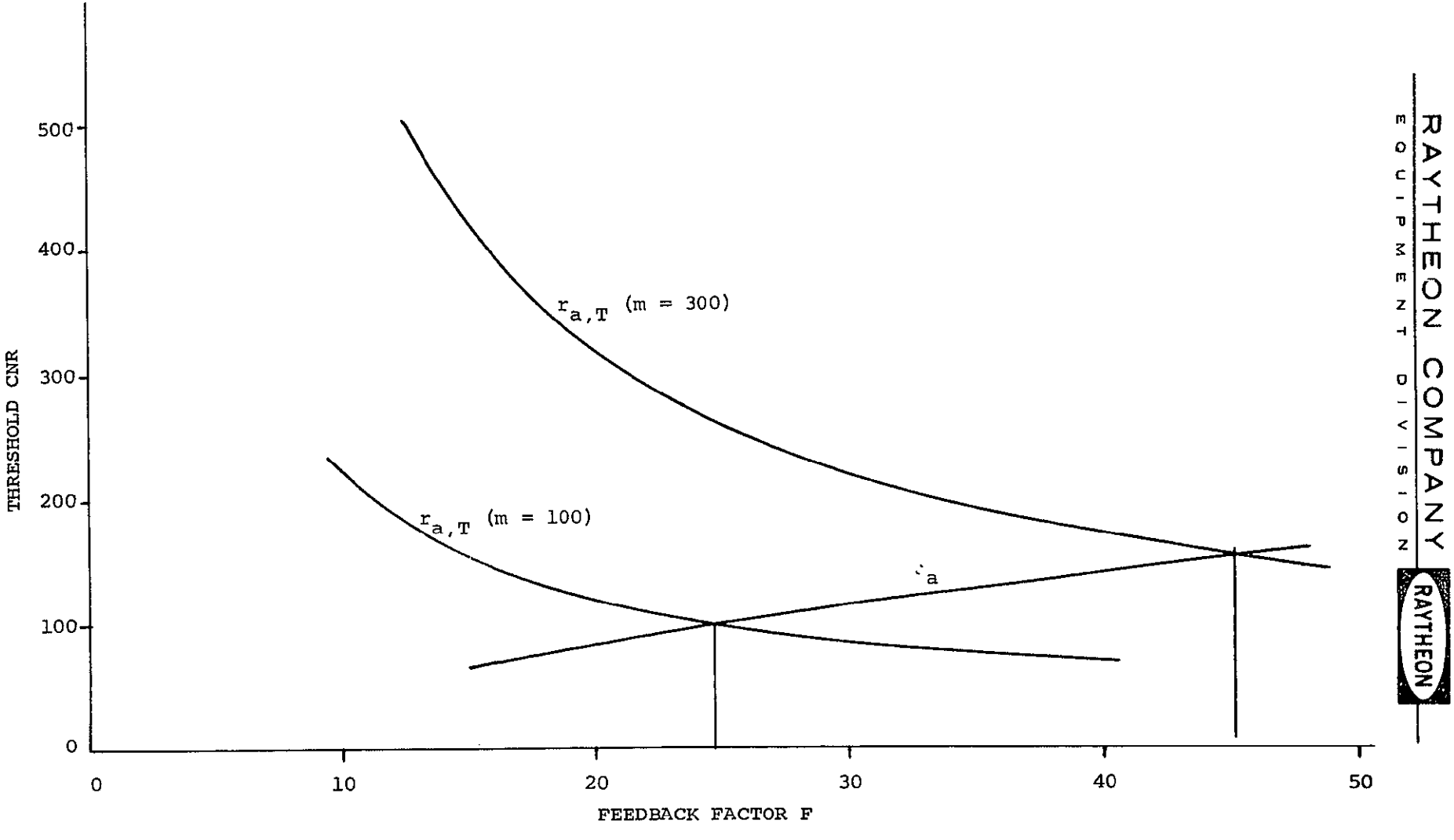

Figure 2-3. Feedback and Discriminator Threshold

factor and the feedback filter, which may take precedence over the F determined from threshold optimization procedures. Marginal stability tends to increase the high frequency tracker output noise and may therefore increase the theoretically expected threshold.

Output signals are derived from the frequency tracker at the input to the VCO. They consist of a DC voltage proportional to the carrier frequency and an alternating voltage proportional in magnitude to the FM deviation and equal in frequency to the modulation.

2.3 MEASUREMENTS WITH STEADY STATE SINUSOID MODULATED FM SIGNALS

2.3.1 EXPERIMENTAL SET-UP

Figure 2-4 is a schematic of the test set-up used in the measurements to determine the operational characteristics of the Tracker. The sinusoid FM inputs to the Tracker under test are generated at the output of a similar Model 200B Tracker. The FM input characteristics of the tracker as shown below:

Carrier Frequency: 5 MHz -- 200 MHz
Deviation Frequency: Up to 30 MHz
Modulation Frequency: Up to 100 kHz

are not reproducible with any standard FM test electronics generators. It is therefore necessary to use a similar Model 200B Tracker in an open-loop configuration to derive the full range of the required test signals.

In the steady-state measurements, as shown in Figure 2-4 , the Tracker-FM-Generator is modulated by a sinusoid signal generator over a baseband frequency range of 100kHz. The frequency deviation and operational carrier frequency is derived by biasing

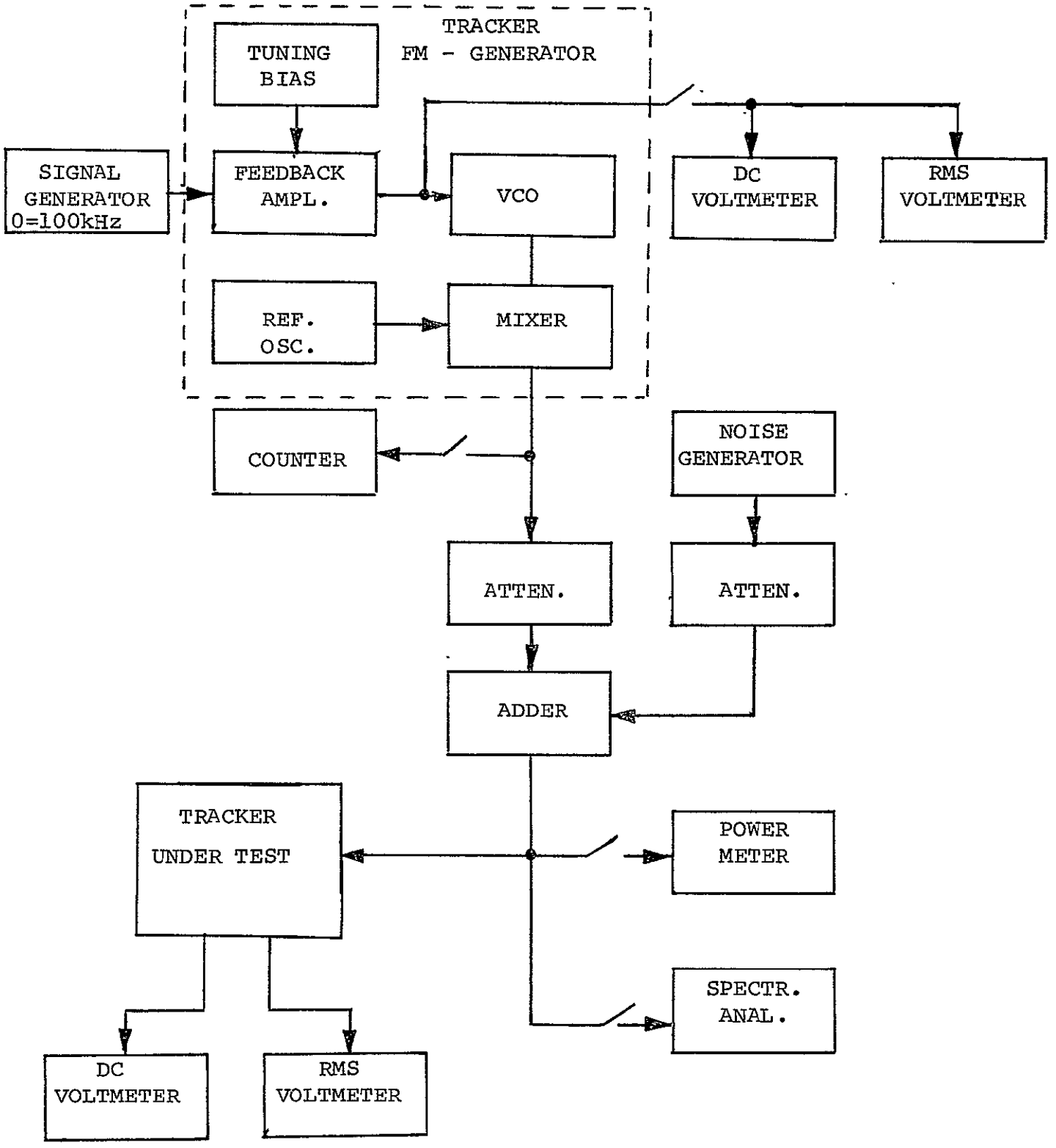

Figure 2-4. Steady State Tracker Measurements

the VCO and heterodyning with a 1.1GHz stable Reference Oscillator. The FM output of the Tracker-FM-Generator is derived at the mixer terminals.

A wide combination of FM signals have been generated in order to study the performance of the Test Tracker through the full range of its specifications, in both its wide and narrow mode of operations.

A noise generator is used to add to the FM signals wide-band noise in order to control the S/N ratio available at the Test Tracker input terminals.

Table I below indicates the range of FM signals that have been generated.

FM PARAMETER	I	II	III
f_c	10	120	200
f_m	1, 10, 50, 100	1, 10, 50, 100	1, 10, 50, 100
Δf	0-6	0-24	0-24
$\frac{S}{N}$	14-25	14-28	10-22

f_c = Carrier Frequency, MHz

f_m = Modulation Frequency, kHz

Δf = Frequency Deviation, MHz, root-mean-square

$\frac{S}{N}$ = Signal-to-Noise Ratio Defined in 1-MHz Bandwidth

TABLE I. Experimental FM Parameters

The carrier frequency, corresponding to a DC voltage at the Tracker-FM-Generator terminals, and the RMS voltage corresponding to the RMS frequency deviation are measured at the Test Generator VCO terminals, as shown. In addition a direct reading of the FM frequency available at the Test Generator mixer output terminals is made with a high accuracy counter, as shown.

The voltage vs. frequency characteristic of the VCO, Figure 2-5 determined by precise and careful measurements, is used to set the input signals to the Test Tracker. A power meter and Spectrum Analyzer at the Test Tracker terminals are used for measuring the signal-to-noise ratio of the FM signals in the Test Program.

2.3.2 MEASUREMENT OF SIGNAL-TO-NOISE RATIOS

Signal-to-noise measurements are usually made with a band-limited noise source corresponding to the signal bandwidth. The power density in the signal and noise can then be measured in turn with a bolometer and their ratio is the desired signal-to-noise parameter. However, such measurements can also be made by means of a spectrum analyzer for FM signals. In this technique, the ratio of the unmodulated signal level to the noise level is read-off directly from the spectrum-analyzer. Since the signal power is the same for the modulated as for the unmodulated signal, the signal-to-noise ratio read-off from the spectrum analyzer is then referred to unit bandwidth. The S/N ratio at the Tracker terminals, however, is determined by the noise equivalent bandwidth. This bandwidth is only limited by the frequency response of the photomultiplier used in the optical homodyne process or any other amplifiers between the photomultiplier output and Tracker. The

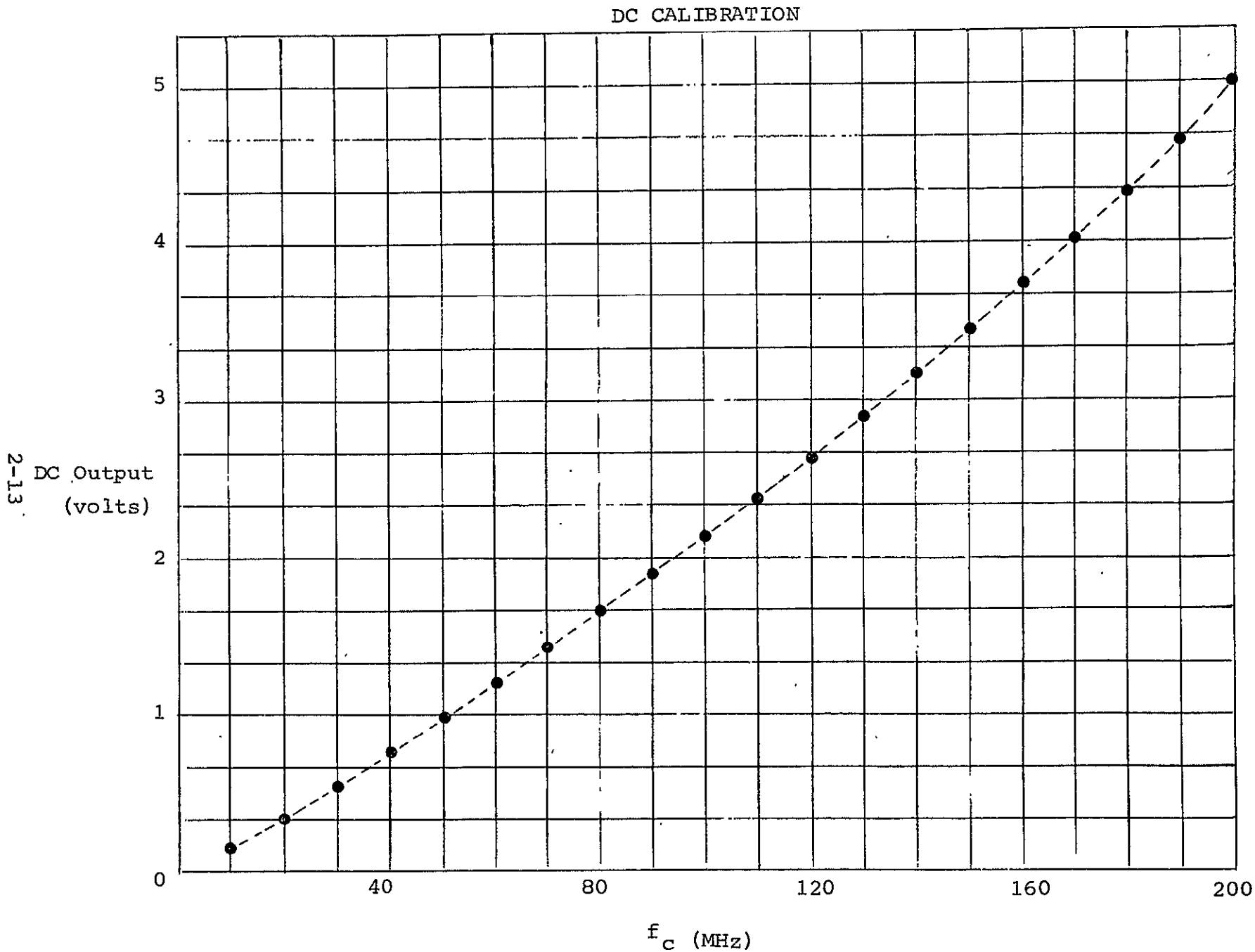

Figure 2-5. Voltage vs. Frequency Characteristic of Tracker

maximum frequency response of the Tracker is 200MHz. It is reasonable to assume that in most experimental turbulence measurements, unless a low-pass filter precedes the Tracker input terminals, the input noise-equivalent bandwidth over which the Doppler shift FM signal is located is 200 MHz. Thus, the S/N measured in a 1-MHz bandwidth can be converted to an experimentally meaningful S/N ratio at the Tracker terminals by the following relationship:

$$\left[\frac{S}{N}\right]_{Db}^{Input} = \left[\frac{S}{N}\right]_{Db}^{Unit\ BW} - 23$$

where: $\left[\frac{S}{N}\right]_{Db}^{Input}$ = Tracker input signal-to-noise ratio referred to noise-equivalent bandwidth of 200MHz,db

$\left[\frac{S}{N}\right]_{Db}^{Unit\ BW}$ = Signal-to-noise ratio defined in a 1-MHz bandwidth

The output of the Test Tracker is measured in terms of its DC level which is proportional to the carrier frequency and its AC root-mean-square level which, in turn, is proportional to the RMS value of the frequency deviation. These quantities are then proportional to the corresponding mean flow velocity and its fluctuations through the Doppler relationship.

2.3.3 RESULTS: STEADY STATE TRACKER MEASUREMENTS

Figure 2-5 shows the non-linear response of the Tracker output as a result of the characteristics of the VCO used in the tracking loop. Departure from linearity is about 10% over a net frequency range of 200MHz. A similar curve, shown in Figure 2-6, relates the

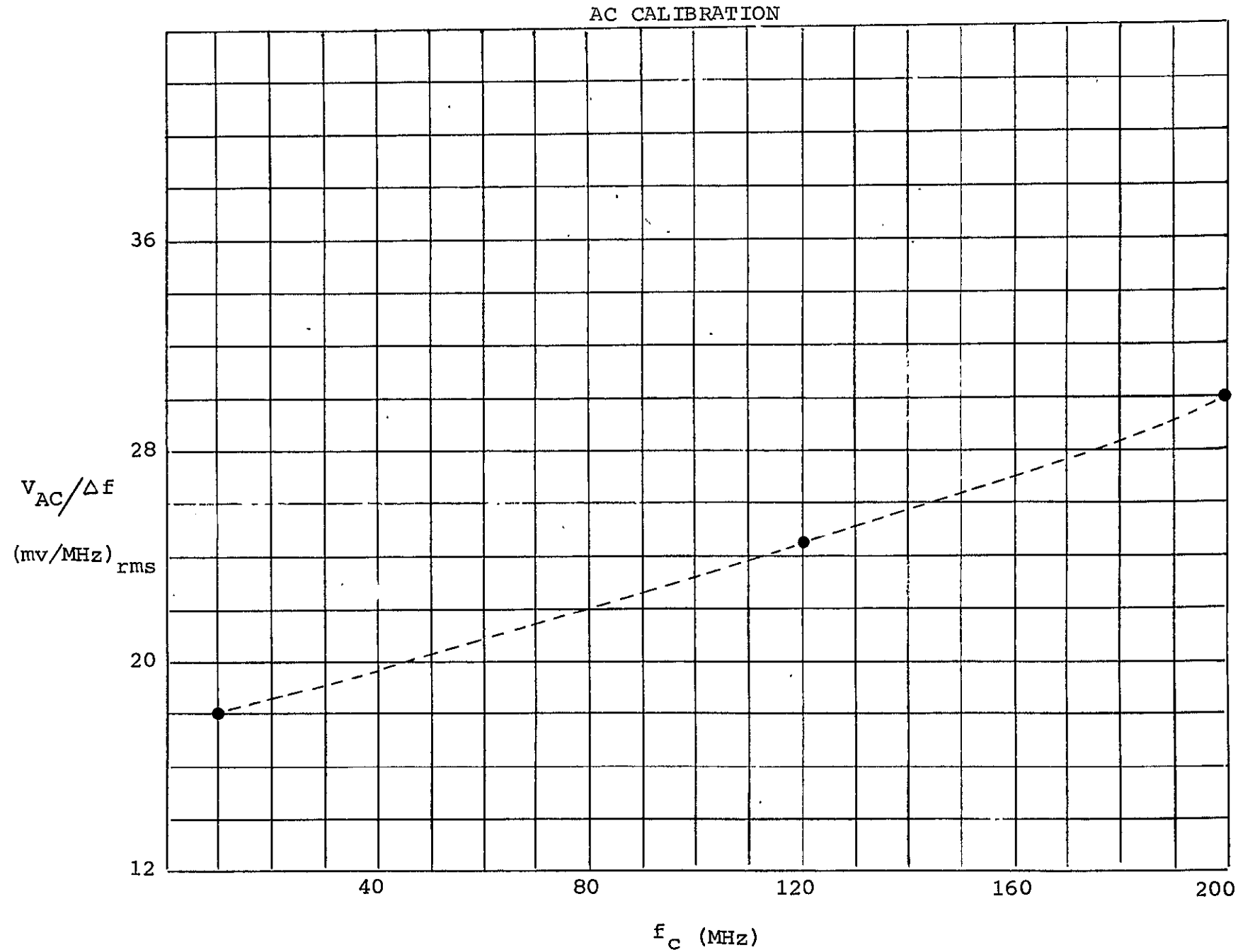

Figure 2-6. Tracker AC Output Characteristic

RMS ratio of the AC voltage output to the frequency deviation, $V_{AC}/\Delta f$, over the same net frequency range. These Tracker characteristics, albeit non-linear, are extremely stable. The VCO's are operated in a thermally controlled environment, with the result that their characteristics do not vary significantly over long time periods. However, as will be ascertained in the operational results to be presented, this inherent non-linearity somewhat limits the overall Tracker performance at the extremes of its operational characteristics

The measurements program has been undertaken to investigate the low carrier frequency (subsonic velocity range) and high carrier frequency (supersonic velocity range) regime of the Tracker in order to experimentally determine the effect of the modulation frequency, signal-to-noise ratio, frequency deviation parameters on the accuracy of Tracker measurements. This information is particularly important in assessing the errors introduced by the Tracker when it is functioning as part of the turbulence measuring Laser Doppler Velocimeter system.

Figures 2-7 and 2-8 illustrate the DC performance of the Tracker for a carrier frequency of f_c = 10MHz, modulation frequency of f_m = 10kHz over a frequency deviation range to Δf = 6MHz, for the wide and narrow modes of operation. The percentage error in the DC measurement is given as a function of the Tracker input S/N ratio for the stated conditions. Operating conditions that yield a performance better than ± 3% have only been included on these figures. Results indicate that the same performance is obtained at lower S/N ratios for the narrow mode of operation. Typically in the wide mode of operation the following results are obtained:

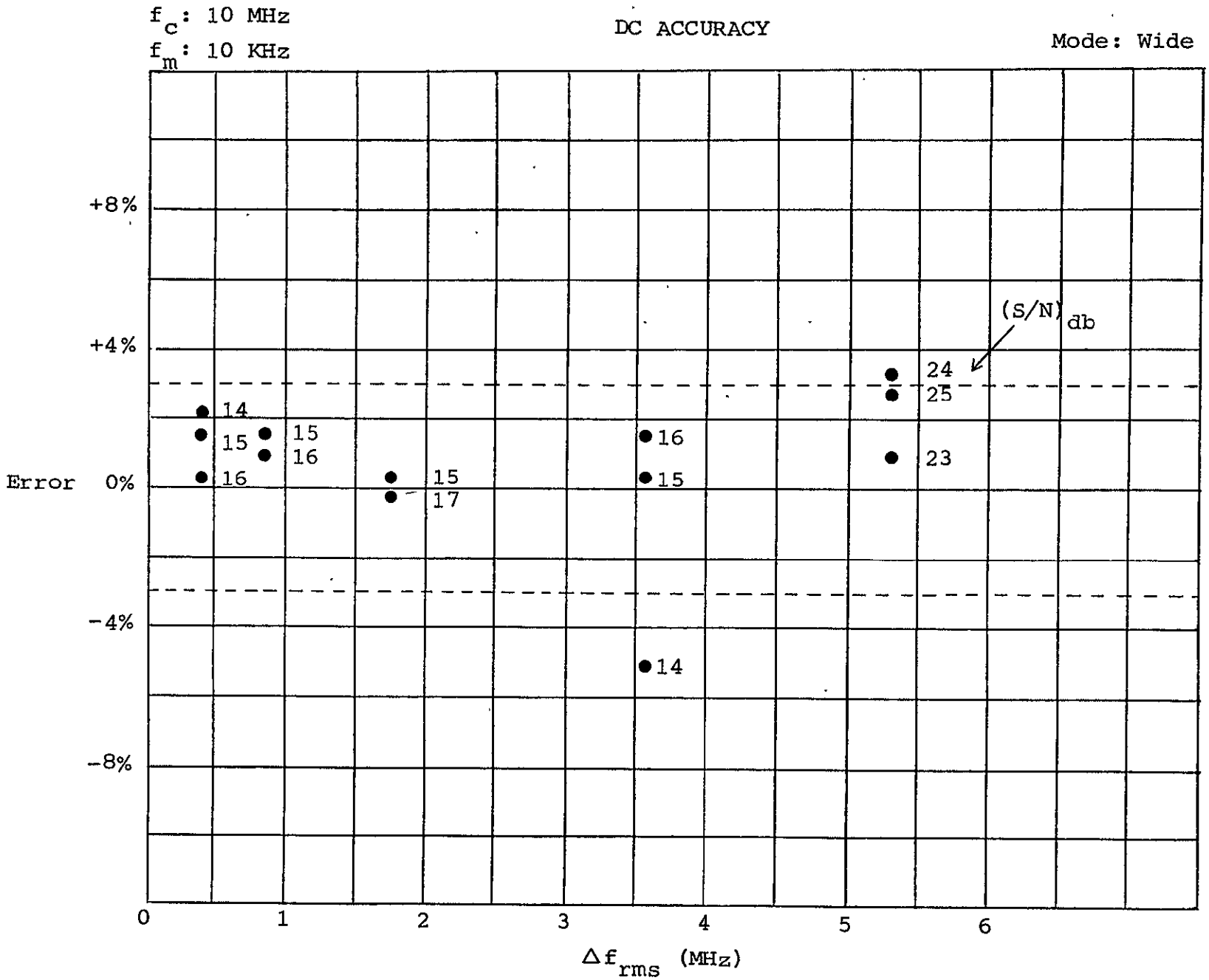

Figure 2-7. DC Performance of Tracker - Wide Mode

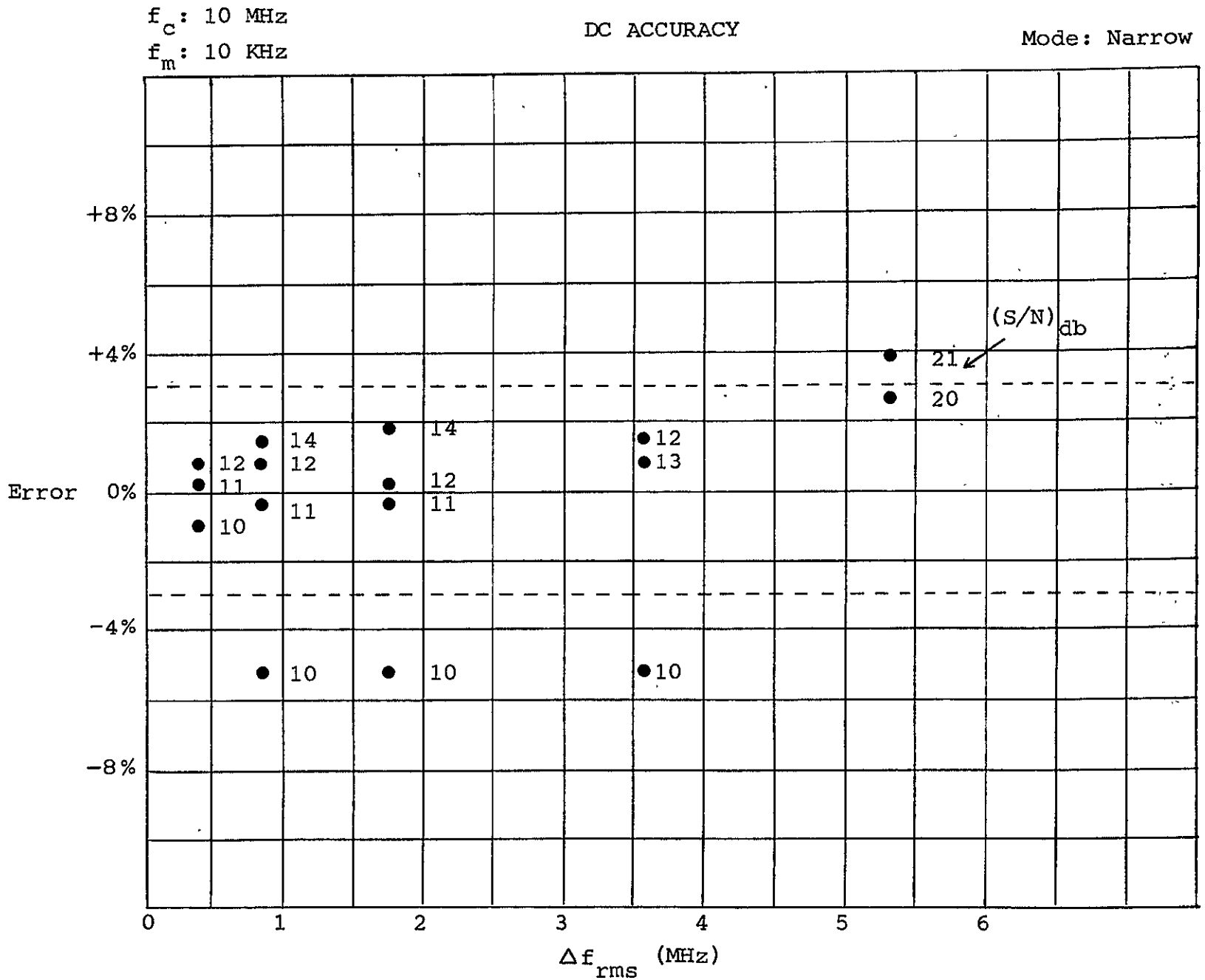

Figure 2-8. DC Performance of Tracker - Narrow Mode

f_c	10MHz	10MHz
f_m	10kHz	10kHz
Δf	1MHz	5.5MHz
S/N	15db	23db
% Error	1%	1%

TABLE II. DC Performance at 10-MHz Carrier, 10-kHz Modulation Frequencies for Wide Mode

Whereas in the narrow mode of operation one obtains:

f_c	10MHz	10MHz
f_m	10kHz	10kHz
Δf	1MHz	5.5MHz
S/N	12db	20db
% Error	1%	3%

TABLE III. DC Performance at 10-MHz Carrier, 10-kHz Modulation Frequencies for Narrow Mode

The improvement in the results for operation in the narrow band mode is due to the additional bandwidth compression resulting from a narrower IF bandwidth. That is, an improvement of about 2 dB can be expected in the narrow mode of operation compared to the wide mode, since the ratio of their respective IF bandwidths is 2/3.

Figures 2-9 and 2-10 illustrate the same relationship under similar input conditions for the AC performance of the Tracker. Table IV summarizes some of the typical results obtained:

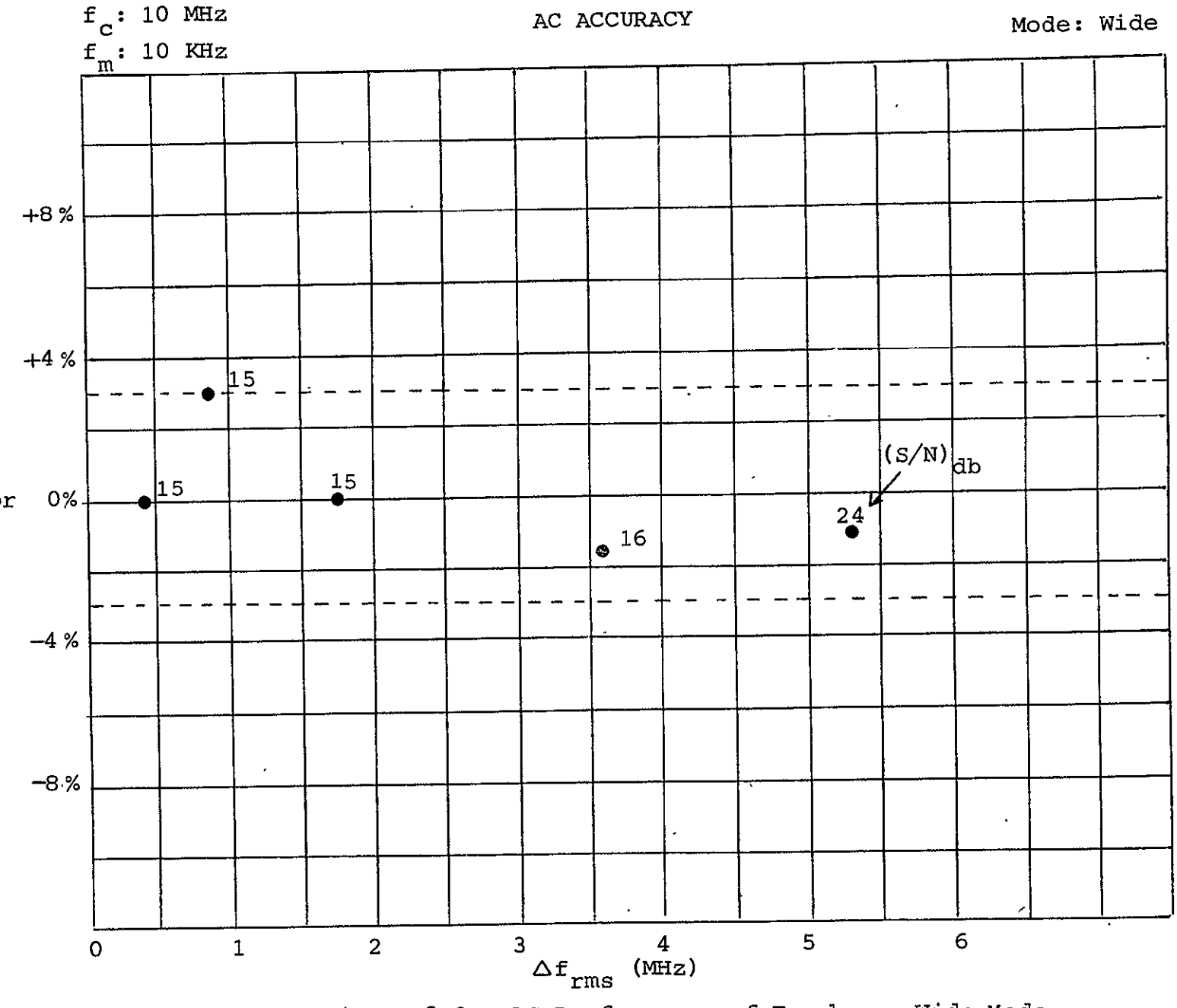

Figure 2-9. AC Performance of Tracker - Wide Mode

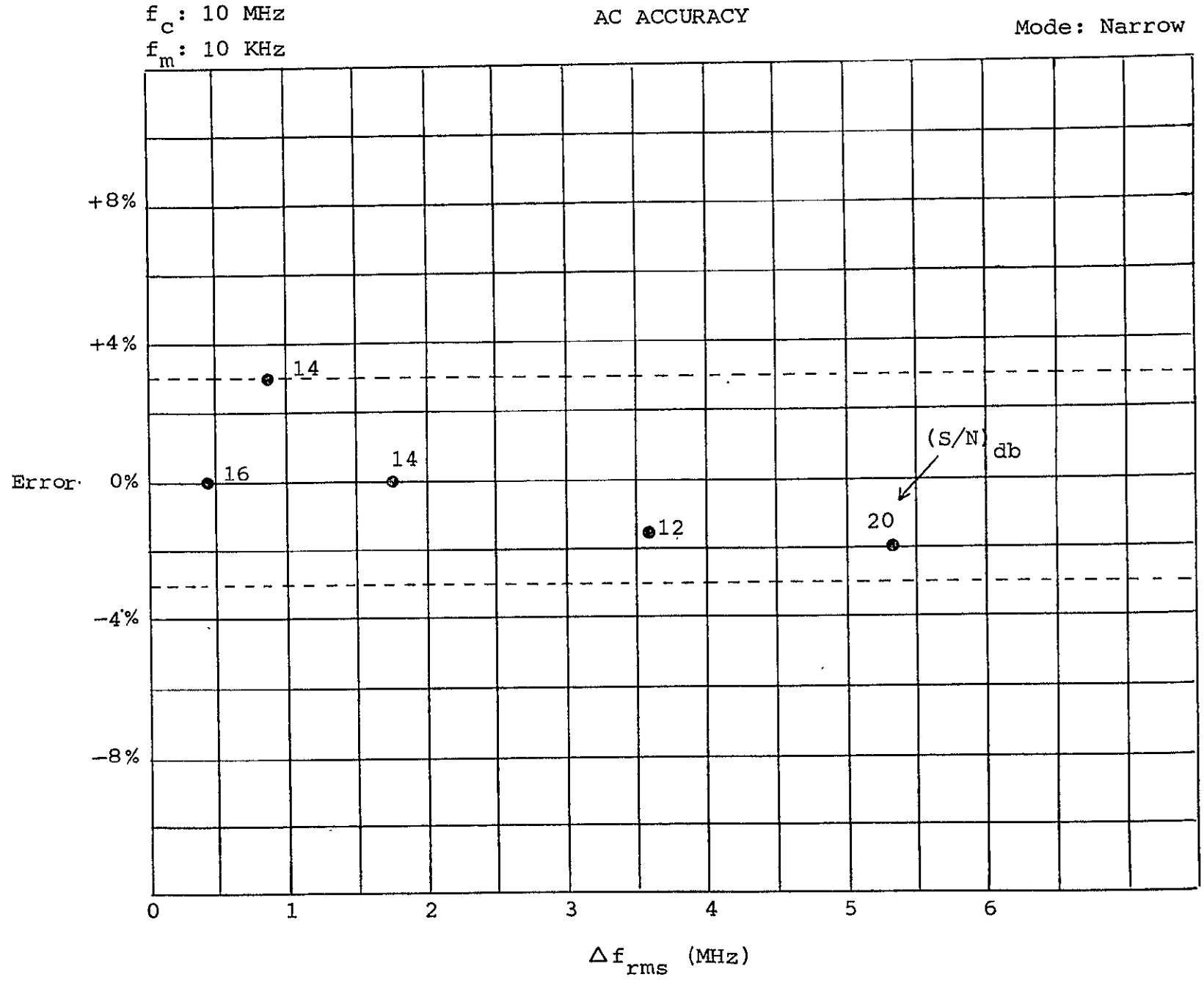

Figure 2-10. AC Performance of Tracker - Narrow Mode

	Wide		Narrow	
f_c, MHz	10	10	10	10
f_m, kHz	10	10	10	10
Δf, MHz	2	5.5	2	5.5
S/N	15	24	14	20
% Error	0	1	0	2

TABLE IV. AC Performance at 10MHz Carrier and 10kHz Modulation Frequencies

These results indicate the same trend previously observed; that is, the narrow mode of tracker operation requires a lower S/N ratio than the wide mode for similar input conditions.

The 10MHz carrier frequency corresponds to a mean flow velocity of 125 ft/second. The low velocity performance of the Tracker at a modulation frequency of 10kHz requires a S/N ratio of 14db in 1MHz for tracking, without errors, a flow with a 2MHz RMS deviation. frequency; that is, a flow at 125 ft/second with a turbulence intensity of 20% can be tracked without any significant errors at actual input S/N ratios of -9db.

In Figures 2-11 and 2-12 the required S/N ratios per MHz bandwidth for a 10MHz input carrier frequency have been plotted as a function of deviation frequency and modulation frequency. All data points that yield a Tracker AC and DC performance better than 3% for the wide and narrow modes, at 1, 10, 50, and 100kHz modulation frequencies are shown. Table V illustrates typical results:

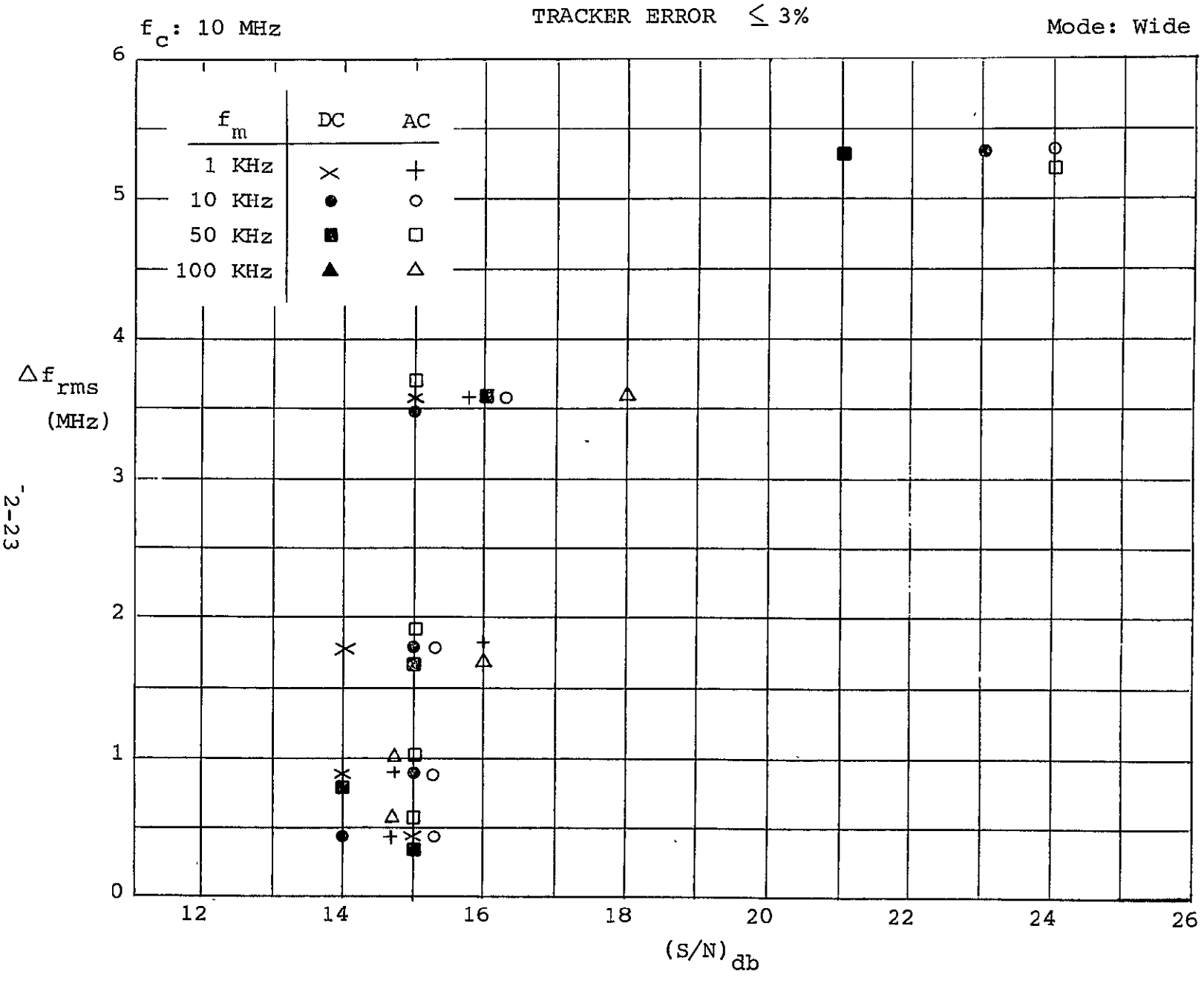

Figure 2-11. AC and DC Tracker Performance Parameters for Errors Less Than 3% -- Wide Mode at 10MHz Carrier Frequency.

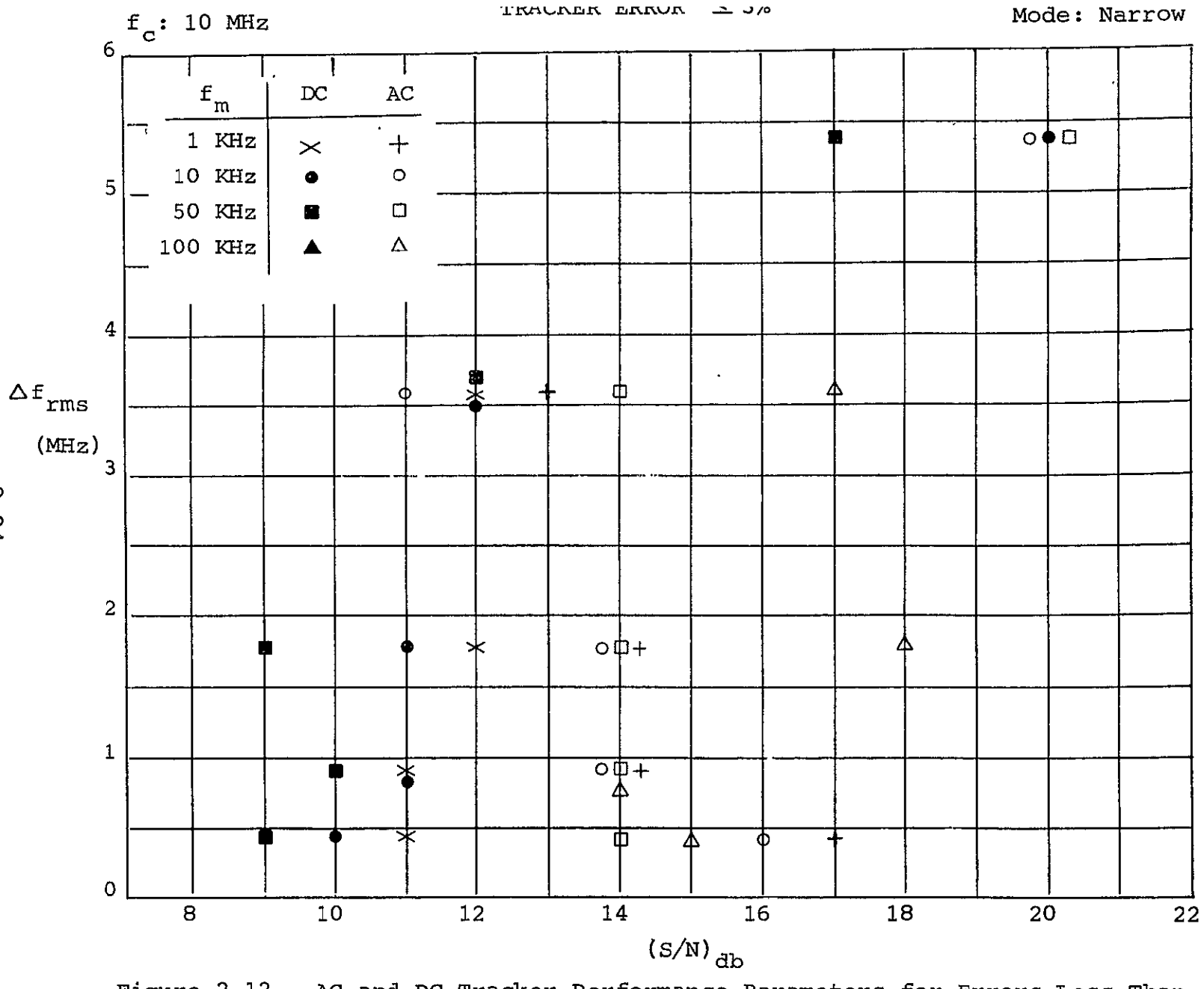

Figure 2-12. AC and DC Tracker Performance Parameters for Errors Less Than 3% -- Narrow Mode at 10MHz Carrier Frequency.

Narrow Mode	DC			AC			
f_c, MHz	10	10	10	10	10	10	10
Δ_f, MHz	3.5	3.5	3.5	1.75	1.75	1.75	1.75
f_m, kHz	1	10	50		10	50	100
S/N, db	12	12	12	14	14	14	14
f_c, MHz	10	10	10	10	10	10	
Δ_f, MHz	.5	1	3.5	.75	3.5	1.75	
f_m, kHz	10	10	10	100	100	100	
S/N, db	10	11	12	14	17	18	

TABLE V. AC and DC Performance at 10MHz Carrier and through 50kHz Modulation Frequencies

The S/N ratio required for a 3% performance is constant for variable modulation frequencies at constant carrier and deviation frequencies; that is, in the DC measurements a modulation index change from 3500 to 70 in the FM signal can be accommodated at a constant S/N ratio of 12 db/MHz at the Tracker input for a 10MHz carrier frequency. The AC measurements, with a change in the modulation index ranging from 1750 to 17.5, also indicate a constant level of the S/N ratio as a function of modulation frequency. This type of performance is theoretically expected over the closed-loop bandwidth of the Tracker response. However, at higher carrier frequencies, as will be ascertained in Figure 2-15, the S/N ratio does not stay constant as a function of modulation frequency when the Tracker is subject to FM signals of different modulation indeces.

The data in the lower half of Table V, however, points to the fact that the larger the deviation frequencies at a constant modu-

lation frequency, the higher are the S/N ratio per unit MHz bandwidth to maintain either lock-on or the 3% performance. The reason for this is that as the FM signal is modulated over a wider bandwidth from a FM signal with a modulation index of 50 to one of 350 at constant modulation frequency, the signal energy spreads out over the bandwidth. Enloe, in his classical paper, "On Decreasing the Threshold in FM by Frequency Feedback", Proc. I.R.E., January 1962, pp. 18-24, makes this point by stating that there is a degradation of threshold as a function of modulation. In the measurements made, a higher S/N ratio must be available at the Tracker input in order to maintain a specified performance level, i.e., errors less than 3%, as the modulation is increased.

Figures 2-13, 2-14, and 2-15 present similar results for input carrier frequencies of 120MHz and 200MHz. Tables VI and VII summarize some results of interest.

In Tables VI and VII a comparison is made between the required input S/N ratios at the Tracker input to maintain an error less than 3% for the AC and DC measurements at 120MHz and 200MHz carrier frequencies at the stated modulation and deviation frequency parameters of the FM signal. The performance of the Tracker at a carrier frequency of 120MHz is from the point-of-view of S/N ratios, poorer than its performance at 200MHz. That is, for the stated deviation frequencies of 1MHz, 5MHz, 9MHz, 20MHz, and 24MHz, the required input S/N ratios at the 10kHz, 50kHz, and 100kHz modulation frequencies is consistently higher than the same at 200MHz carrier frequency. These trends are demonstrated in Figure 2-16, where the required S/N ratio for Tracker performance better than 3% is plotted against the carrier frequency for the stated FM

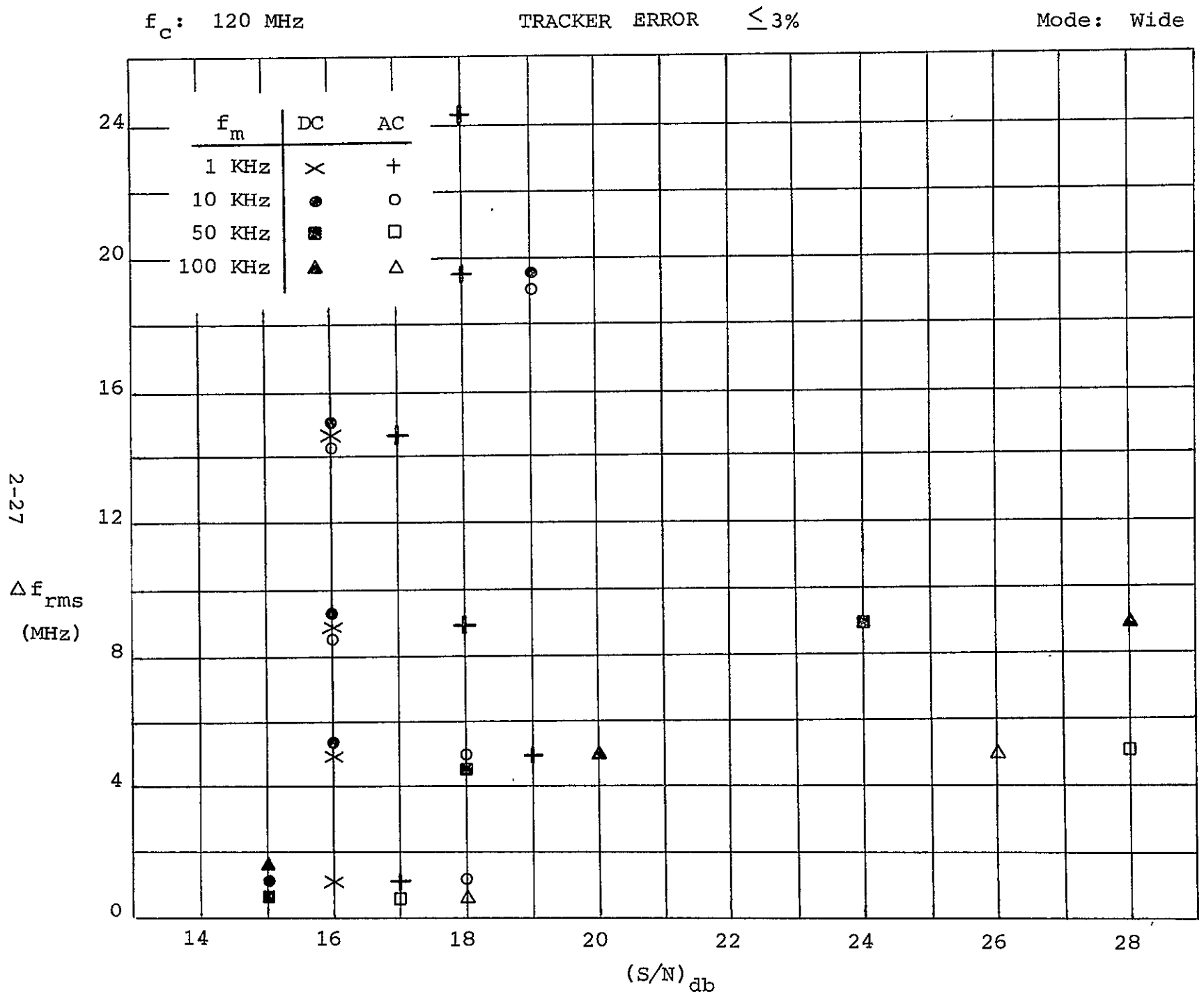

Figure 2-13. AC and DC Tracker Performance Parameters for Errors Less Than 3% -- Wide Mode at 120MHz Carrier Frequency

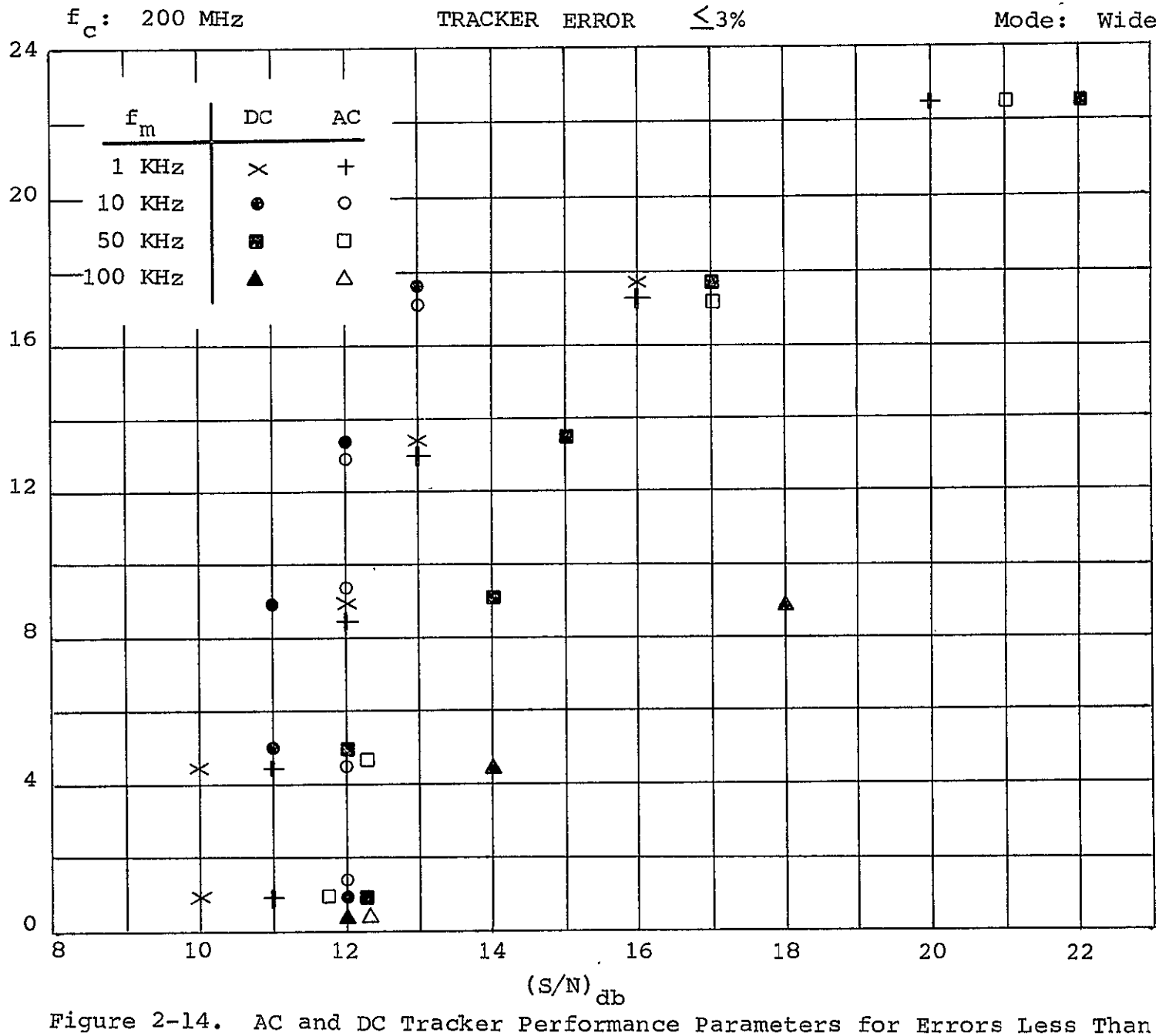

Figure 2-14. AC and DC Tracker Performance Parameters for Errors Less Than 3% -- Wide Mode at 200MHz Carrier Frequency

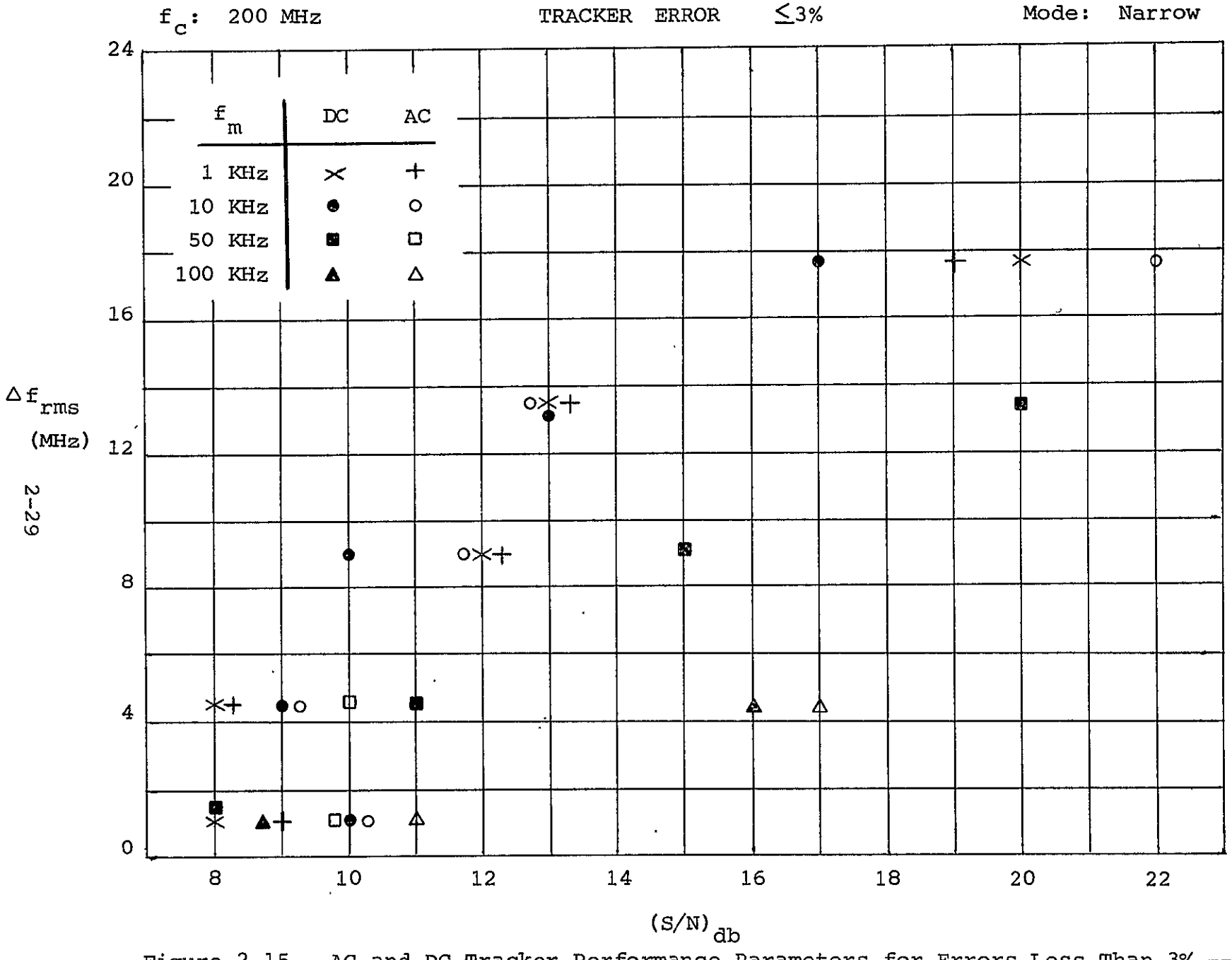

Figure 2-15. AC and DC Tracker Performance Parameters for Errors Less Than 3% -- Narrow Mode at 200MHz Carrier Frequency

	I	II	III	IV	V	VI	VII
f_c	120	120	120	120	120	120	120
Δ_f	1	1	5	5	5	5	5
f_m	10,50,100	10,50,100	1,10,50	100	1,10	50	100
S/N	15	17-18	16-18	20	17-18	28	26
Mode	Wide	Wide	Wide	Wide	Wide	Wide	Wide
Output	DC	AC	DC	DC	AC	AC	AC
f_c	200	200	200	200	200	200	200
Δ_f	1	1	5	5	5	5	5
f_m	10,50,100	10,50,100	1,10,50	100	1,10	50	100
S/N	12	12	10-12	14	11-12	12	--
Mode	Wide	Wide	Wide	Wide	Wide	Wide	--
Output	DC	AC	DC	DC	AC	AC	--
f_c	200	200	200	200	200	200	200
Δ_f	1	1	5	5	5	5	5
f_m	10,50,100	10,50,100	1,10,50	100	1,10	50	100
S/N	8-10	10	8-11	16	8-9	10	17
Mode	Narrow	Narrow	Narrow	Narrow	Narrow	Narrow	Narrow
Output	DC	AC	DC	DC	AC	AC	AC

TABLE VI. AC and DC Performance at 120MHz and 200MHz Carrier Frequencies and Through 100kHz Modulation Frequencies

Output	f_c	Δ_f	f_m	S/N	Output	f_c	Δ_f	f_m	S/N
DC Wide Mode	120	9	1	16	DC Wide Mode	200	9	1	12
			10	16				10	11
			50	24				50	14
			100	28				100	18
DC and AC Wide Mode	120	20	1	18-19	DC and AC Wide Mode	200	18	1	16
		24	1	18			18	10	13

TABLE VII. Comparison of Performance at 120MHz and 200MHz Carrier Frequencies at Selected Frequency Deviations and Modulation Frequencies

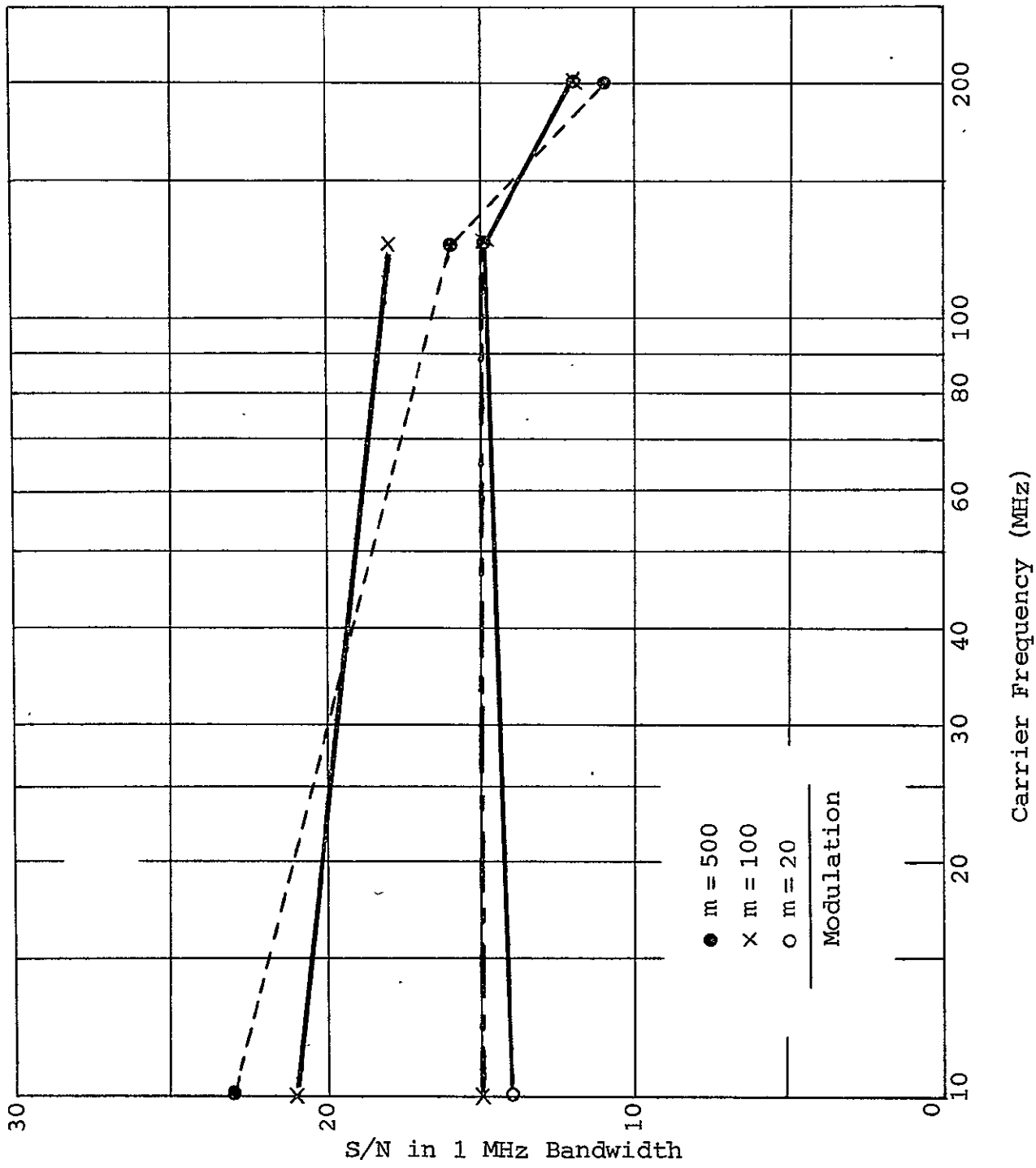

Figure 2-16. Variation of S/N Ratio as a Function of Carrier Frequency and Modulation Index

modulation indeces. Whereas ideally one does not expect any variation in the S/N ratio required for a defined Tracker performance as a function of modulation index and carrier frequency, the non-linearities in the Tracker loop components and the modulation of the FM signal degrade performance. It is clear, however, that at the upper range of its operating characteristic the Tracker performs far better over the full range of its modulation frequency and deviation frequency than at its low end. We attribute this to the characteristics of the VCO and Stable Local Oscillator in the Tracker loop. These components, both designed to operate in the 1.1GHz to 1.5GHz range, are mutually heterodyned in the Tracker loop. The response of the individual IF filter and limiter-discriminator at 30MHz,operational amplifiers and feedback circuits at baseband over 100kHz, microwave mixers and VCO at S-band, all in turn contribute to the observed overall Tracker response. Noise generated in any one of these networks and non-linearities in their frequency response combine to contribute to the observed experimental results. The basic theory of the Frequency Tracker as originally proposed by Chaffee[1], Enloe[2], Wojnar[3], and Baghdady[4] does not take any such effects which may be due individual component characteristics or noise sources into account.

At its 200MHz operating point, the Tracker does fulfill the full range of its operating characteristics. Referring to Table VI, it is clear that in the narrow mode of operation, when the IF bandwidth of the Tracker is 1MHz, as a result of the additional frequency spectrum compression the performance of the Tracker is substantially improved. Hence, for input signals whose frequency

deviation is less than 10MHz, operation in the Tracker narrow mode can be performed at a S/N ratio improvement of about 7 to 10 db.

2.4 MEASUREMENTS WITH NOISE MODULATED FM SIGNALS

2.4.1 INTRODUCTION

In its true operational environment, the Frequency Tracker must demodulate Doppler shifted FM signals that are generated by a Laser Doppler Velocimeter. As such, the FM modulation which is representative of the micro-turbulence in the gas-dynamic environment under observation, is generated at all times over a turbulence power spectrum density extending from a few Herz to tens of kHz. Within this range of turbulence, the instantaneous velocity of the flow, defined by a carrier frequency representative of the mean flow and a superimposed frequency deviation representative of the velocity fluctuations in the flow, can vary over large turbulence frequencies. Thus in order to study Frequency Tracker performance it is necessary to simulate such real signals. This is best performed by a) generating FM signals that are noise modulated over well defined bandwidths so that Tracker performance may then be measured at specified carrier frequencies, frequency deviations and S/N ratios, and b) simulating the shape of the turbulence amplitude or power spectrum density by means of filters and noise sources to measure the statistical response of the Tracker by the use of correlation functions. Both these approaches have been taken and are described in the following two sections.

2.4.2 STATIC MEASUREMENTS

Figure 2-17 is a diagram of the experimental set-up. It is identical to the set-up used in performing sinusoidally modulated FM measurements, except that the signal generator is replaced with a white noise source and low pass filter. Measurements were made at a carrier frequency of 200MHz over modulation frequencies noise modulated through 10kHz, 50kHz, and 100kHz at frequency deviations through 24MHz. Figure 2-18 is a display of the parametric results obtained for a Tracker operating in its Wide Mode at a performance better than 3%. These measurements are more realistic in terms of the true performance of the Tracker than those presented in Figure 2-14. Table VIII is a comparison of the required S/N ratios for the defined 3% performance of the Tracker obtained by the sinusoidal and noise modulation techniques.

In I, II, and III we compare the respective performance of the Tracker over the full range of modulation frequencies through 100kHz at frequency deviations of 1MHz, 4MHz, and 8MHz. The trend in the results indicates that the Tracker when noise modulated requires somewhat larger input S/N ratios for the same 3% performance. The difference, however, of the order of 2 db in some cases, is not significant. In Figure 2-19, the AC output of the Tracker at 200MHz is shown to be independent of the modulation frequency when noise modulated over 100kHz. This is an important fact because it is indicative of the flat frequency response of the Tracker and its linear response over a FM modulation index range from 10 to 2.2×10^5.

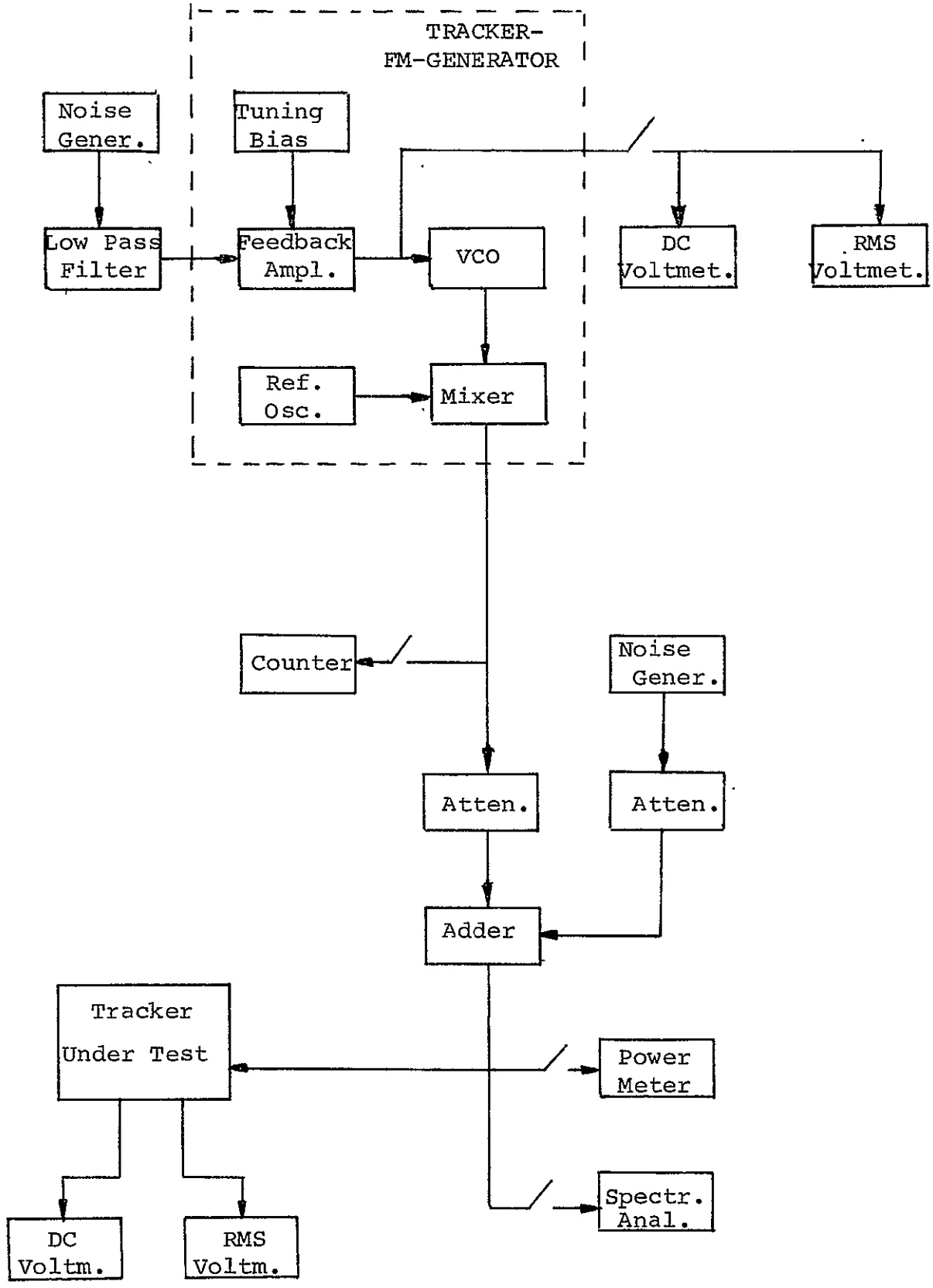

Figure 2-17. Noise Modulated Tracker Measurements

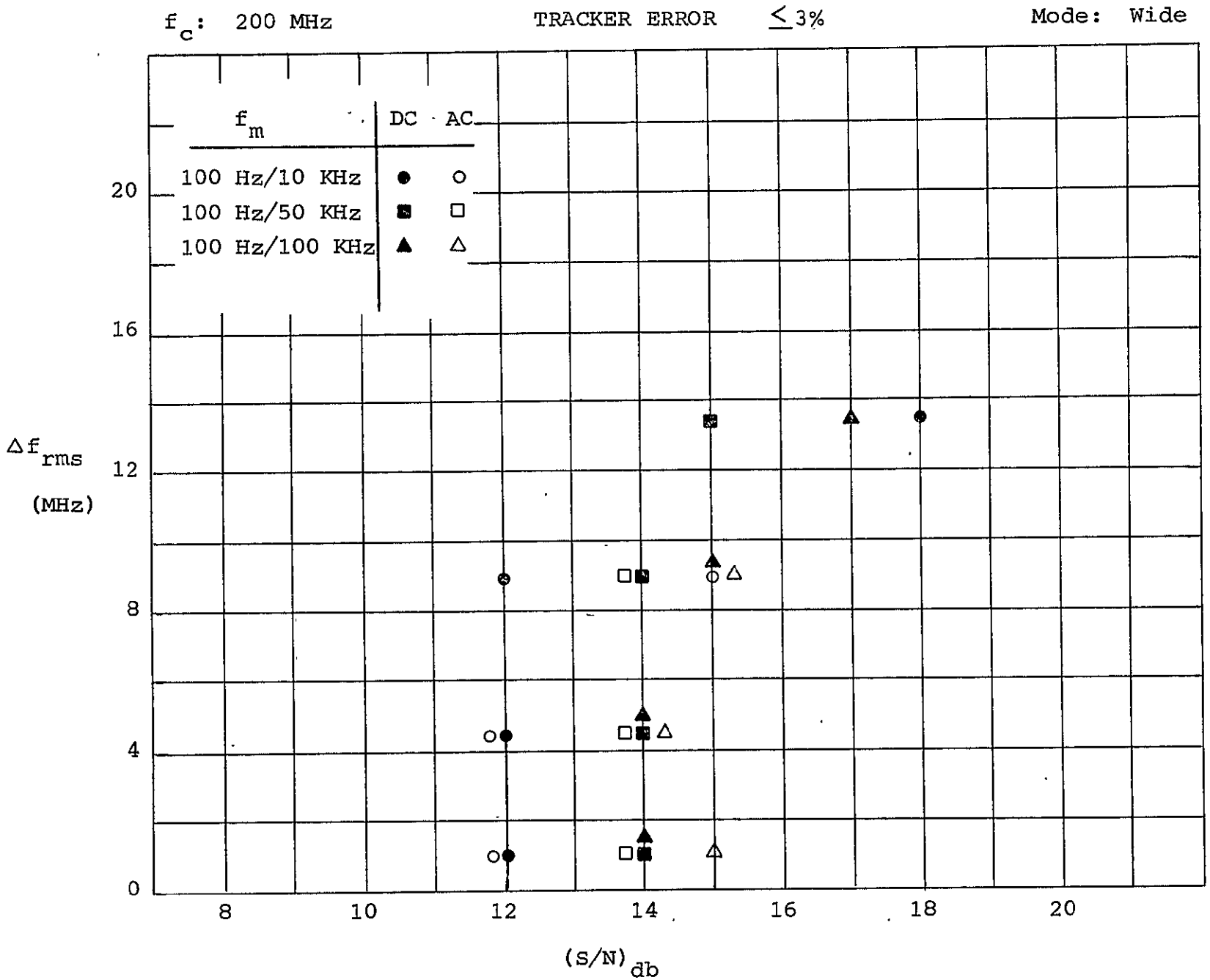

Figure 2-18. Noise Modulation of Tracker

	I		II		III	
Modulation	Sinusoid	Noise	Sinusoid	Noise	Sinusoid	Noise
Output	DC	DC	DC	DC	DC	DC
Mode	Wide	Wide	Wide	Wide	Wide	Wide
f_c	200	200	200	200	200	200
Δ_f	1	1	4	4	8	8
f_m, kHz	10,50,100	10,50,100	10,50,100	10,50,100	10,50,100	10,50,100
S/N	12,12,12	12,14,14	11,12,14	12,14,14	11,14,18	12,14,15
Modulation	Sinusoid	Noise	Sinusoid	Noise	Sinusoid	Noise
Output	AC	AC	AC	AC	AC	AC
Mode	Wide	Wide	Wide	Wide	Wide	Wide
f_c	200	200	200	200	200	200
Δ_f	1	1	4	4	8	8
f_m	10,50,100	10,50,100	10,50,100	10,50,100	10,50,100	10,50,100
S/N	12,12,12	12,14,15	12,12,--	12,14,14	12,--,--	15,14,15

TABLE VIII. Comparison of Sinusoidal and Noise Modulated FM Signals at 200 MHz Carrier Frequency

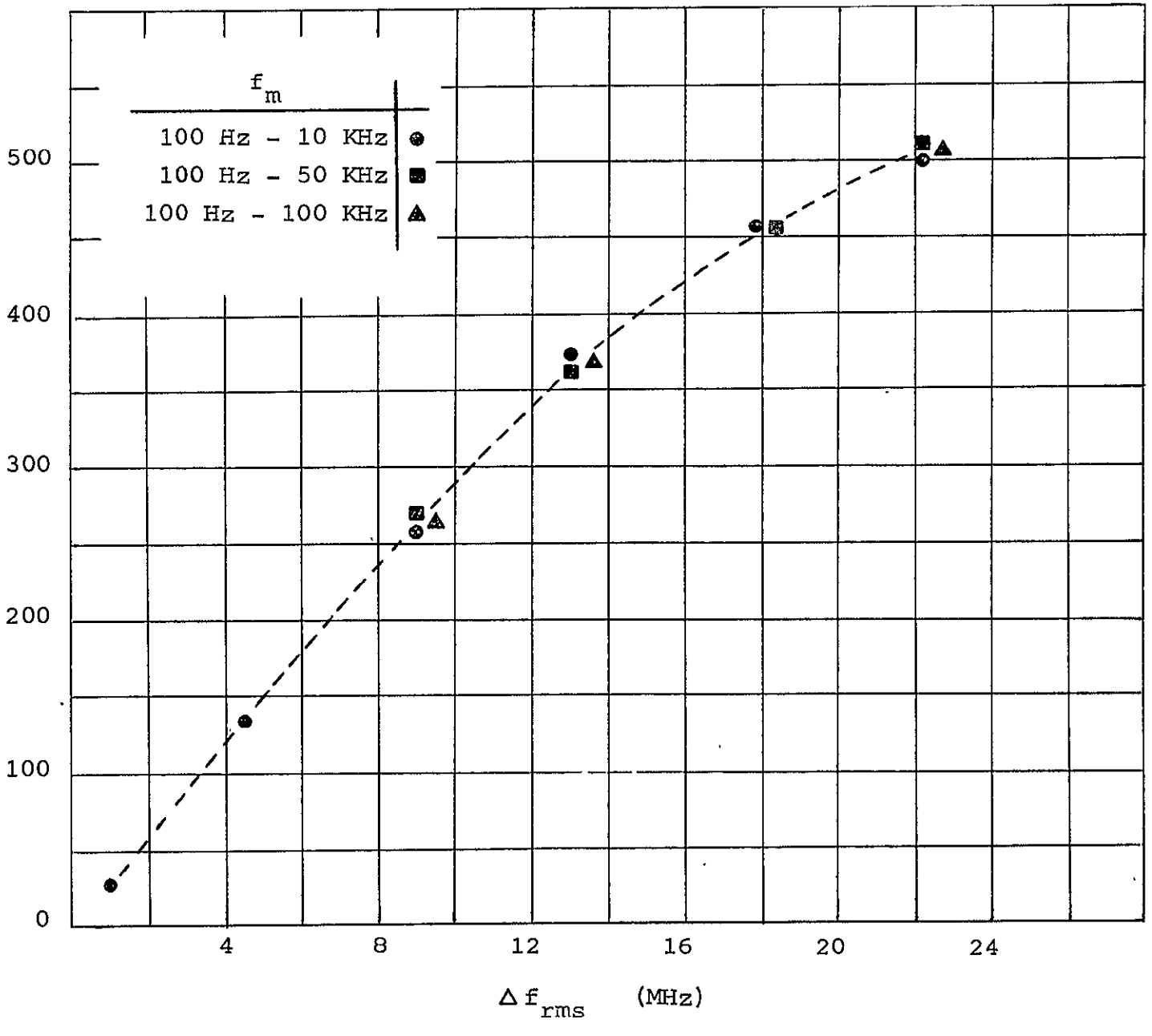

Figure 2-19. AC Output Independent of f_m

2.4.3 DYNAMIC MEASUREMENTS

2.4.3.1 Turbulence as a Random Process

A definition of turbulence may be formulated as follows: "Turbulent fluid motion is an irregular condition of flow in which the various quantities show a random variation with time and space co-ordinates, so that statistically distinct average values can be discerned."[5] In turbulence, all phenomena are random processes arising from a purely non-linear behavior of the fluid environment. Thus, the description of such processes can best be conveyed in terms of a correlation analysis for the characterization of the random process. Basic to the characterization of signals and random processes are the auto- and cross-correlation functions.

Assume that we have some physical process that in various channels gives rise simultaneously to signals $f_A(t)$, $f_B(t)$, $f_C(t)$, etc. Assume further that the physical process is not changing its character with time, such that we have a stationary situation. Further assume the time function $f_n(t)$ are not zero, nor do they have a DC component. The signals may be simple or complex periodic waves or they may have the character of noise; that is, randomly varying. Now imagine that we pass one of the signals, say $f_A(t)$, through a perfect delay line which introduces a non-dispersive variable delay of amount τ. We now have available the signal $f_A(t-\tau)$, identical to $f_A(t)$ but just delayed in time. Multiply the instantaneous value of $f_A(t)$ by the value of $f_A(t-\tau)$ and obtain the average of the product over a sufficiently long time. We now arrive at a quantity which has the following properties:

(1) The product will be a maximum at $\tau = 0$.

(2) The value at $\tau = 0$ is related to the total power of the signal. If $f_A(t)$ is a voltage, then the average of the product for $\tau = 0$ is simply $f_A^2(t)$, or the power that the signal dissipates.

(3) The average value of the product will be a function of τ, the form of which will be characteristic of the original signal, $f_A(t)$.

(4) If the averaging time is long compared to the reciprocal of the lowest frequencies present in $f_A(t)$, then repetitions of the measurement for a given τ will give values very close to one another.

(5) The average value of the product for a negative value of τ is identical to that for the same positive τ.

The above is a description of the auto-correlation function for any time function, $f_A(t)$ which is rigorously defined as:

$$C_{AA}(\tau) = \lim_{T\to\infty} \frac{1}{2T} \int_{-T}^{T} f_A(t) f_A(t-\tau)\, dt. \qquad (10)$$

Consider what information the function $C_{AA}(\tau)$ can give about $f_A(t)$. First compare $f_A(t)$ with $f_A(t-\tau)$ for very large values of τ. Any physically realizable process that might give rise to a signal will be such that the value of the signal at time t will become more independent of the value at $t-\tau$ as τ grows larger. Turbulence and thermal noise introduce randomness into a signal that causes a gradual loss of its coherence. Hence, for a signal arising from real processes, $C_{AA}(\tau)$ will tend to zero as τ becomes sufficiently

large. The value of τ that gives a significant diminuation of $C_{AA}(\tau)$ is a measure of the coherence time of the original signal, and the coherence time of a physical process is an important quantity in its characterization.

A very important property of the auto-correlation function is given by:

$$\Phi_{AA}(\omega) = \frac{1}{2\pi} \int_{-\infty}^{\infty} C_{AA}(\tau) \cos\omega\tau d\tau \tag{11}$$

and

$$C_{AA}(\tau) = \int_{-\infty}^{\infty} \Phi_{AA}(\omega) \cos\omega\tau d\omega \tag{12}$$

These expressions are the cosine Fourier transform pair. It can be shown that $\Phi_{AA}(\omega)$, the cosine Fourier transform of the auto-correlation function, is identically the power density spectrum of $f_A(t)$. Hence, an experimental determination of the auto-correlation or of the Fourier density spectrum are completely equivalent, equations (11) and (12) being used for transforming from one to the other.

In experimental work the measurement of the power density spectra of a complex signal has been the preferred way of obtaining information for characterizing the signal. Thus, the general characteristics of a turbulent flow, whether measured by the well-known hot wire techniques or by the more recent Laser Doppler Velocimetry approach is represented by its spectral power density.[6]

While determining the auto-correlation time function of a signal is in every respect equivalent to the traditional technique of power density spectra analysis, there is no classical analog for cross-correlation analysis. In cross-correlation one is concerned

with investigating the nature of the relationship between two signals that arise in some common process. The cross-correlation function is obtained by averaging the product of a time function with a delayed replica of a second time function.

Formally, the cross-correlation function is defined by:

$$C_{AB}(\tau) = \lim_{T\to\infty} \frac{1}{2T} \int_{-T}^{+T} f_A(t) f_B(t-\tau) dt. \tag{13}$$

The cross-correlation function can be described as representing the degree of conformity between two signals as a function of their mutual delay.

Hence, if $f_A(\tau)$ and $f_B(\tau)$ arise from two completely separate processes, then $C_{AB}(\tau)=0$. As in the case of the auto-correlation function, we can again define a reciprocal Fourier pair.

$$\Phi_{AB}(\omega) = \frac{1}{2\pi} \int_{-\infty}^{\infty} C_{AB}(\tau) e^{-j\omega\tau} d\tau \tag{14}$$

$$C_{AB}(\tau) = \int_{-\infty}^{\infty} \Phi_{AB}(\omega) e^{j\omega\tau} d\omega \tag{15}$$

In this case, however, the physical meaning of $\Phi_{AB}(\omega)$ is not so clear. $\Phi_{AB}(\omega)$ is the spectrum of cross-correlation of $f_A(t)$ and $f_B(t)$.

The method of cross-correlation analysis of two signals provides a powerful analytical tool that far transcends any technique

available in classical communication theory.[7] The ability to measure the alikeness of two signals that might arise from a common physical phenomenon as a function of their relative delay is generally capable of providing a much deeper insight into the phenomenon than any analysis of the properties of either or both of the signals separately.

Let us now examine random noise. The auto-correlation function for very wide bandwidth, uniform (white) noise of RMS value E_m is an impulse function at $\tau=0$ of amplitude E_m^2. This tells us that a characteristic of wide band noise is that the value of the signal at any instant is completely independent of the value the instant before and after; in other words, that the coherence time of the process giving rise to the noise is very short.

Since turbulence is a random process, white noise may be used to simulate the power spectral density or amplitude spectrum of a turbulent process. When the noise source is used with an appropriate shaping filter to modulate a FM generator, the equivalent Doppler shift obtained by the turbulent process may be reproduced.

2.4.3.2 Experimental Set-up .

Figure 2-20 is the set-up used to simulate the amplitude spectrum of a typical turbulent signature. A shaping filter which may have the bandwidth and form of any turbulence amplitude spectrum, driven by white noise, is used to modulate the Tracker-FM-Generator. The output of the FM Generator is then the Doppler shift resulting from the simulated turbulence that has a given amplitude spectrum or power spectral density. This Doppler signal at a given carrier frequency and noise modulated through the shaping

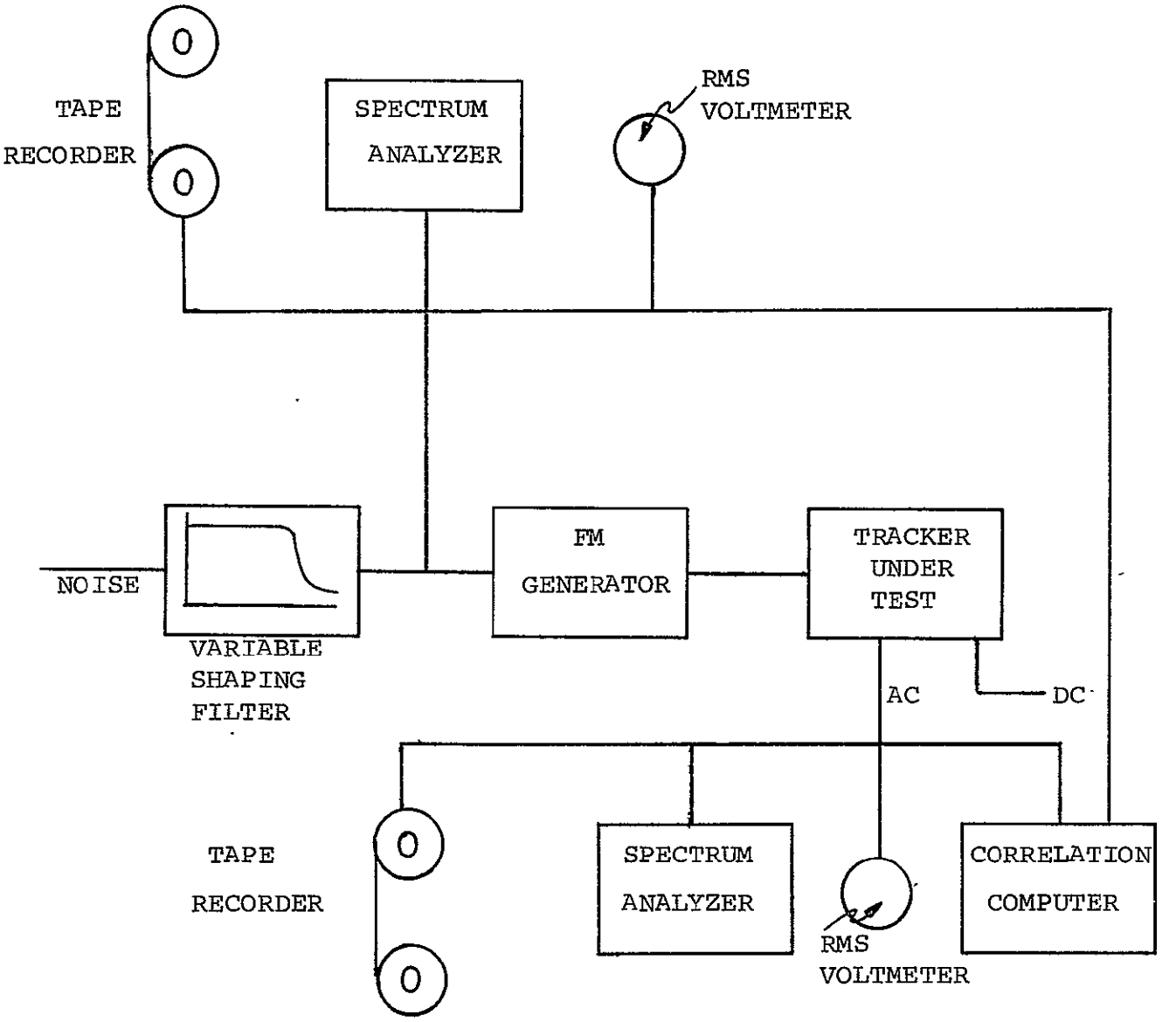

Figure 2-20. Turbulence Spectrum Simulation

filter is applied to the Frequency Tracker terminals. The Frequency Tracker then demodulates this signal, and if operating true to its characteristics must reproduce the signal in its time domain. Thus, one must compare the time-domain signal at the input to the FM Generator with that at the output of the Frequency Tracker. In order to perform this comparison as shown in Figure 2-20, the signals are observed on spectrum analyzers, recorded on tape recorders and in order to achieve in real-time a dynamic comparison of their statistical properties, their correlation functions computed by means of a Correlation Computer. The purpose for recording the signals on tape recorders has been so that data is available for later processing to compute the correlation functions and power spectral densities of the signals. A number of parametric combinations of carrier frequency, frequency deviation, modulation frequency, and signal-to-noise ratios have thus been processed. Table IX is a listing of tape recorded data that has been submitted to NASA Marshall Space Flight Center for computation of its auto- and cross-correlation functions and its power spectral density. This data, however, has not yet been reduced by appropriate computer programs to the desirable form so that a comparison of the Frequency Tracker performance will be made with respect to the results available from the real-time Correlation Computer used.

PAR Model 101A Correlation Computers have been used in the measurements set-up.[8]

The PAR Model 100 Correlation Function Computer computes the autocorrelation of a signal, or the crosscorrelation of two signals for 100 values of lag simultaneously. The range of delay is selectable from 100 microseconds to 10 seconds. The correlation function.

Output Level: 1 Volt RMS (all channels)
Tape Speed: 30 in./sec.

FREQUENCY TRACKER TEST TAPE (NASA)

Channel
1 - 1KHz Sine Wave
2 - Voice Identification
4 - Input Spectrum
5 - Output Spectrum

Test No.	Index	f_c-MHz	f_m-KHz	Δf-MHz	(S/N)db
1	000	200	10	1	24
2	055	200	10	1	15
3	110	200	50	1	24
4	164	200	50	1	15
5	216	200	100	1	24
6	266	200	100	1	15
7	316	200	10	5	24
8	368	200	10	5	16
9	416	200	50	5	24
10	464	200	50	5	17
11	509	200	100	5	25
12	554	200	100	5	17
13	598	200	10	10	24
14	642	200	10	10	14
15	684	200	50	10	24
16	724	200	50	10	14
17	763	200	100	10	24
18	803	200	100	10	14
19	842	200	10	18	24
20	888	120	10	5	24
21	926	120	10	5	16
22	964	120	50	5	24
23	1000	120	50	5	16
24	1039	120	100	5	24
25	1074	120	100	5	16
26	1109	120	10	10	24
27	1145	120	10	10	16
28	1180	120	50	10	24
29	1213	120	50	10	16
30	1247	120	100	10	24
31	1282	120	100	10	16
32	1315	120	10	18	24
33	1349	120	10	18	16
34	1381	120	50	18	24
	Data interrupted: Tracker unlocked				
35	1408	"	"	"	

TABLE IX. Frequency Tracker Test Tape Parametric Data

FREQUENCY TRACKER
TEST TAPE
(NASA)

Test No.	Index	f_c-MHz	f_m-KHz	Δf-MHz	(S/N) db
36	1408	10	10	1	24
37	1435	10	10	1	16
38	1458	10	50	1	24
39	1482	10	100	1	24
40	1507	10	10	1.75	24
41	1536	10	50	1.75	24
	Data interrupted: Tracker unlocked				
42	1561	10	50	1.75	24
43	1584	10	100	1.75	24
44	1616	10	10	3.50	24

The above simulated FM turbulence signals are noise modulated from 100Hz to f_m as indicated.

TABLE IX. (continued)

is stored in a 100 element analog memory, and may be displayed on an oscilloscope or an X-Y recorder. Alternatively, it may be fed into the Model 102 Fourier Analyzer for further processing.

The correlator functions by sampling one of the input signals at a frequency that depends on the delay selected, and representing it by a sequency of plus or minus "ones" with a ratio of probability that depends on the value of the input signal. The method is similar but not identical to that of a one bit digitizer. The signal is then delayed in a shift register, and multiplied either by its original self in the case of autocorrelation, or by the second signal in the case of crosscorrelation. The lagged products are averaged in one hundred RC integrating circuits for a time that is usually chosen to be 20 seconds. A choice of values between 1 and 400 seconds is available at the time of order; a field change is possible.

The advantage of using a correlation computer for statistical signal analysis is that it allows an enormous amount of calculation to be performed continuously as the data enters the instrument. Thus, a display of the auto- and cross-correlation functions is a direct indication of the statistical properties of the signals analyzed.

In addition to the PAR Correlation Computer, the PAR Fourier Analyzer has also been used for the real-time calculation of the input-output power spectral density of the simulated turbulence spectrum. Unfortunately an operational malfunction of the device did not enable the calculation of the power spectral density for every case that was simulated.

The PAR Model 102 Fourier Analyzer operates on the correlation

function $C(\tau)$ stored in the correlator, computing the sine and cosine Fourier transforms. When $C(\tau)$ is the autocorrelation, the cosine Fourier transform is the power spectrum of the input to the correlator.

2.4.3.3 Results

Let $f_A(t)$ and $f_B(t)$ be input and output sets of random signals to and from a signal processor. Then, as previously established, their auto- and cross- correlation functions are given by:

$$C_{AA}(\tau) = \lim_{T\to\infty} \frac{1}{2T} \int_{-T}^{T} f_A(t) f_A(t-\tau)\, dt \tag{16}$$

$$C_{BB}(\tau) = \lim_{T\to\infty} \frac{1}{2T} \int_{-T}^{T} f_B(t) f_B(t-\tau)\, dt \tag{17}$$

$$C_{AB}(\tau) = \lim_{T\to\infty} \frac{1}{2T} \int_{-T}^{T} f_A(t) f_B(t-\tau)\, dt \tag{18}$$

If $f_A(t) = f_B(t)$, i.e., the input and output sets of random signals are equal, then

$$C_{AA}(\tau) = C_{BB}(\tau) = C_{AB}(\tau) \tag{19}$$

Thus, two sets of random statistical signals that are identical, have equal auto- and cross-correlation functions, i.e., their power spectrum densities, see equations (14) and (15), are

also identical. This then, is the final test to establish the performance level of the Frequency Tracker.

In Figure 2-21A the amplitude modulation spectrum of turbulence that has been simulated by the set-up in Figure 2-19 is shown.

The shaping filter is noise swept across its bandwidth and the resultant signal is used to modulate the Tracker-FM-Generator, with the following FM output characteristics:

Carrier frequency: 200MHz
Modulation frequency: 10kHz
Frequency Deviation: 9MHz RMS
S/N = 25db in 1MHz bandwidth

Figure 2-21B is the resultant FM signal, i.e., simulated turbulence Doppler shift, as seen on the Frequency Tracker input spectrum analyzer. Figure 2-21C is the demodulated amplitude spectrum of the simulated turbulence at the Tracker AC output. Figure 2-21D is the auto-correlation of the input, auto-correlation of the output, and cross-correlation between the Tracker input and output signals, measured in real time, directly from the Frequency Tracker terminals. The resultant Doppler shift shown in Figure 2-22 will be recognized to be very similar to the actual Laser Doppler Velocimeter Doppler shifts obtained in practise. The demodulated amplitude spectrum, shown in Figure 2-23, is seen to be very similar to the input amplitude spectrum shown in Figure 2-21. The final certification that this is so is clearly seen in Figure 2-24, because $C_{AA}(\tau)$, $C_{BB}(\tau)$, and $C_{AB}(\tau)$ are seen to be one and the same.

Figure 2-22 is a similar set of data for the following FM,

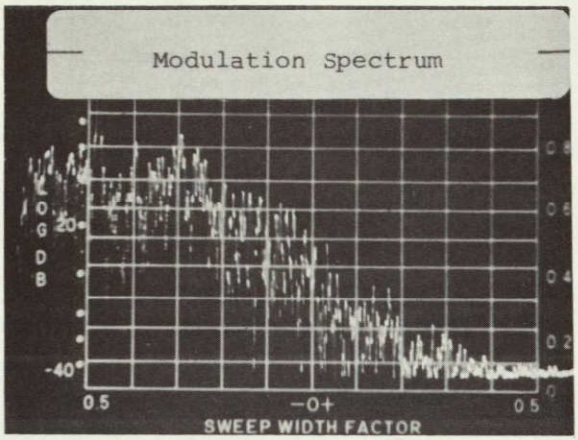

20 kHz

A. Amplitude spectrum of simulated turbulence.

Figure 2-21. Tracker Response to Simulated Turbulence Parameters:

f_c: 200MHz f_m: 10KHz

Δf: 9MHz S/N = 25db in 1MHz

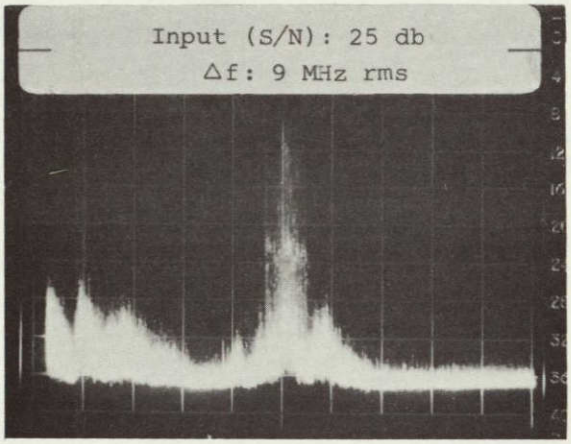

300 MHz

B. Simulated FM signal corresponding to turbulence spectrum.

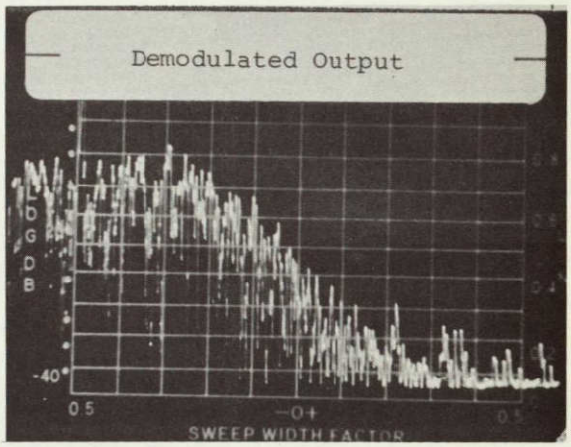

20 kHz

C. Amplitude spectrum of turbulence at Tracker output.

REAL TIME MEASUREMENTS

Autocorrelation, Input

Autocorrelation, Output

Crosscorrelation, Input-Output

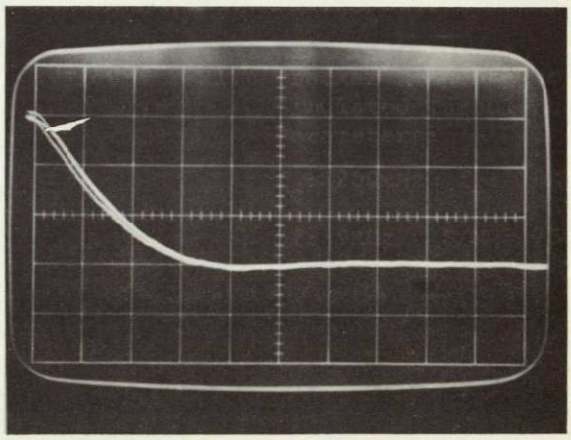

D. Correlation functions.

simulated Doppler shift, signals:

Carrier Frequency: 200MHz
Modulation Frequency: 10kHz
Frequency Deviation: 9MHz RMS
S/N: 15db in 1MHz bandwidth

Figure 2-22A is the FM, simulated Doppler shift, at the input of the Tracker terminals. Figure 2-22B is the Tracker demodulated output, which must be compared with Figure 2-21A. In Figure 2-23A and Figure 2-23B the auto-correlation functions of the input and output signals, derived under very similar, if not precisely exact, conditions, are shown. This case differs from the previous one in that its S/N ratio is at 16db rather than 25db. The auto-correlation of the input signals is ascertained to be very similar to that of the output signals. This data was first recorded on a tape recorder, on different channels for the Tracker input and output signals. The cross-correlation between the two channels was not superimposed on this data because of a tape channel time sequencing mismatch. However, comparison of Figures 2-21A, 2-22B, 2-23A, and 2-23B yields the conclusion that the Tracker operates properly over these input signal parameters.

The capability of the Tracker to demodulate accurately and reproduce a turbulence amplitude spectrum breaks down at the extremes of its frequency deviation. This is shown to be the case in Figure 2-24, where the following FM parameters are simulated:

Carrier frequency: 200MHz
Modulation frequency: 10kHz

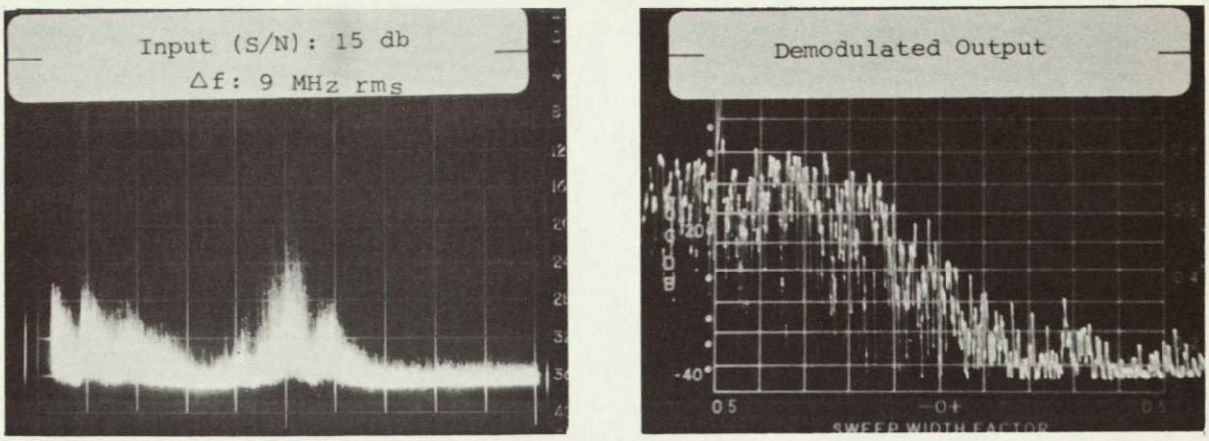

A. 300 MHz B. 20 kHz

Figure 2-22. Tracker Response to simulated turbulence parameters: f_c: 200MHz, Δf: 9MHz, f_m: 10kHz, S/N = 15db in 1MHz.

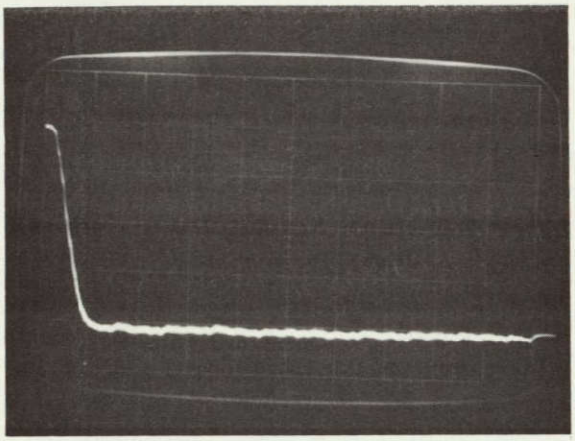

A.

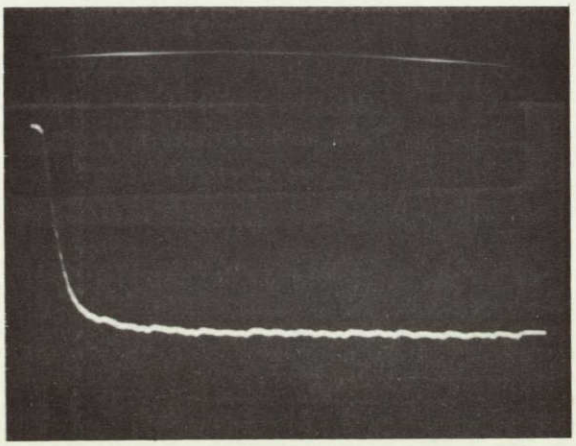

B.

AUTOCORRELATION, INPUT

f_c = 200 MHz
Δf = 10 MHz
f_m = 10 kHz
S/N= 16 dB

Correlation Computer: T = 1 msec

AUTOCORRELATION, OUTPUT

Figure 2-23. Correlation Functions

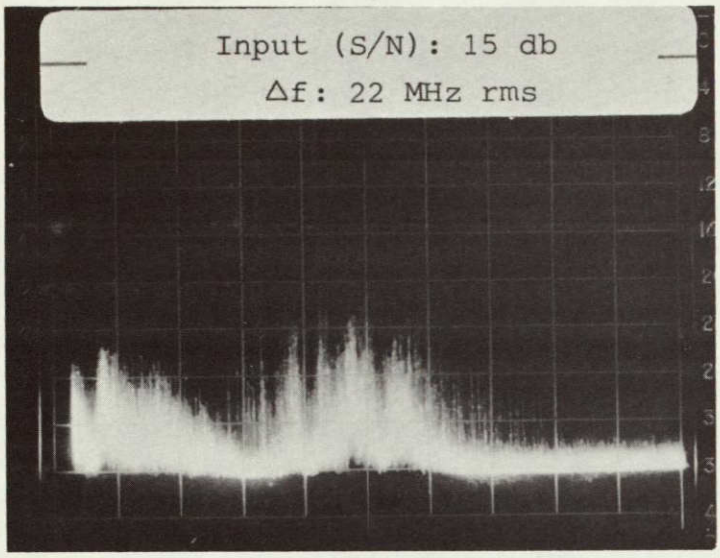

300 MHz

A.

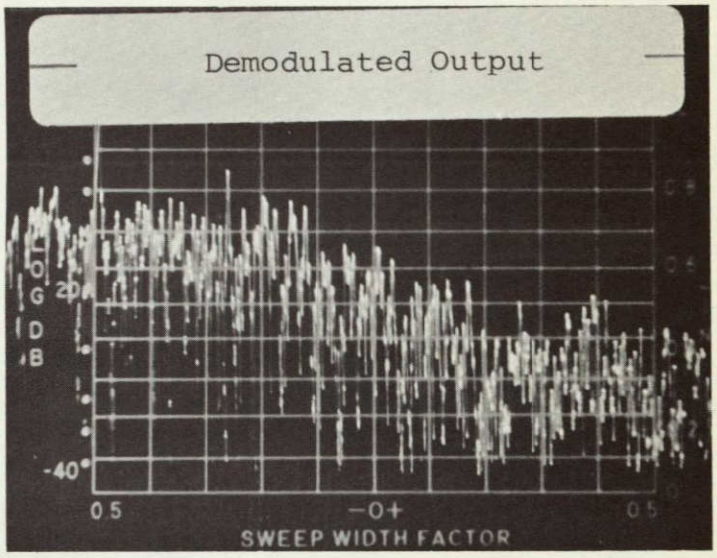

20 KHz

B.

Figure 2-24. Tracker Response to Simulated Parameters

f_c: 200MHz, Δf: 22MHz, f_m: 10kHz, S/N:15db in 1MHz

Frequency deviation: 22MHz RMS

S/N: 15db in 1MHz

Data taken under steady state sinusoid modulation input conditions, see Figure 2-14, in the Wide Mode Tracker operation, have resulted in similar conclusions. For a frequency deviation in excess of 18MHz RMS, i.e., 25MHz center-to-peak, to operate the Tracker within a 3% accuracy the S/N must be increased to 22db, measured in a 1MHz bandwidth. The dynamic simulation of this sinusoid steady state measurement bears this conclusion out. In Figure 2-24A the effect of such a large frequency deviation on the spectrum analyzer displayed FM signal is apparent. The distortion in the resultant amplitude spectrum, compare Figure 2-24B to Figure 2-21A, is seen to be effective in the tail-end of the distribution.

In Figure 2-25 the following set of FM parameters are simulated:

Carrier frequency: 200MHz

Modulation frequency: 50kHz

Frequency deviation: 9MHz RMS

S/N: 14db in 1MHz bandwidth

In Figure 2-26 the auto-correlation functions at the Tracker input and output, recorded at slightly different frequency deviation and S/N parameters are shown. This difference in frequency deviation, 10MHz RMS vs. 9MHz RMS in Figure 2-25, and 16db in S/N vs. 14db in S/N in Figure 2-25, is due to the experimental difficulties incurred in this type of measurement work, when reproducing such FM data. Again, comparison of Figure 2-25A and Figure 2-25B,

Figure 2-25. Tracker Response to Simulated Turbulence Parameters

f_c: 200MHz, Δf: 9MHz, f_m: 50kHz
S/N: 14db in 1MHz

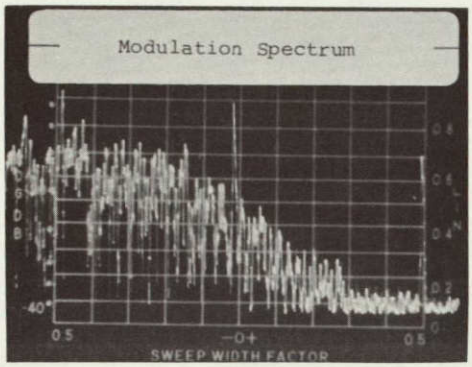

A. 100 kHz

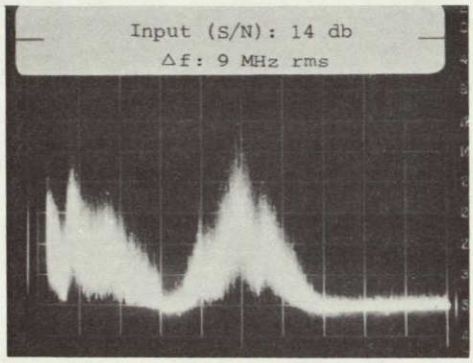

B. 300 MHz

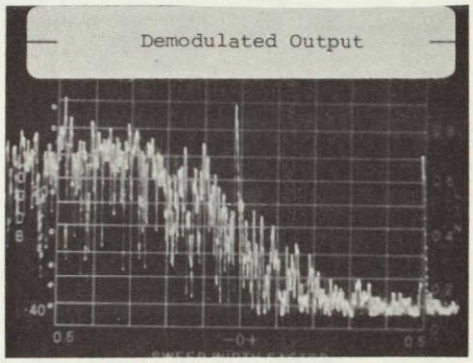

C. 100 kHz

Figure 2-26. Correlation Functions

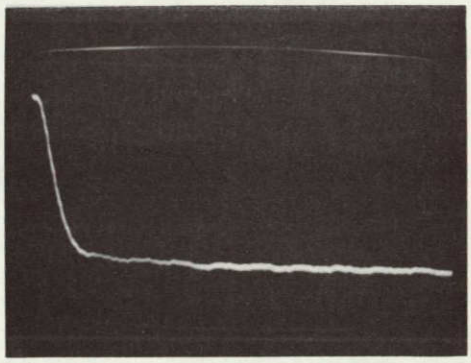

A. AUTOCORRELATION, INPUT

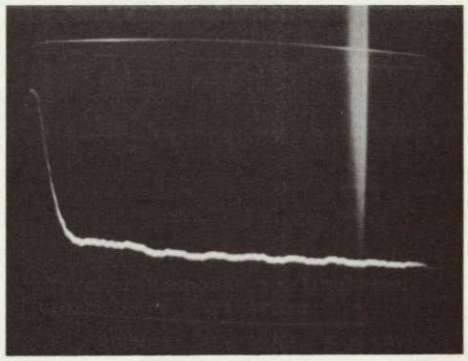

B. AUTOCORRELATION, OUTPUT

f_c = 200 MHz
Δf = 10 MHz
f_m = 50 kHz
S/N= 16 dB
Correlation Computer: T = 0.2 msec

and Figure 2-26A and Figure 2-26B, show that the Tracker has reliably and accurately performed its function. Similar data, shown in Figures 2-14 and 2-15, taken under steady state sinusoid input modulation conditions, concur with this.

In Figure 2-27 the resultant Tracker demodulation is shown to be somewhat less accurate. The simulated FM conditions are:

Carrier frequency: 200MHz
Modulation frequency: 50kHz
Frequency deviation: 22MHz RMS
S/N: 17db in a 1MHz bandwidth

Here again, Tracker performance at the frequency deviation of 22MHz RMS, about 30MHz center-to-peak, is seen to be somewhat off at the tail-end of the amplitude turbulence spectrum. (Compare Figures 2-25A, 2-25B, 2-27A.) This general conclusion, viz., that at the extremes of the frequency deviation, 30MHz center-to-peak, the Tracker does not precisely reproduce the amplitude (or power) spectrum of a signal, may be due to two causes:

a) Limitations in the closed loop frequency response of the Tracker electronics

b) The experimental noise-source used for these measurements did not have a good white, flat response across its bandwidth.

Thus, at high frequency deviations, the FM signal bandwidth at times coincided with a distortion present in the noise-source. This may result in a signal convolution, distorting under these conditions the demodulated amplitude spectrum. The cause of the

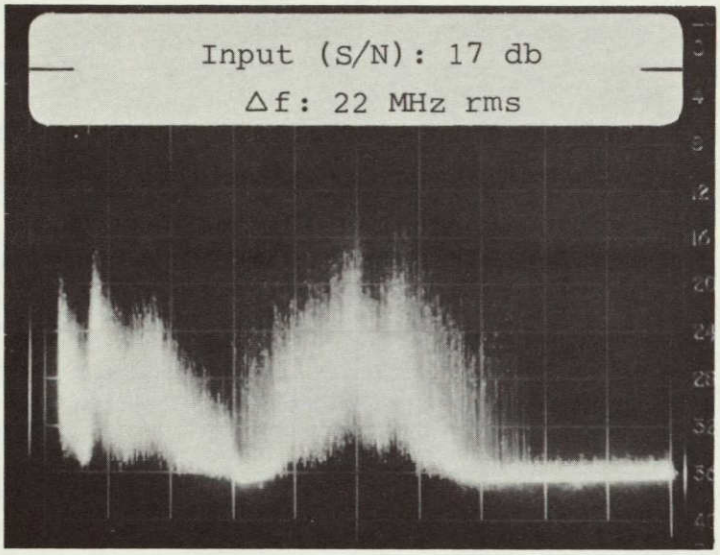

300 MHz

A.

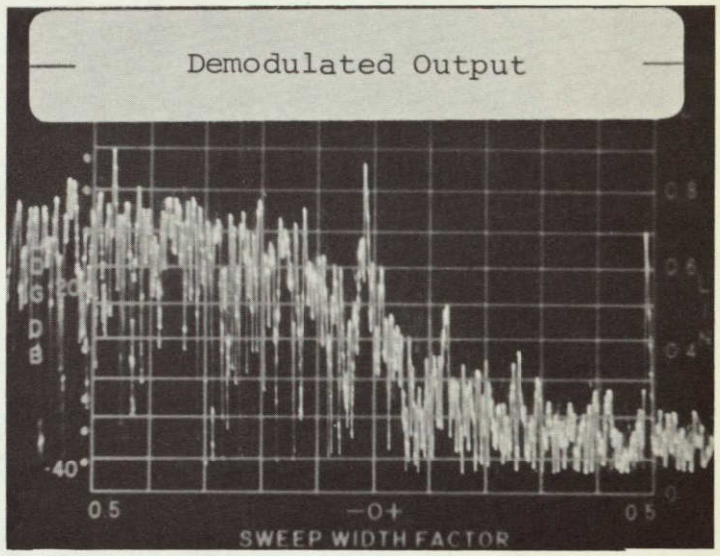

100 kHz

B.

Figure 2-27. Tracker Response to Simulated Turbulence Parameters
f_c: 200MHz, Δf: 9MHz, f_m: 50kHz, S/N: 17db in 1MHz

above-mentioned problem most probably lies in a combination of the reasons given in (a) and (b).

Figure 2-28 shows the response of the Tracker through a modulation frequency of 100kHz, for the following simulated FM parameters:

Carrier frequency: 200MHz
Modulation frequency: 100kHz
Frequency deviation: 9MHz RMS
S/N: 15db in a 1MHz bandwidth

The input amplitude spectrum, the corresponding FM spectrum, the Tracker demodulated output, and the real-time auto- and cross-correlation functions are shown in 2-28A, B, C, and D respectively. Figure 2-29 is a display of the Tracker input and output auto-correlation functions taken under somewhat different input signal conditions. (Δf: 10MHz, S/N:16db)

The correlation functions shown in Figure 2-28D and Figure 2-29 completely concur with one another. That is, the Tracker is fully responsive to these simulated signals at a modulation frequency of 100kHz. Better similarity between Figure 2-28A and Figure 2-28C is expected; however, these two amplitude spectra differ in their tail-end structure. Such differences that have occurred in these measurements may be attributed to the fact that they were not performed necessarily on the same day, so that an experimental error factor must be considered in all such interpretations. Again, as in the above results, a departure from accurate performance is observed at frequency deviations of the order of 22MHz RMS.

The statistical evaluation of the Frequency Tracker performance that has been presented in the above displays, Figures 2-21 through

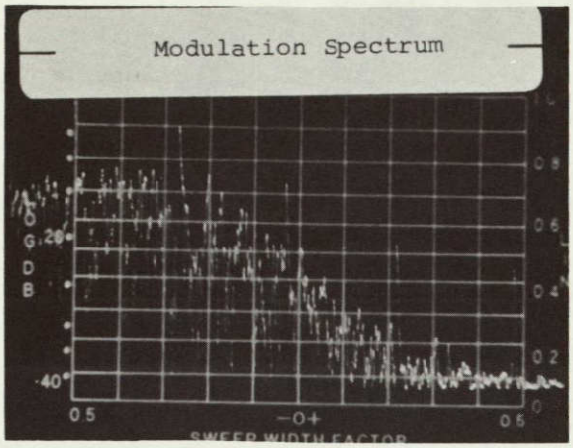

200 KHz

A. Amplitude spectrum of simulated turbulence.

Figure 2-28. Tracker Response to Simulated Turbulence Parameters:

f_c: 200MHz f_m: 100KHz
Δf: 9MHz S/N = 15db in 1MHz

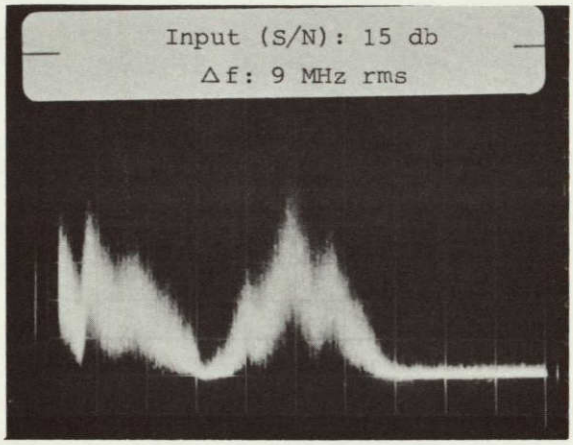

300 MHz

B. Simulated FM signal corresponding to turbulence spectrum.

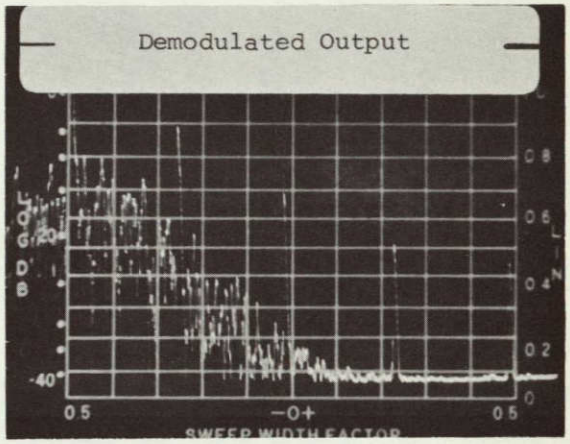

200 KHz

C. Amplitude spectrum of turbulence at Tracker output.

Real-Time Measurements

Auto-correlation input

Auto-correlation output

Cross-correlation input-output

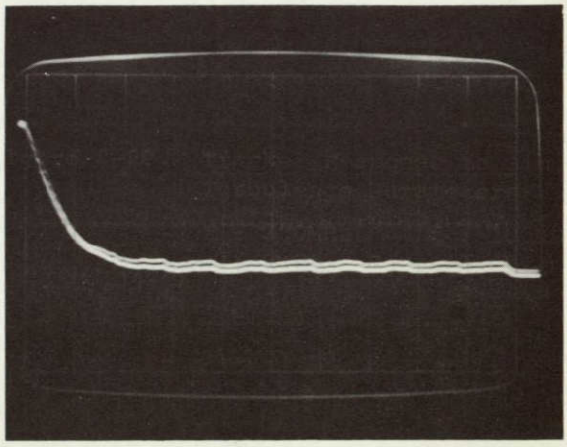

D. Correlation Functions.

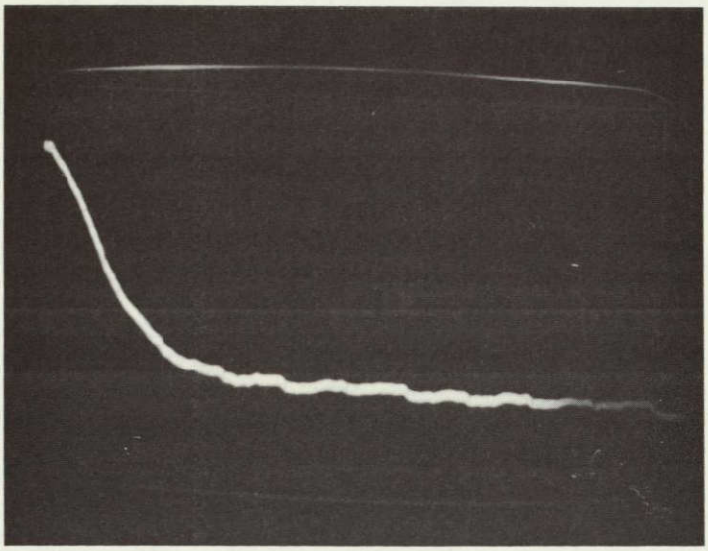

AUTOCORRELATION, INPUT

A.

f_c = 200 MHz
Δf = 10 MHz
f_m = 100 kHz
S/N= 16 dB

Correlation Computer: T = 0.1 msec

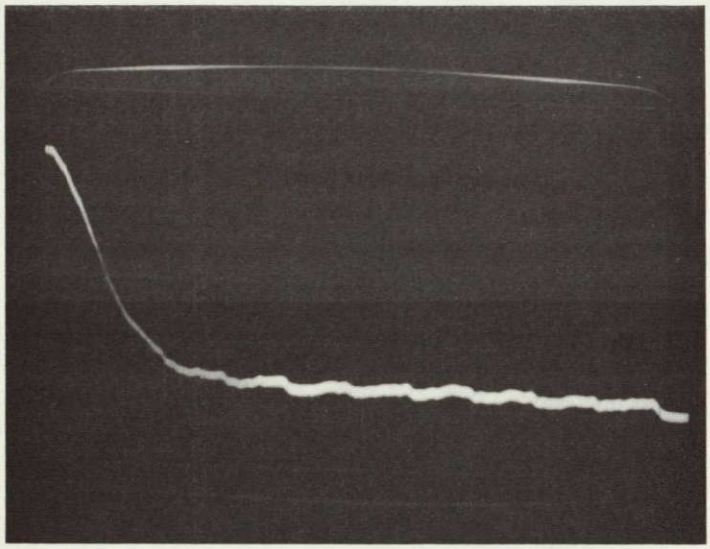

AUTOCORRELATION, OUTPUT

B.

Figure 2-29. Correlation Functions

2-29, have been limited to a carrier frequency of 200MHz. In each case proper correlation to the static results shown in Figures 2-14 and 2-15 has been found. The very nature of these measurements are tedious, time consuming, and difficult to perform. We have not been able to make as many such measurements by use of the correlation computers for a similar detailed study of other sampled carrier frequencies across the tracking band. However, many cases of interest, as shown in Table IX, have been tape recorded, and when finally analyzed by digital computer programs, will be an interesting and useful complement to the above study.

2.5 OUTPUT NOISE OF FREQUENCY TRACKER

The Frequency Tracker, like any other electronic network, has an output noise associated with it. This noise generates a systematic error in the AC output channel of the Tracker, such that it effectively limits the accuracy with which any turbulent flow measurement can be made. However, it will be shown that improvements in this systematic error can be made by limiting the modulation frequency at the output by the use of low-pass filters. All flow and turbulence measurements do not necessarily extend over turbulence frequencies of 100kHz. As a matter of fact, turbulence power spectra of subsonic flows may peak at about 2kHz, trailing out to a maximum turbulence frequency of 10kHz. Similar frequency constraints may be assigned to hypersonic flows, in where the turbulence intensity information of interest may extend only over 25kHz to 50kHz. Hence, a trade-off between increasing the accuracy in the measurement of the instantaneous flow and reducing the turbulence frequency over which the measurement is

made can be achieved.

An analysis of the noise output of a frequency tracker is now presented. The minimum detectable Δf (sensitivity of frequency tracker) is then related to the loop parameters (feedback factor, modulation frequency, closed loop bandwidth) and to the input signal-to-noise ratio. It is also shown that the sensitivity can be increased considerably by adding an output filter to the frequency tracker.

2.5.1 NOISE ANALYSIS OF FREQUENCY TRACKER

The input to the frequency tracker can be written as:

$$s(t) = A \cos (\omega t + \varphi(t)) + n(t) \qquad (20)$$

where: A = amplitude of Doppler signal (assumed to be constant)
ω = average Doppler frequency (carrier frequency)
$\varphi(t)$ = modulation of Doppler due to turbulence
$n(t)$ = white noise

The noise term can be represented by two quadrature components:

$$n(t) = n_1(t) \cos \omega t + n_2(t) \sin \omega t \qquad (21)$$

In the case of no modulation ($\varphi(t) \equiv 0$), the input takes the form of:

$$s(t) = A \cos \omega t + n_1 \cos \omega t + n_2 \sin \omega t \qquad (22)$$

which can be reduced to:

$$s(t) = \sqrt{(A + n_1)^2 + n_2^2} \cos \left(\omega t - \text{arc tan} \frac{n_2}{A + n_1} \right) \qquad (23)$$

Since this analysis is only applicable above threshold, where $A >> n$, we can write:

$$s(t) = \sqrt{(A + n_1)^2 + n_2^2} \cos\left(\omega t - \frac{n_2}{A}\right) \quad (24)$$

This expression represents a signal which is simultaneously amplitude and phase modulated. Since the tracker contains an amplitude limiter, the AM can be disregarded. The discriminator, however, is sensitive to the phase noise n_2/A, which causes the tracker output noise.

It can be shown that the spectral densities of n_1 and n_2 in equation (21) are equal to the spectral density of $n(t)$, which is $N_o/2$. Therefore, the normalized input phase noise n_2/A can be directly related to the input carrier-to-noise ratio. The spectral density of n_2/A is $N_o/2A^2$, the normalized noise spectral density, and the carrier-to-noise ratio in an arbitrarily selected reference bandwidth (B_r) is:

$$r_r = A^2/N_o B_r \quad (25)$$

Let us now consider the tracking loop, which is diagrammatically shown in Figure 30, and assume that the equivalent transfer function of the IF filter is included in $G(s)$. The open loop transfer function is:

$$H_o(s) = k_D s G(s) \frac{k_v}{s} = k_D G(s) k_v \quad (26)$$

The noise voltage at the VCO input, which is of particular interest, is, according to elementary feedback theory:

$$v_{VCO}(s) = \frac{k_D s G(s)}{1 + H_o(s)} \varphi_{IN}(s) \quad (27)$$

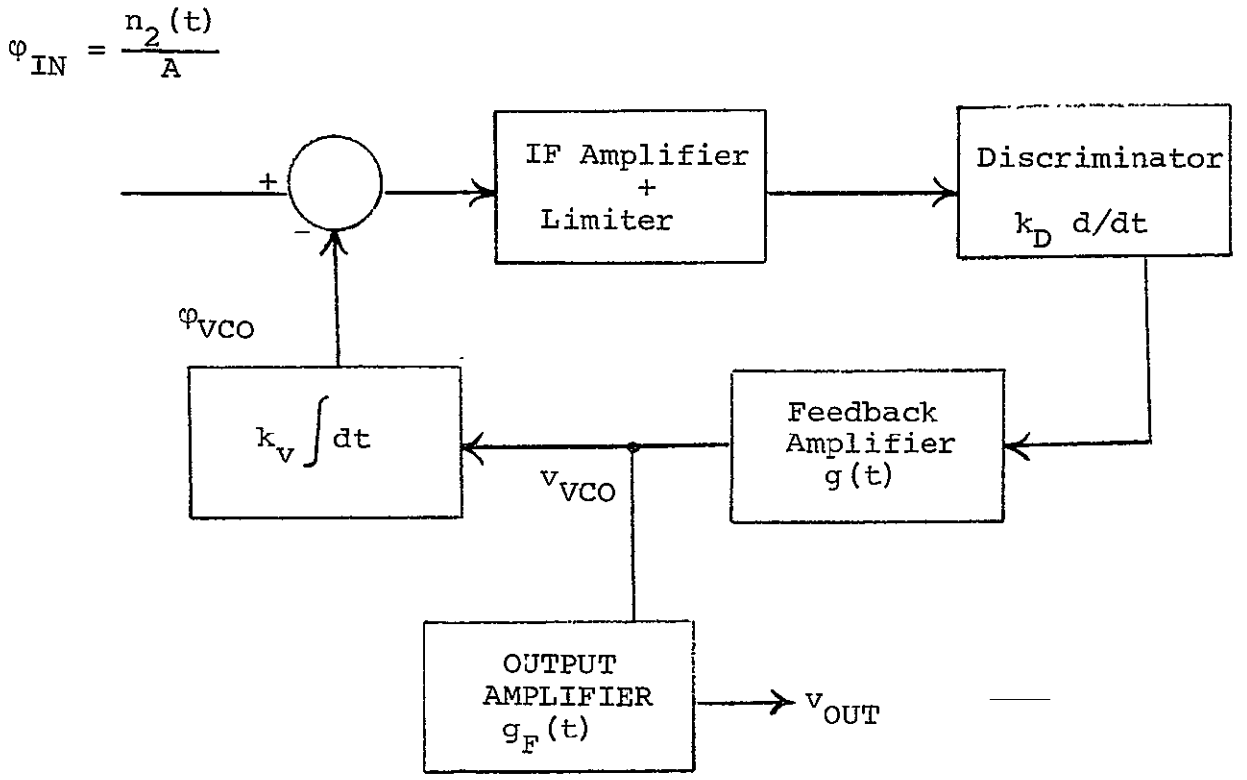

Figure 2-30. Feedback Loop

which can be rewritten as:

$$v_{VCO} = \frac{H_o}{1 + H_o} \cdot \frac{s}{k_v} \cdot \varphi_{IN} = H_c \frac{s}{k_v} \varphi_{IN} \tag{28}$$

where H_c designates the closed loop transfer function. The mean square VCO voltage is related to the input phase noise spectral density by:

$$\overline{v_{VCO}}^2 = \frac{N_o}{2A^2} \cdot \frac{1}{2\pi} \int_{-\infty}^{+\infty} \frac{s^2}{k_v^2} \cdot |H_c(s)|^2 \, d\omega \tag{29}$$

Substituting

$$T(\omega) = |H_c|^2 \tag{30}$$

which is the squared magnitude of the closed loop gain function, we obtain:

$$\overline{v_{VCO}}^2 = \frac{N_o}{2\pi \cdot 2A^2} \int_{-\infty}^{+\infty} \frac{\omega^2}{k_v^2} \cdot T(\omega) \, d\omega$$

$$\overline{v_{VCO}}^2 = \frac{N_o}{4\pi \, k_v^2 \, A^2} \int_{-\infty}^{+\infty} \omega^2 \, T(\omega) \, d\omega \tag{31}$$

Equation (31) gives the desired relation between the VCO input noise voltage, the loop parameters (which determine $T(\omega)$) and the input carrier-to-noise ratio.

2.5.1.1 Frequency Tracker Sensitivity

The sensitivity of the frequency tracker; i.e., the minimum detectable frequency deviation Δf_{min}, can be defined to be equal to the rms frequency deviation of the VCO due to loop noise; i.e., the Δf resulting in an output signal-to-noise ratio of 1.

$$\Delta f_{min} = \sqrt{\overline{\Delta f}_{VCO}^{\,2}} \tag{32}$$

The variance of the VCO frequency due to the loop noise is obtained by multiplying equation (31) by k_v^2, the VCO sensitivity:

$$\overline{\Delta f}_{VCO}^{\,2} = \frac{N_o}{4\pi A^2} \int_{-\infty}^{+\infty} \omega^2 \, T(\omega) \, d\omega \tag{33}$$

With equation (32), we obtain:

$$\Delta f_{min} = \sqrt{\frac{N_o}{4\pi A^2} \int_{-\infty}^{+\infty} \omega^2 \, T(\omega) \, d\omega} \tag{34}$$

It has been shown that $A^2/N_o B_r$ is the signal-to-noise ratio in a reference bandwidth B_r. The integral expression is the second moment of the function $T(\omega)$ with respect to the axis $\omega = 0$. With the open loop parameters (feedback factor, poles, zeros) given, $T(\omega)$ is uniquely determined, and the integral can be evaluated analytically, or numerically. It can also be obtained by numerical or graphical integration of the actually measured $T(\omega)$.

2.5.1.2 Characteristics of T(ω)

The open loop function $H_o(j\,\omega)$ generally used in frequency trackers has a low pass characteristic; i.e., $|H(j\,\omega)|$ is approximately constant up to f_m and then cuts off at the fastest possible rate. $T(\omega)$ therefore approximates unity in the frequency range to f_m, and has a resonance peak near the frequency where $|H_o(j\,\omega)|$ is unity, since there $|1 + H_o(j\,\omega)|$ can become rather small, depending on the open loop phase margin (see Figure 2-31).

It can easily be seen that with such a function $T(\omega)$ the frequencies in the vicinity of the open loop unity gain crossover contribute a considerable part to the second moment, and therefore to the loop noise.

2.5.1.3 Tracker Output Filter

An obvious solution to increase the tracker sensitivity is to make the loop as stable as possible, and to make $T(\omega)$ as narrow and as flat as possible. This is however not always practical due to the requirements of high f_m and high open loop gain, connected with unavoidable residual phase shifts and delay effects in the loop.

Another possibility is to pass the tracker output through a low pass filter. The frequencies of interest are no higher than f_m, and since a considerable amount of noise is at frequencies higher than f_m, it can be filtered out. Ideally, a rectangular filter with cutoff at f_m is desirable. Since the filter is outside the loop, it has no effect on the loop stability. With the output filter included, the input-to-output relation is: (see Figure 2-30)

$$v_{out}(s) = \varphi_{IN}(s) \cdot \frac{s}{k_v} \cdot H_c(s) \cdot G_F(s) \qquad (35)$$

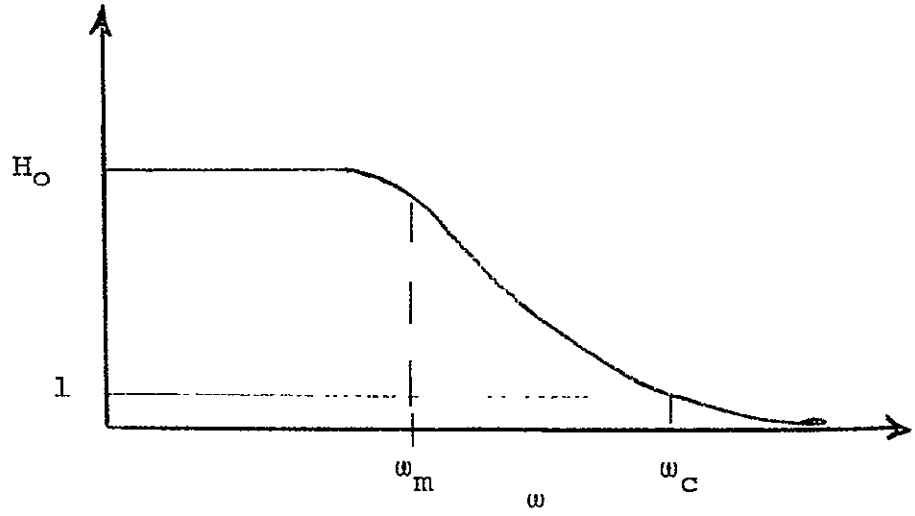

Figure 2-31(a) Open Loop Gain Function

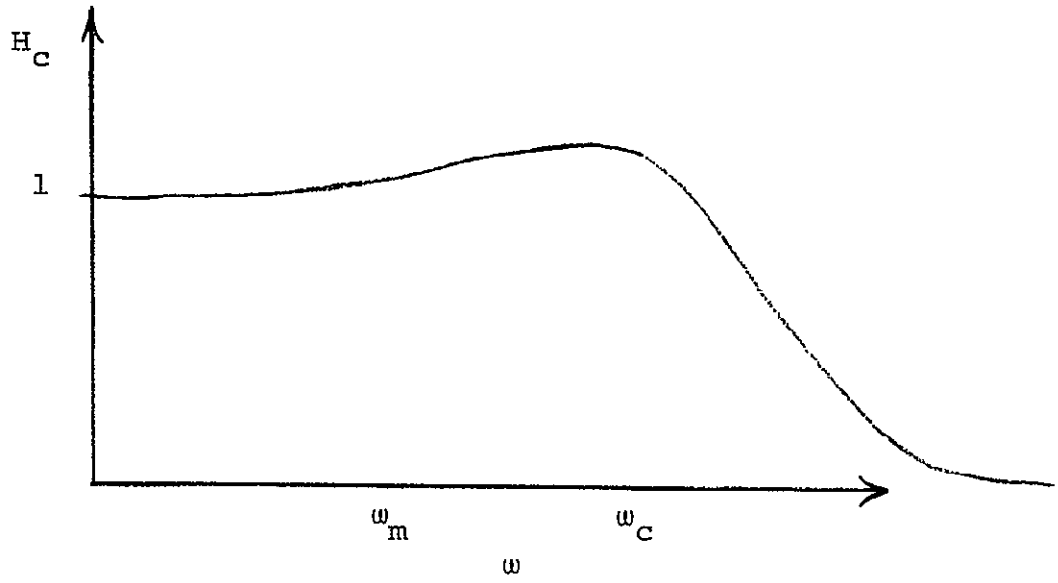

Figure 2-31(b) Closed Loop Gain Function

The output mean square noise voltage due to the input phase noise is now:

$$\overline{v_{out}^2} = \frac{N_o}{2A^2} \cdot \frac{1}{2\pi} \cdot \int_{-\infty}^{+\infty} \left| \frac{j\omega}{k_v} \cdot H_c(j\omega) \cdot G_F(j\omega) \right|^2 d\omega$$

$$= \frac{N_o}{4\pi A^2 k_v^2} \int_{-\infty}^{+\infty} \omega^2 T(\omega) \left|G(j\omega)\right|^2 d\omega \qquad (36)$$

i.e., it is a function of the second moment of $T(\omega) \left|G(j\omega)\right|^2$ instead of $T(\omega)$.

It was stated earlier that $T(\omega)$ is nearly constant ($\approx$ unity) over the modulation frequency range f_m. If, therefore, a sufficiently sharp output filter is used, the function $T(\omega) \left|G(j\omega)\right|^2$ reduces to $\left|G(j\omega)\right|^2$; i.e., the tracker sensitivity is independent of the loop characteristics. For a rectangular filter with unity gain and a cutoff frequency f_m, the output noise is:

$$\overline{v_{out}^2} = \frac{N_o}{4\pi A^2 k_v^2} \cdot \int_{-\omega_m}^{\omega_m} \omega^2 \, d\omega$$

$$= \frac{N_o}{4\pi A^2 k_v^2} \cdot \frac{2}{3} \omega_m^3$$

$$= \frac{2 N_o \cdot 8 \pi^3 f_m^3}{12\pi A^2 k_v^2} \qquad (37)$$

$$\overline{v_{out}^2} = \frac{4\pi^2 N_o f_m^3}{3 A^2 k_v^2} \tag{38}$$

The sensitivity is obtained by multiplying the output noise voltage by k_v:

$$\Delta f_{min} = 2\pi \sqrt{\frac{N_o f_m^3}{3A^2}} \tag{39}$$

With $A^2/N_o f_m$ being the carrier-to-noise ratio r_m referred to the baseband-bandwidth f_m, equation (19) becomes:

$$\Delta f_{min} = 2\pi f_m \sqrt{\frac{1}{3r_m}} \tag{40}$$

From equation (19) it can be seen that for any given normalized noise spectral density $N_o/2A^2$ (above threshold) the sensitivity increases with decreasing modulation bandwidth f_m. The sensitivity at threshold can be calculated considering that the threshold signal-to-noise ratio $(r_c)_t$, referred to the closed loop bandwidth B_c, for an optimally designed tracking loop is:[5,6]

$$(r_c)_t = 5 \left(\frac{F - 1}{F}\right)^2 \tag{41}$$

For high feedback factors, equation (41) reduces to:

$$(r_c)_t \approx 5 \tag{42}$$

With equation (25),

$$r_c = \frac{A^2}{N_o B_c} \tag{43}$$

Therefore:

$$\left(\frac{N_o}{2A^2}\right)_t = \frac{1}{2\ (r_c)_t\ B_c} \tag{44}$$

Combining equations (39), (42) and (44), the sensitivity at threshold is obtained to be:

$$\left(\Delta f_{min}\right)_t = 2\pi\ f_m \sqrt{\frac{1}{15}\ \frac{f_m}{B_c}} \tag{45}$$

The closed loop bandwidth can be found following the procedure given in Reference 6, or experimentally. For the tracker model 200B, B_c is approximately 800 kHz, and f_m is 100 kHz. $(\Delta f_{min})_t$ is therefore:

$$\left(\Delta f_{min.}\right)_t = 57 \text{ kHz}$$

2.5.2 EXPERIMENTAL RESULTS

The Frequency Tracker output noise is plotted, in Figure 32, in terms an AC RMS voltage as a function of signal-to-noise ratios for an unmodulated input carrier frequency at 120MHz. Since the output noise is input frequency independent, and this is experimentally established, the significance of the carrier frequency is only to enable measurements to be performed over a wide range of carrier-to-noise (C/N) ratios. As previously stated, these C/N ratios are defined in a 1MHz unmodulated bandwidth.

Without an output filter at its terminals, the noise output of the Tracker is at its maximum and monotonically decreases with C/N ratio. At a carrier-to-noise ratio of 16db, the output noise level is at 3.5 mv. Reference to Figure 2.6, where the AC voltage/

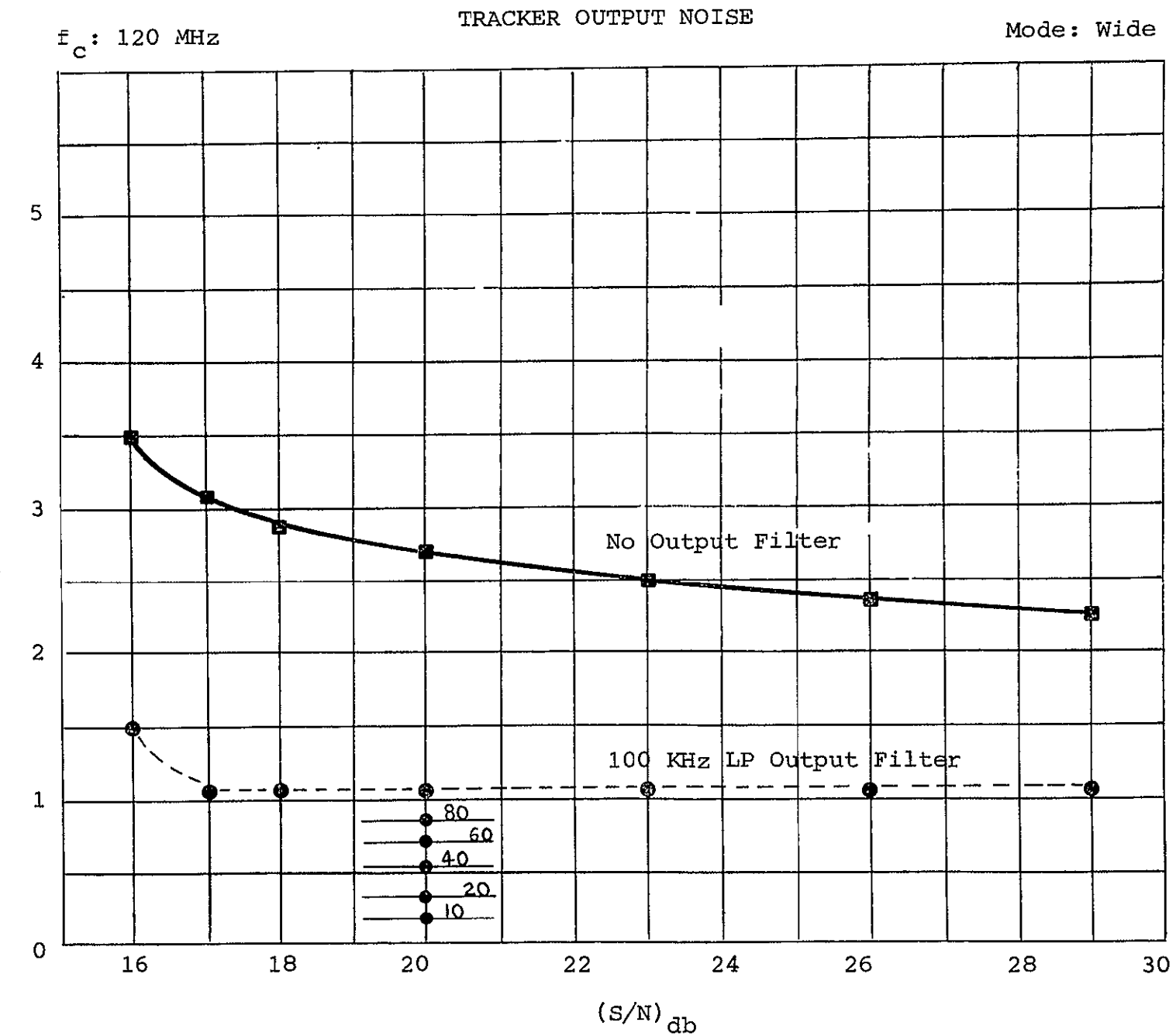

Figure 2-32. Output Noise of Frequency Tracker

MHz deviation frequency vs. carrier frequency of the Tracker is plotted, yields a Δf of 140kHz. This implies an error in the measurement of flow velocity of about 2 ft/second. At low C/N ratios, less than 16db, the output noise of the Tracker sharply increases because of the conventional noise generated by the discriminator at its threshold. The effect of loop regenerative noise also contributes, at low input carrier-to-noise ratios, to the total Tracker noise output. As the carrier-to-noise increases, the total output noise of the Tracker is reduced. Thus, at a C/N ratio of 23db, the systematic error is at 100kHz, or close to a velocity error of 1 ft/second. (We assume an 8° scattering angle in the Laser Doppler Velocimeter).

The Tracker output noise level can be substantially decreased by connection of a low-pass filter to the AC output terminals. Figure 2-32 shows the results, where the reduction in output noise level as a function of the low-pass filter bandwidth is shown. Table X summarizes the results.

2.6 EFFECTIVENESS OF FREQUENCY TRACKER AGC (AUTOMATIC GAIN CONTROL) FEATURE

The Model 200B Frequency Tracker has a built-in AGC feature that extends the sensitivity of the Tracker input down to -50dbm, at 50 ohm, input impedance. It is important to establish the fact that this feature does not in any way change the performance of the Tracker, irrespective of signal level and operating frequency. Figure 2-33 clearly shows the results, in where the DC output level of the Tracker, corresponding to its tracking range, is at all times independent, down to -50dbm, of the input signal level.

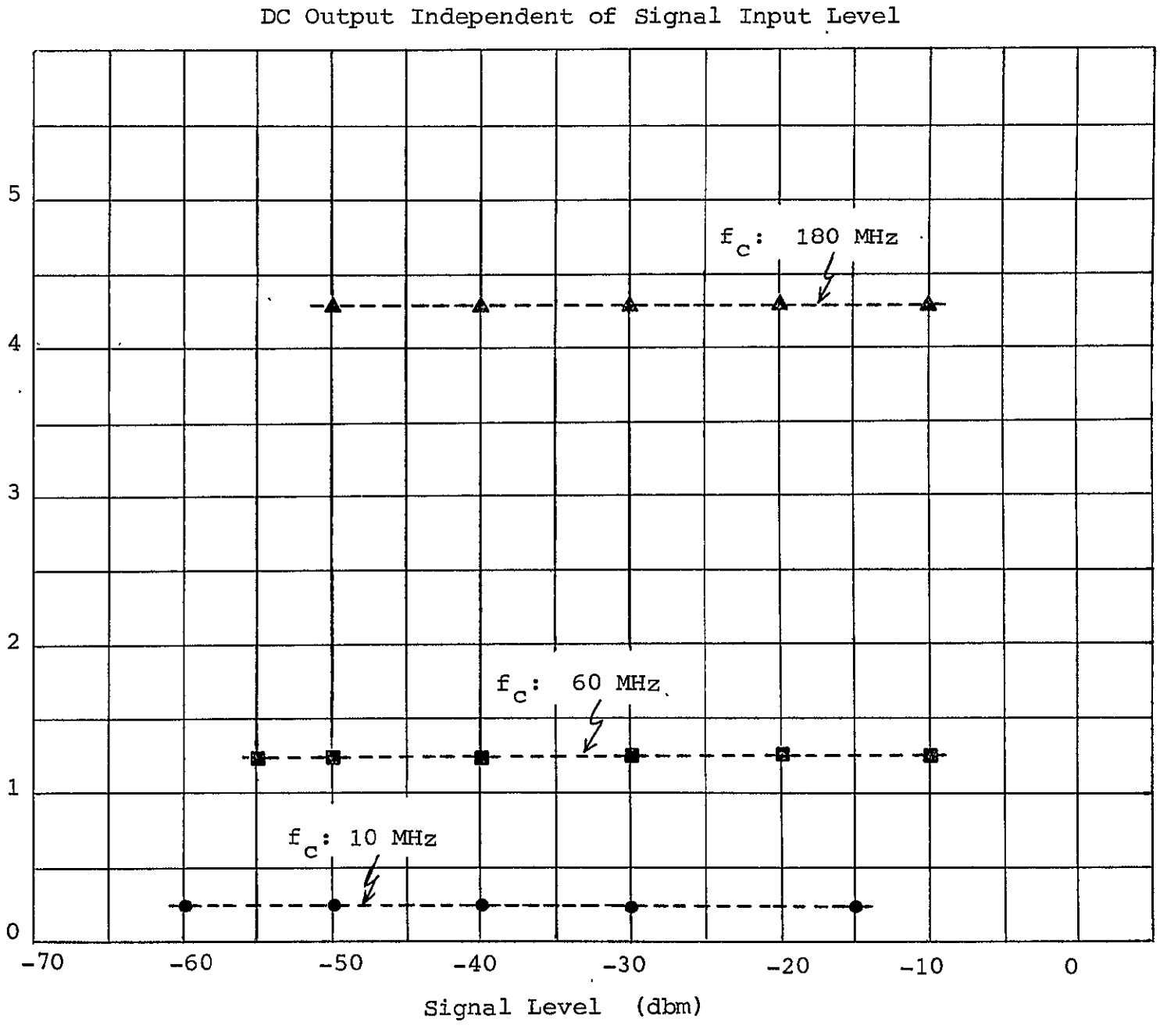

Figure 2-33. Frequency Tracker AGC Feature

f_c, MHz	C/N	Low Pass Filter Cut-off, kHz	Output Noise Voltage, MV	Equivalent Output Noise Frequency, kHz	Velocity Error ft/sec
120	20	None	2.7	108	1.35
		100	1.1	44	0.55
		80	0.9	36	0.45
		60	0.75	30	0.375
		40	0.55	22	0.275
		20	0.35	14	0.175
		10	0.20	8	0.100

TABLE X. Output Noise Reduction of Frequency Tracker

2.7 CONCLUSIONS

The Wide Band Frequency Tracker Model 200B has been thoroughly analyzed and subjected to a range of input signals representative of its operating parameters. Results have been established based on steady state, as well as turbulence-type signals that have been simulated. Levels of Tracker performance as a function of carrier frequencies, modulation frequencies, frequency deviations, and signal-to-noise ratios have been established over representative data points across the total tracking range. Tracking performance within a 3% accuracy constraint has been found to be satisfactory for frequency deviations as large as 18MHz RMS at reasonable signal-to-noise ratios. In general, signal-to-noise ratio has to be increased as a function of modulation frequency and frequency deviation to maintain track within the desired accuracy band. Results and their interpretation have been presented in Sections 2.3 and 2.4. The Tracker performance on simulated turbulence spectra at a carrier frequency of 200MHz have been found to be a useful adjunct to the extensive steady state and noise modulated FM measurements. In particular the interpretation of Tracker response via the statistical auto- and cross-correlation concept has been found to be useful and meaningful. This work has been a pioneering study in the simulation of turbulence spectra by electronic means. For the amplitude spectra selected, the Tracker has been shown to demodulate correctly and reliably. However, it has not been possible to perform exhaustively an analysis of all types of spectra, to indicate under what power spectral density conditions the Frequency Tracker will not demodulate correctly. Obviously only CW signals have been considered and any extension of the results to a

pulsed Doppler case has not been performed.

In conclusion, typical subsonic flow parameters of interest will be presented and the expected Tracker demodulation performance criteria evaluated.

SUBSONIC VELOCITY FLOW PARAMETERS

MEAN FLOW:	125 FT/SEC.
TURBULENT INTENSITY:	2.5%--12%
PEAK-TO-PEAK FLUCTUATIONS:	8.75 FT/SEC.--44 FT/SEC.
FREQUENCY OF TURBULENCE:	25 kHz

EQUIVALENT DOPPLER SHIFT PARAMETERS

CARRIER FREQUENCY:	10 MHz
FREQUENCY DEVIATION:	350 kHz--1.75 MHz
MODULATION FREQUENCY:	25 kHz

EXPECTED FREQUENCY TRACKER PERFORMANCE

1)	CARRIER FREQUENCY:	10 MHz
	INPUT S/N:	15 db
	MODULATION FREQUENCY:	50 kHz
	MEAN FLOW OR DC ACCURACY:	≤ 3%

or

2)	CARRIER FREQUENCY:	10 MHz
	INPUT S/N:	20 db
	MODULATION FREQUENCY:	50 kHz
	MEAN FLOW OR DC ACCURACY:	1%

FOR MODULATION FREQUENCY: 25 kHz
AC NOISE THRESHOLD, WITH FILTER 26 kHz

IN FLUID DYNAMIC TERMS ONE THEREFORE MEASURES:

	MEAN FLOW VELOCITY:	125 ± 3.75 ft/sec at S/N:15 db
	TURBULENT INTENSITY:	12%
	PEAK-TO-PEAK FLUCTUATION:	44 ± 0.3 ft/sec
or	MEAN FLOW VELOCITY:	125 ± 3.75 ft/sec at S/N:15 db
	TURBULENT INTENSITY:	2.5%
	PEAK-TO-PEAK FLUCTUATION:	8.75 ± 0.3 ft/sec

For typical subsonic flow parameters, the Frequency Tracker will therefore demodulate an equivalent Doppler shift at a mean velocity of 125 ft/sec (10-MHz carrier frequency) with a ±3% accuracy at 3.75 ft/second when the signal-to-noise ratio at the Tracker terminals is 15 dB, defined in a 1-MHz bandwidth. Equivalently, the instantaneous Doppler shift over a modulation frequency of 25 kHz with a 5-dB signal-to-noise ratio defined over a 10-MHz tracking range will be demodulated by the Frequency Tracker with an accuracy of 44 ± 0.3 ft/second or 8.75 ± 0.3 ft/second for 12% and 2.5% turbulent intensities, respectively. This predicted performance of the LDV-Frequency Tracker is outstanding and surpasses in its accuracy similar measurements that can be made with the conventional hot-wire probe techniques.

Supersonic measurements at Mach 6 (about 200-MHz equivalent Doppler shift) can be performed over a 50-kHz modulation frequency at signal-to-noise ratios of -8 dB, defined over the full tracking range, for turbulent intensities of the order of 10% at an accuracy of ±3%. Thus, the application of the Wide-Band Frequency Tracker to process the Doppler shifted signals obtained from Laser Doppler Velocimetry measurements can be performed at very high accuracies, reliably.

2.8 REFERENCES

(1) Chaffee, J.G.: "The Application of Negative Feedback to Frequency Modulation Systems", Bell Sys. Tech. J., 403-437, July 1939.

(2) Enloe, L.H.: "Decreasing the Threshold in FM by Frequency Feedback", Proc. IRE, January 1962, pgs. 18-30.

(3) Wojnar, A.: "An Analysis and Synthesis Procedure for Feedback FM Systems", MIT Technical Report 415, September 1963.

(4) Baghdady, E.J.: "The Theory of FM Demodulation with Frequency-Compressive Feedback", IRE Trans. Comm. Syst., September 1962.

(5) Hinze, J.O.: "Turbulence", McGraw-Hill Co., 1959.

(6) Huffaker, R.M.: "Laser Doppler Detection Systems for Gas Velocity Measurement", Applied Optics, Vol. 9, No. 5, May 1970.

(7) Lee, Y.W.: "Statistical Theory of Communication", John Wiley and Sons, 1960, N.Y.

(8) Ridgway, S.L.: "The Measurement of Power Spectra with the P. A. R. Correlation Function Computer and Fourier Analyzer", Princeton Applied Research Corporation, Princeton, N. J.

SECTION 3

ALL ANGLE LASER DOPPLER OPTICAL HOMODYNE RECEIVER

3.1 GENERAL SPECIFICATIONS

The All Angle Laser Doppler Optical Homodyne Receiver is a versatile one-dimensional receiver, with a variable scattering angle and variable position angle that effectively makes it a multi-dimensional instrument, useful for monitoring flows from the subsonic to the supersonic when used in conjunction with the Wide Band Frequency Tracker.

The general specifications of the All Angle Optical Homodyne Receiver are as follows:

1. The Optical Homodyne Receiver is designed to operate with any laser in the visible range, encompassing CW powers up to 10 watts. (The appropriate filter must be used.)

2. The scattering angle can be varied from 5° to 12° in 1° steps.

3. The instrument can be positioned about the laser local oscillator axis approximately 260° to allow alignment with any velocity vector and locked in position.

4. The unit has equal optical path lengths of both the local oscillator and the scatter beam, making it an equal path length interferometer.

5. A minimal number of lenses consistent with reliable optical mixing design concepts are used.

6. There is a minimal use of reflective optical surfaces; i.e., mirrors and beamsplitters, consistent with a variable scattering angle, all angle, and optical mixing design concepts.

7. An easy and direct line-up procedure is incorporated into the instrument design. Vertical, crossways and rotary adjustment is provided for easy and precise boresighting of the instrument with the laser beam. Boresighting is obtained when the beam falls on the cross-hair center.

8. Access for viewing the diffraction patterns of the optically mixed local oscillator and scatter beams is available. This feature allows optimum line-up of the two beams. An alignment microscope permits visual observation on a screen of local oscillator and scatter beam relative alignment.

9. The alignment microscope is on a rotatable right angle viewer to allow comfortable use at any instrument angle.

10. The alignment microscope may be swung out of the way to allow direct access to the beams for external measurements.

11. Provisions for eye safety while aligning the instrument have been incorporated into the instrument, in that a fail safe electric shutter interrupts the laser beam if and when its power density exceeds safe eye threshold levels.

12. There are six field stops on an index wheel to allow resolving different sizes of scatter volumes. The field stops are 12.5 μ, 25 μ, 50 μ, 100 μ, 200 μ and 400 μ in size.

13. Local oscillator and scatter beams are in configurations focused on the field stop by lens systems compensated for the variations in the air and glass path of the beams.

14. Easy access to the interior is provided to view the beam paths with the field stop being in full view.

15. Local oscillator beam plane of polarization can be matched to the plane of the scatter beam at any viewing angle for maximum S/N, by rotating a Glan - laser polarizing prism and polarizer as needed.

16. Continuous variable attenuation of the local oscillator is provided over a range of 1 to 10^5, by use of a Glan - laser prism.

17. Continuous variable attenuation is provided at each of the view ports for eye safety. The boresight screen has additional fixed attenuation.

18. A measuring rod is provided to allow easy and exact setting of the scatter volume distance.

19. The instrument is designed for ease of operation, mechanical stability, ruggedness and flexibility of controls.

3.2 DESCRIPTION OF OPTICAL INSTRUMENT

The All Angle Laser Doppler Receiver instrument is shown in Figure 3-1, and a schematic of the optical paths, appropriately labeled, is shown in Figure 3-2. The laser Doppler instrument is contained in a case that supports the lenses, mirrors, beam-splitters, polarizers, apertures, photomultiplier tube and viewing screens in their proper positions. The case is supported on two bearings that are concentric with the laser-local oscillator beam optical axis of the instrument. These bearings allow the instrument to be rotated approximately 120° counterclockwise and approximately 140° clockwise from the initial vertical position when viewed from the laser. This permits the instrument to be aligned with any chosen velocity vector over 260°, effectively permitting 1-, 2- or 3-dimensional measurements to be made. These multi-dimensional measurements can only be made independent of each other, one at a time. The angular position of the instrument can be read on a degree dial located on the front bearing. As the case is counterweighted, it is quite easy to rotate into the desired position. A positive friction lock on the front bearing holds the instrument in the set position. The two bearings are supported by hinge members (to allow alignment flexibility) on vertical

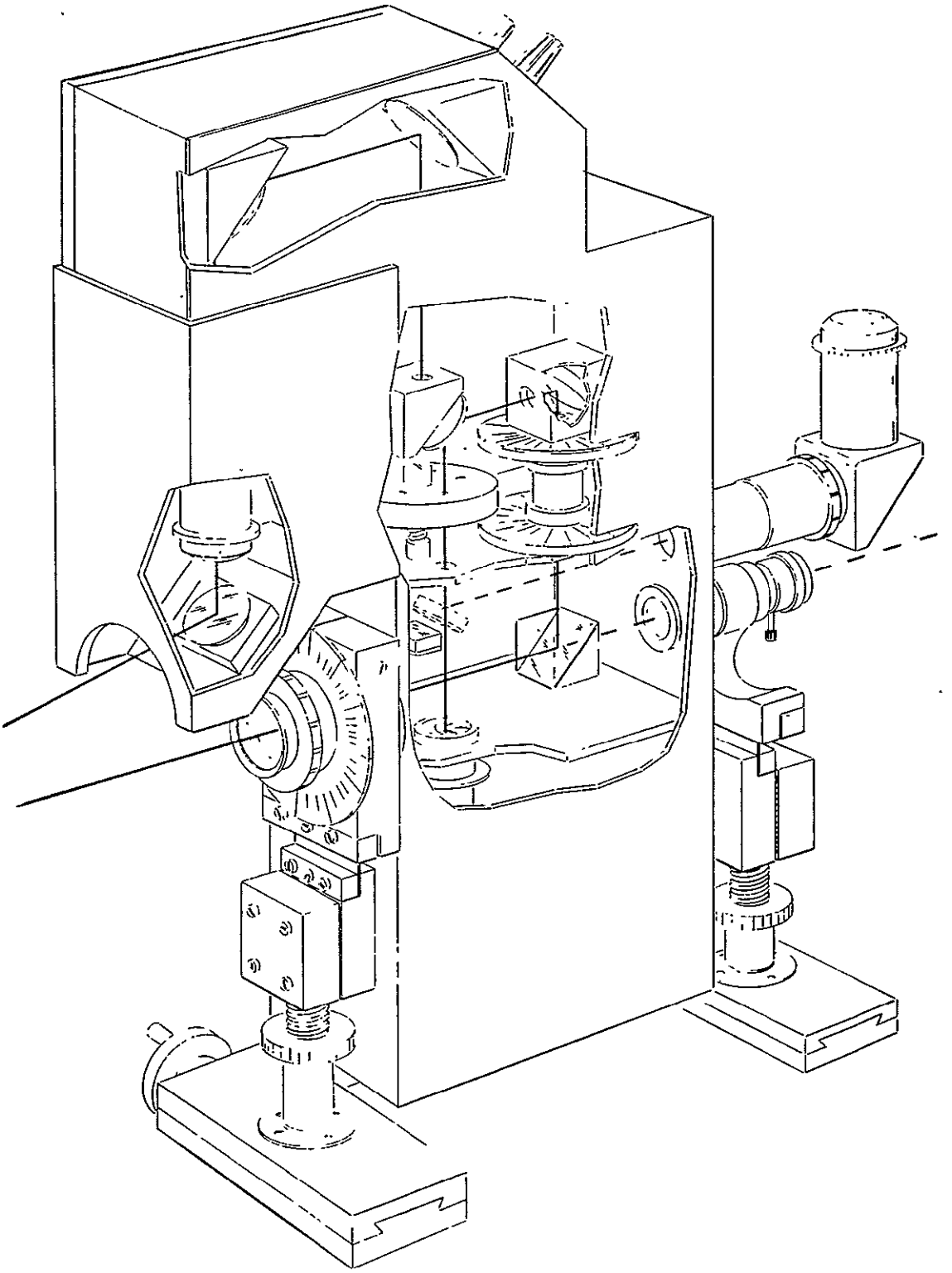

Figure 3-1 Variable Angle Optical Homodyne Receiver

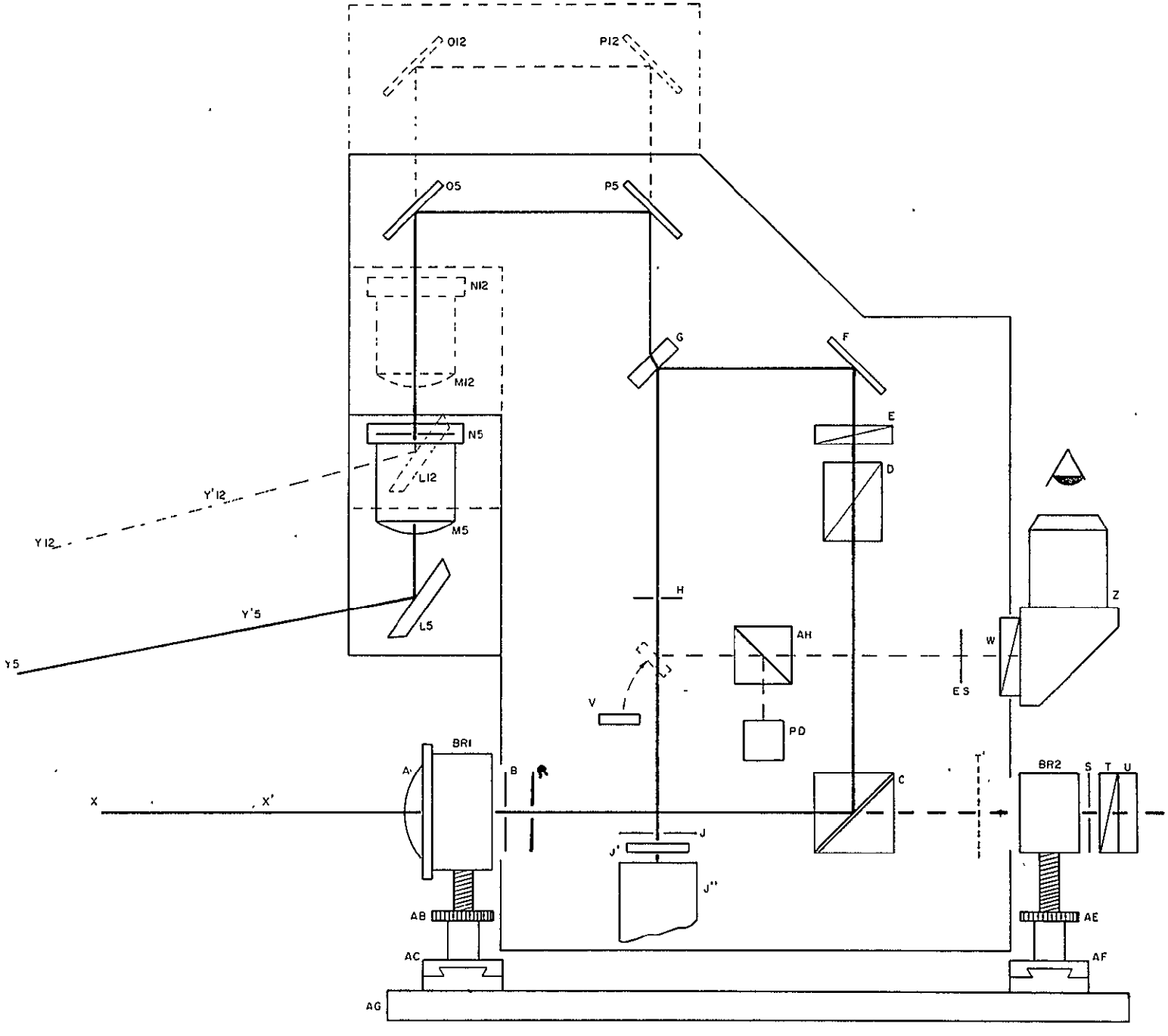

Figure 3-2 Schematic of the Optical Homodyne Receiver

adjustment screws which are, in turn, supported by machine tool slides that allow adjustment at right angles to the laser beam. This adjustment system allows the instrument to be precisely and easily aligned with the laser beam as the instrument can be translated and rotated as needed (within the adjustment range of the supports). The whole instrument rests on a plate that has holes to match the existing support of the 3-dimensional Laser Doppler Velocimeter presently installed at the NASA Marshall Space Flight Center, Huntsville, Alabama.

3.2.1 ALIGNMENT PROCEDURE

The instrument is attached to the 3-D, three-way support by bolting down plate AG. The instrument is approximately positioned in boresight alignment with the local oscillator beam by means of the support slides. The correct focal distance to the scatter volume is set by use of the appropriate support slide and the measuring rod. The instrument is then aligned with the laser beam $x-x^1$ by means of the vertical adjustments AB and AE and cross horizontal adjustments AC and AF while observing the two alignment check points R and U. The boresight alignment ring R is inserted in the case opening in back of iris B. This then gives a visual observation of the beam and the instrument can be adjusted so that the beam is concentric with the alignment rings. The laser beam is focused by lens A on the field stop H and slightly beyond the cross hair screen U. The intensity of this spot on screen U is controlled by a fixed attenuation filter T^1 that transmits 1% of the light and by rotating the polarizing plate T until comfortable viewing intensity is obtained. The spot can be positioned in the center of the cross hairs by means of the vertical and horizontal adjustment, thus achieving proper boresighting of the instrument. It will be found necessary to

When the Glan prism is rotated to attenuate the L. O. beam, it also rotates the plane of polarization of the beam. To maintain the beam in a fixed plane of polarization desirable for photomixing at G, the polarizing plate E is placed after the prism D. The plane of polarization of E determines the polarization plane of the L. O. beam. E is set in a rotating holder with a degree dial so that the exact plane of polarization of the L. O. can be set, thus matching its plane of polarization with the plane of the scatter beam to give optimum photomixing at G. The Glan prism dial also is marked in degrees. Both dials are set so that with the instrument set in the 0^{o} position (scatter lens directly above the L. O.) there is maximum transmission with dials set at 0^{o} for a horizontally polarized beam.

The scatter beam Y5 - $Y5^{1}$ is reflected by adjustable mirror L_5 through lens M_5 which focuses the beam on field stop H. Non-adjustable mirror O_5 and adjustable mirror P_5 direct the beam through the combining beamsplitter G, through the field stop H, iris J, 5145A filter J' and onto the photocathode of the photomultiplier tube J". Adjustable mirrors L_5 and P_5 allow moving the scatter beam so that it is in exact coincidence with the local oscillator beam from G to J". This is necessary for optical mixing and homodyning to take place efficiently. To assist in this adjustment of the mirrors, mirror V is swung across the beam to deflect it onto the viewscreen of the magnifier eyepiece Z. By observing the two beam spots on the viewscreen, one can quickly adjust the mirrors L and P to bring the scatter beam into coincidence with the local oscillator beam. The intensity on the viewscreen in Z can be controlled by rotating the polarizing plate W. Of course, the eye safety shutter, previously described, protects the eye at all times. The eyepiece can be swung out of the way to let the beams emerge from the instrument to allow external measurements as desired.

The five degree scatter path is represented by path Y_5 - Y'_5 - L_5 - M_5 - N_5 - O_5 - P_5 - G - H - J". The twelve degree scatter path is represented by path Y_{12} - Y'_{12} - L_{12} - M_{12} - N_{12} - O_{12} - P_{12} - G - H - J". L, M, and N are all mounted on one movable carriage. As the scatter angle is changed by moving the carriage on one-degree dowel pins, mirror L is tilted to always direct the beam along the required path. Approximately one turn of the mirror adjustment knob is required for each degree change. Lens M must be set to a separate position for each degree of adjustment. A scale located on the barrel of the lens mount allows setting the lens in its nominal position. Slight adjustment may be necessary to obtain exact focus. As lens A does not move to change angles, only a nominal mark is provided on the barrel. Both lenses have been positioned for 5145A light.

Mirrors O and P are also on a movable carriage that is dowel pinned in one-degree increments. The positions of the carriage dowel pins are so chosen that the distance M-H remains constant with the change of scatter angles. Mirror P requires no change with movement of the carriage except possibly slight peaking.

The positions of O and P have been chosen so that the air equivalent distance from the scatter volume through the path L - M - O - P - G - H is exactly the same as the air equivalent distance from the scatter volume through the path A - C - F - G - H. This path length is kept constant for all scatter angles of the instrument. This path equalization frees the instrument from any loss of signal/noise ratio resulting from a short coherence length laser.

The distance from the scatter volume to lens A and lens M in any position is equal to 809 mm. The equivalent air distance from lens A to H and lens M in any position to H is always 431.5 mm. Thus the instrument is always an equal path length interferometer.

The ratio of the image distance to the object distance of a lens system is its magnification factor. In this system it is 809/431.5 or 1.9. Therefore, the scatter volume is approximately twice the diameter of the field stop being used. The beam size in the instrument is controlled by iris B in the local oscillator beam and iris N in the scatter beam. The beam size must be adjusted to the proper size, corresponding to the field stop being used for optimum resolution of the scatter volume.

The photomultiplier tube J", a RCA Type 8645 photomultiplier, is beyond the field stop H, which is the focus point of the system. Thus, the joint L. O. and scatter signal impinging on it will be defocused. The P. M. tube is therefore spared from high intensity spot overloading and small spot variations in the sensitivity of the photocathode are eliminated. The load resistor of the P. M. tube is 50 ohms, which gives approximately a 250-MHz wide frequency response of the system. The load resistor can be changed if a different value is desired.

3.2.1.1 Alignment of Field Stop

The field stops (pinholes) are cemented into field stop holders which have been precisely aligned and fastened to the index wheel with screws. No further adjustment should be required.

The following procedure is used in setting the field stops: The index wheel is first adjusted and pinned in place such that the L. O. beam goes through the center of the clearance hole. The field stop holders are then roughly positioned in their respective index position and lightly fastened in place. The field stop adjusting tool is then screwed to the index wheel at the position being adjusted and the clamp tightened on the field stop holders. Then, by means of the two adjusting screws, the field stop is moved in x and y directions until it is in precise alignment

with the L. O. beam. This position is when the Airy disc pattern is the most complete. The two mounting screws are then tightened to hold the field stop holder in place. The adjusting tool is then removed, the index wheel rotated one notch, and the adjusting procedure repeated until all six field stops are in precise alignment. A photograph of the field stop adjusting tool in position is shown in Figure 3-3.

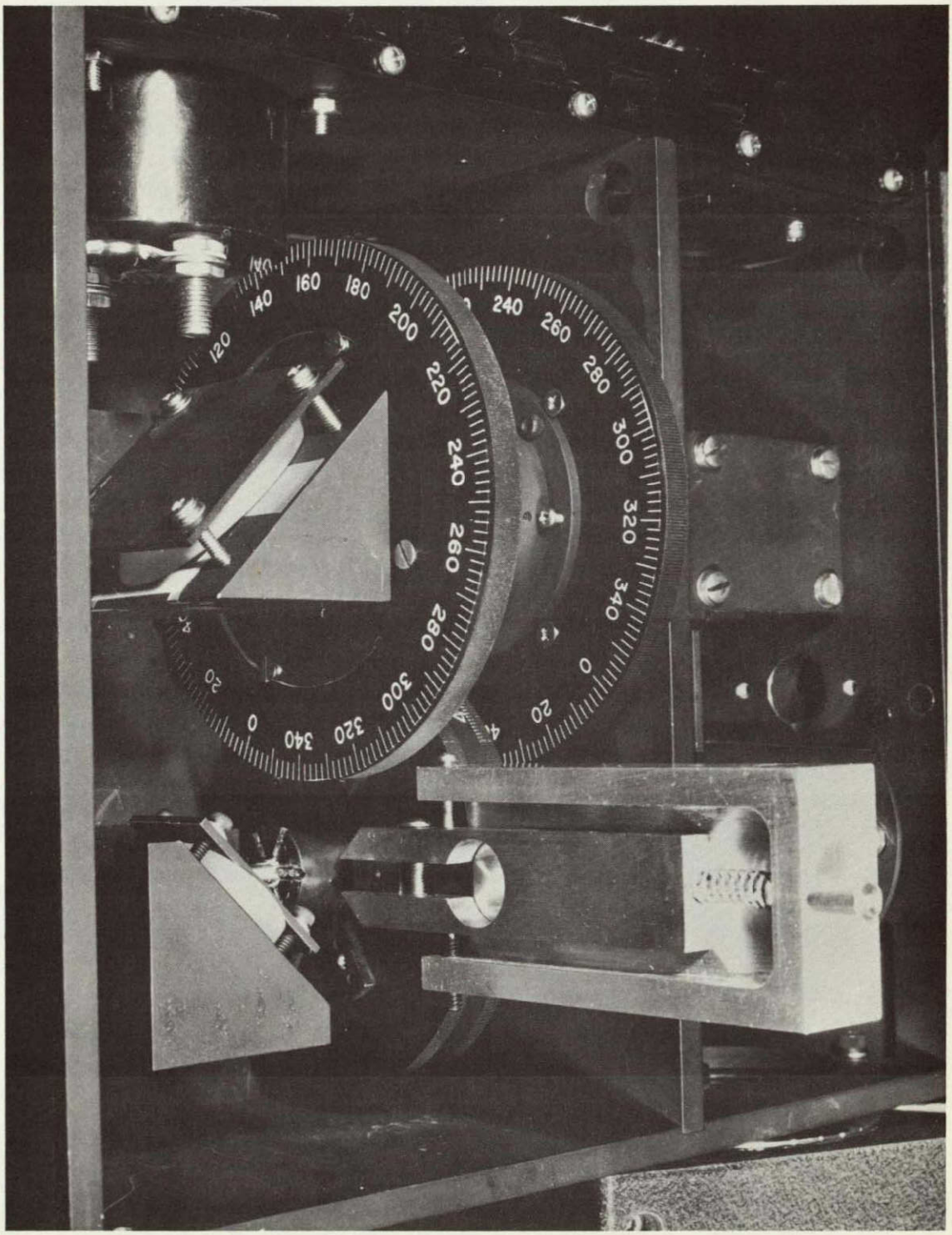

Figure 3-3 Adjustment of Field Stop with Special Tool

3.2.2 EQUAL PATH LENGTH COMPUTATION

The All Angle Velocimeter has an equal air path length between the resolution volume and the field stop H, for both scatter and L. O. beam paths. However, appropriate compensations in the actual path lengths of the respective beams must be made in order to take into account a) the effect of focal shortenings for the laser beam propagating through the relatively thick optical glass components and b) the equivalent air path length of the laser beam propagating through these components, identified by their respective index of refraction.

With reference to Figure 3-2, the following optical glass components are identified in the L. O. beam:

COMPONENT	n	OPTICAL PATH LENGTH mm	AIR PATH EQUIVALENT mm	AIR PATH INCREMENT mm
Cube Beamsplitter, C	1.5	30.0	45.0	+15.0
Glan Prism, D	1.49	22.5	33.5	+11.0
Polarization Plate, E	1.5	2.0	3.0	+ 1.0
TOTAL			81.5	+27.0

The scatter beam propagates through the combining beamsplitter, G, with an index of refraction of 1.46 and a thickness 6.35 mm. Thus, the optical path length through G, which is placed at an angle of 45°, is given by:

$$\text{Optical Path Length: } \frac{6.35}{\cos\left[\sin^{-1}\left(\frac{\sin 45}{1.46}\right)\right]} = \frac{6.35}{\cos 29^{\circ}\ 1^{1}} = 7.25 \text{ mm}$$

The equivalent air path in the scatter beam is therefore longer by:

COMPONENT	n	OPTICAL PATH LENGTH mm	AIR PATH EQUIVALENT mm	AIR PATH INCREMENT mm
Combining Beam-splitter, G	1.46	7.25	10.6	+3.3

Therefore the scatter beam path length must be lengthened by 27.0 - 3.3 = 23.7 mm in order to match the equivalent air path length in the L. O. beam. The initial uncompensated mechanical length between lens A and field stop H, and lens M5 and field stop H in the All Angle LDV is 404.5 mm. Compensation of the paths, as described above, results in a scatter path that is now 428.2 mm. The air equivalent is 404.5 + 27.0 = 431.5 mm for the L. O. path and 428.2 + 3.3 = 431.5 mm for the scatter path.

The amount of defocusing d introduced by an optical slab of thickness t and index of refraction n is given by:

$$(-)\ d = \frac{(n - 1)\ t}{n} \qquad (46)$$

Since the L. O. and scatter beams are focused onto H, the field stop, and propagate through the optical components, this effect must be taken into account. Thus in the L. O. and scatter paths one calculates:

PATH	COMPONENT	RETRACTION IN FOCUS, mm
L. O.	Cube Beamsplitter, C	10.0
	Glan Prism, D	7.4 Total: 18.1
	Polarization Plate, E	0.7
Scatter	Combining Beamsplitter, G	2.3

The front focal distance between lenses A and M5 and the resolution volume is 809 mm. Therefore, using the net air path equivalent L. O. and scatter beam back focal lengths result in the following lens parameters:

PATH	LENS	AIR PATH EQUIVALENT BACK FOCAL LENGTH	FOCAL LENGTH, mm
L. O.	A	404.5 - 18.1 = 386.4	261.5
Scatter	M5	428.2 - 2.3 = 425.9	279.0

Thus, to preserve an equivalent equal air path length configuration in the LDV, the focal length of the L. O. and scatter lenses are 261.5 mm and 279.0 mm, respectively. Their effective net diameters are 31 mm.

3.2.3 LOSSES SUFFERED BY L. O. AND SCATTERED BEAMS DUE TO POLARIZATION EFFECTS ON REFLECTION AND REFRACTION

Reflectivity and transmissivity of an incident light beam on a surface depend on the polarization of the incident wave. They may best be expressed in terms of the reflectivity and transmissivity associated with polarizations in the parallel and perpendicular directions, respectively. While metallic surfaces are the best reflectors, dielectric surfaces exhibit attenuation characteristics as a function of the angle of incidence. These considerations are very important for the All Angle LDV because the polarized scatter and L. O. beams interact with metallic surface mirrors and dielectric beamsplitters. Thus, the reflectivities and transmissivities that the beams exhibit as they propagate through the optical paths of Figure 3-2 relate to the net power available for photomixing of the scattered and L. O. beams. The instrument rotates about the L. O. beam. The orientations that it can assume modify the polarization of the L. O. beam as it becomes incident on the metallic and dielectric surfaces. Since efficient photomixing requires alignment between the L. O. and scatter beam polarization directions, it is necessary to assess the attenuation introduced in the polarizations in the parallel and perpendicular directions, respectively.

The intensity of reflected or transmitted light on a dielectric surface as a function of the angle of incidence is given by the following[1] Fresnel formulae. Figure 3-4 identifies the directions of polarization.

$$\tau_{\parallel} = \frac{\sin 2\theta_i \sin 2\theta_t}{\sin^2(\theta_i + \theta_t)\cos^2(\theta_i - \theta_t)} \tag{47}$$

$$\tau_{\perp} = \frac{\sin 2\theta_i \sin 2\theta_t}{\sin^2(\theta_i + \theta_t)} \tag{48}$$

$$R_{\parallel} = \frac{\mathrm{Tan}^2(\theta_i - \theta_t)}{\mathrm{Tan}^2(\theta_i + \theta_t)} \tag{49}$$

$$R_{\perp} = \frac{\sin^2(\theta_i - \theta_t)}{\sin^2(\theta_i + \theta_t)} \tag{50}$$

where: $\tau_{\parallel}$ = transmissivity parallel to plane of incidence

$\tau_{\perp}$ = transmissivity perpendicular to plane of incidence

$R_{\parallel}$ = reflectivity parallel to plane of incidence

$R_{\perp}$ = reflectivity perpendicular to plane of incidence

θ_i = angle of incidence

θ_t = angle of refraction

The above formulae relating to the transmissivity and reflectivity through a dielectric medium remain valid for metallic surfaces. Hence, we can now budget out the losses at transmission and

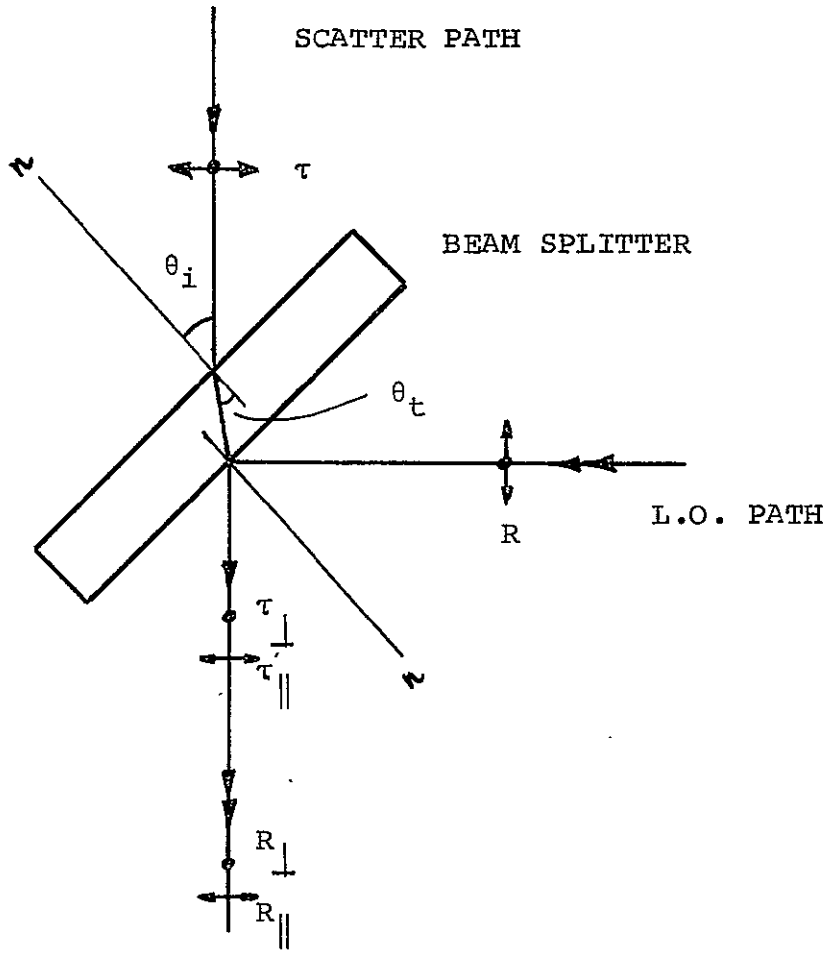

Figure 3-4. Interaction of L. O. and Scatter Beam on Dielectric Photomixing Beam Splitter

reflection suffered by the respective L. O. and scatter beams as follows:

PATH	COMPONENT	TYPE	$T_{\parallel}$	$T_{\perp}$	$R_{\parallel}$	$R_{\perp}$
L. O.	Beamsplitter, C	Metallic	----	----	0.45	0.45
	Mirror, F	Metallic	----	----	0.89	0.93
	Combining Beam-splitter, G	Dielectric	----	----	0.0089	0.0932
Scatter	Mirror, L5	Metallic	----	----	0.88	0.94
	Mirror, O5	Metallic	----	----	0.89	0.93
	Mirror, P5	Metallic	----	----	0.89	0.93
	Combining Beam-splitter, G	Dielectric	0.96	0.83	------	------

∴ Loss suffered by L. O. beam:

Parallel Component: 0.00356 ≈ 104 dB

Perpendicular Component: 0.039 ≈ 14 dB

Loss suffered by scatter beam:

Parallel Component: 0.67 ≈ 1.7 dB

Perpendicular Component: 0.675 ≈ 1.7 dB

With the All Angle LDV in its vertical position, when the polarization of the incoming laser L. O. beam is parallel to the direction of propagation, an attenuation of 104 dB matches up the respective power levels between the scatter and L. O. beams for photomixing. However at other positions of the instrument, it becomes important to use the Glan - laser prism polarizer combination to provide the proper level of L. O. signal for photomixing. The scatter beam, already several orders of magnitude below the L. O. beam, does not suffer any appreciable losses, irrespective

of instrument position as a result of reflecting from the metallic mirrors or propagating through the dielectric photomixing beam-splitter.

3.2.4 LASER EYE SAFETY CONSIDERATIONS

A fail-safe laser eye safety electro-optical feature has been designed and built into the All Angle Laser Doppler Velocimeter in order to insure that any precise alignment between the L. O. and scatter beams, as described in Section 3.2.1, be performed at laser power levels that will not create an eye-hazard problem. In particular, it is important to assess the power level into the eye due to the L. O. beam, when it is focused out the field stop H. Since the Glan prism is in the L.O. path of the LDV, it is important to perform the L. O. beam alignment at maximum Glan prism attenuation. This attenuation is of the order of 10^5.

Let us now perform a worst-case computation to assess the total power reaching the eye, under conditions of minimum attenuation through the optical components. The transmittances of the optical elements, under these conditions, are shown in Figure 3-5 which is a schematic of the L. O. path during alignment, when movable mirror V is turned on to deflect the laser beam into the aligning microscope. Beamsplitter AH apportions 45% of the total energy reaching it onto the laser eye-safety level photodetector P. D., which in turn initiates the mechanical flag FL through the circuit shown in Figure 3-7.

Transmission through beamsplitter AH and at eye-safety level photodetector P. D. is given by:

T_{AH}: $0.45 \times 0.90 \times 0.50 \times 0.93 \times 0.093 \times 0.93 \times 0.45 = 0.735\%$

Transmission through polarizer W, ahead of the diffuser in the microscope, is given by:

$$T_{AP} = 0.735 \times 10^{-2} \times 0.50 = 0.367\%$$

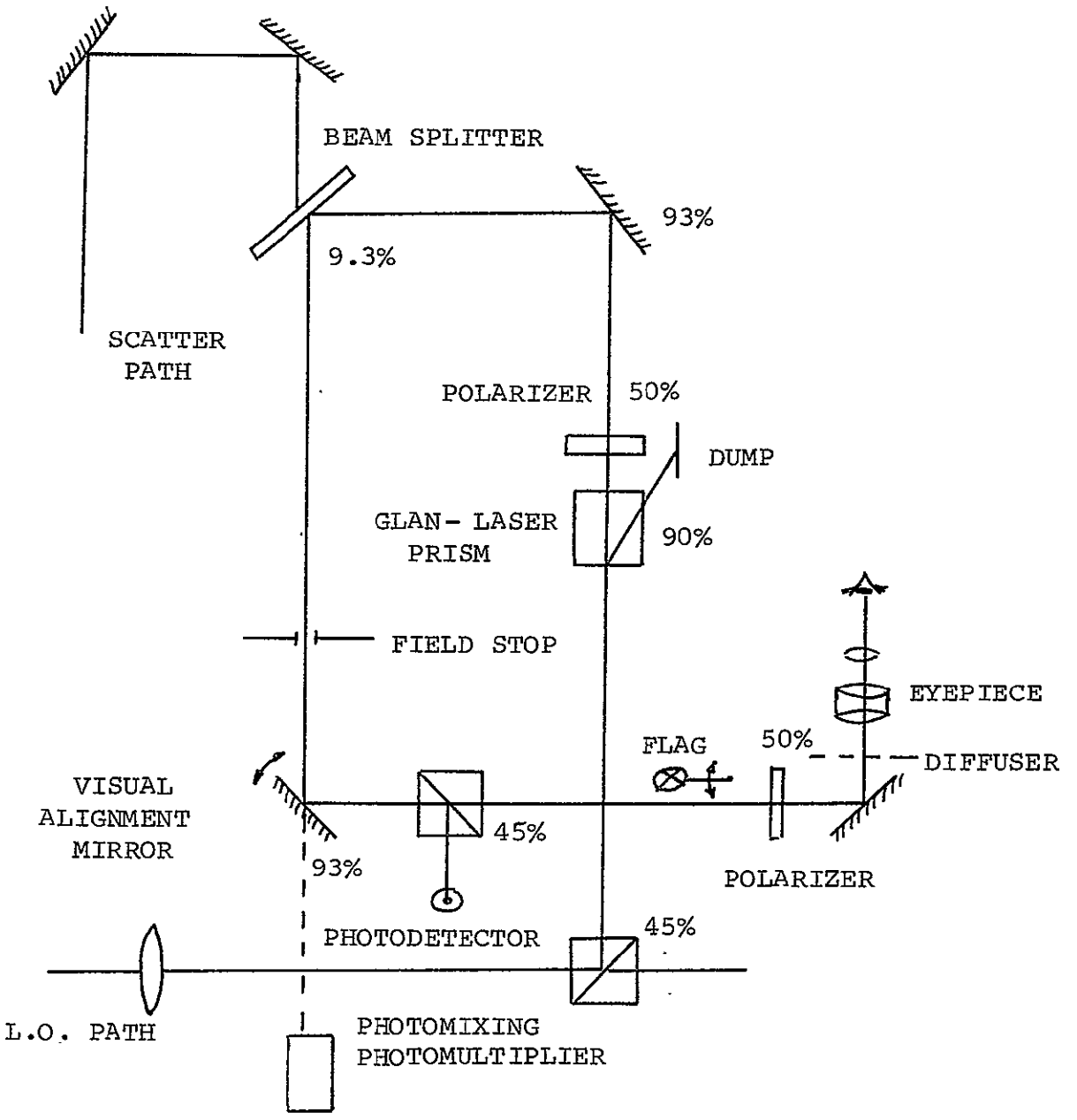

Figure 3-5. Visual Alignment Optical Path

A 10-watt, CW Argon laser beam will have an effective power of 73.5 milliwatts at the photodetector and 36.7 milliwatts at the diffuser. The diffuser has a diameter of 1.7 cm, and is placed 34.6 cm from H. The size of the beam at the diffuser as a result of its divergence is calculated at 2.24 cm, illuminating the total surface of the diffuser.

In order to calculate the power/unit area reaching the eye, we assume that the diffuser is Lambertian. Thus, as shown in Figure 3-6, the illuminance into the eye will be given by:

$$E = \frac{dF}{dS} = \frac{\pi}{K^2} \sin^2 \theta \; B \qquad (51)$$

where: E = illuminance, lumen/ft^2 or ft-candle
B = luminance, foot-candle/steradian onto diffuser
K = microscope magnification
θ = as shown, about 19°

To evaluate the luminous flux density into the eye, one must use appropriate conversion constants at the wavelength of interest between radiometric and photometric units. For the eye[2]

$$9.29 \times 10^{-2} \text{ foot-candles} \equiv (680.2\ \alpha)^{-1} \text{ watts/m}^2$$

where $\alpha(\lambda = 5113, \text{eye}) = 0.0255$ for the photopic and 0.2544 for the scotopic response of the eye. Thus, for the photopic response

$$1 \text{ foot-candle} = 0.62 \times 10^{-4} \text{ W/cm}^2$$

and for the scotopic color response

$$1 \text{ foot-candle} = 0.62 \times 10^{-5} \text{ W/cm}^2$$

Thus, energy density on diffuser is:

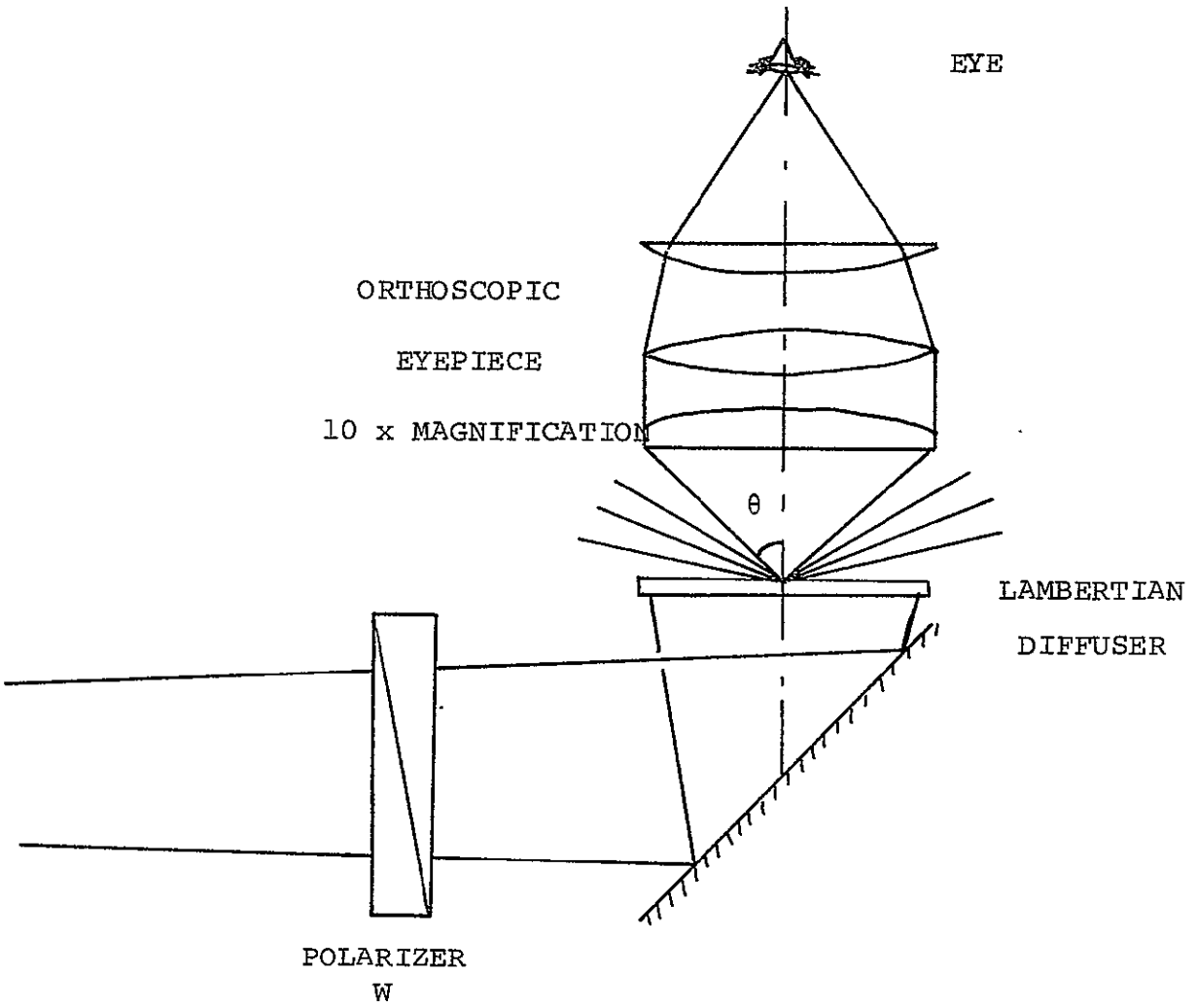

Figure 3-6. Microscope Alignment

$$\frac{36.7 \times 10^{-3}}{\frac{\pi}{4} \times (1.7)^2} = 15.9 \times 10^{-3} \text{ W/cm}^2 = 2560 \text{ foot-candles}$$

The diffuser subtends a total solid angle of:

$$\Omega = \frac{A}{r^2} = \frac{\pi \times (0.85)^2}{34.6 \times 34.6} = 1.9 \times 10^{-3} \text{ steradians}$$

∴ The luminance B, at the diffuser, is:

$$B: \frac{2560}{1.9 \times 10^{-3}} = 1.35 \times 10^6 \frac{\text{foot-candles}}{\text{steradians}}$$

Hence, the illuminance E at the diffuser is:

$$E = \frac{dF}{dS} = \pi \sin^2 \theta \, B = \pi \times (0.326)^2 \times 1.35 \times 10^6 = 4.52 \times 10^5 \text{ ft-candles}$$

The illuminance at the eye results in

$$E = \frac{\pi}{K^2} \sin^2 \theta \, B = 4.52 \times 10^5 \times 10^{-2} = 4.52 \times 10^3 \text{ ft-candles}$$

∴ In radiometric units, at the eye, the energy density is:

$$E = 2.8 \times 10^{-2} \text{ watts/cm}^2$$

when a 10-watt, CW Argon laser beam is propagated across the L. O. beam path.

At the photodetector, with a typical 5.7-mm diameter surface, the corresponding energy density is:

$$\frac{73.5 \times 10^{-3}}{\pi \times (2.8)^2 \times 10^{-2}} = 0.3 \text{ watts/cm}^2$$

Thus between the detector and the eye, the following power density relationship holds:

$$P_{eye} \approx 10^{-1} P_{Detector} \text{ watts/cm}^2$$

A safe laser level on the eye, which is very conservative in its estimate, is of the order of 1 $\mu W/cm^2$. Obviously, the energy density of the order of 10^{-1} watts/cm^2 computed above is five orders of magnitude above the desirable safe level. Thus, at no time should the All Angle Velocimeter, when used in conjunction with a 10-watt, CW Argon laser, be visually aligned with the microscope, unless the full attenuation available in the Glan prism-polarizer combination, D and E, is used to attenuate the primary L. O. beam through the device. This is precisely the role that the eye-safety circuit triggered by the photodetector fulfills.

The solenoid drive circuit is shown in Figure 3-7. When the mirror V is positioned to deflect the L. O. and scatter beams into the microscope, a microswitch, as shown, connects a 16.8-V battery across the circuit. With power applied to the circuit the variable resistor (50 kΩ Pot) controls the base current into the transistor.

The solenoid trigger level has been measured to be 20 mA, and the release level is 5 mA. Under the given illumination conditions, the photocell resistance is approximately 1 kΩ, which increases to over 5 kΩ with no illumination. If the photocell illumination is at a "safe" level, the cell drains less than 0.1 mA corresponding to a resistance of > 5 kΩ, and the transistor is on, which means that the solenoid is energized and the shutter is open. As soon as the light level increases, the cell resistance drops and drains more current, thereby reducing the base current and turning the transistor off. <u>With the solenoid de-energized, the shutter is closed</u>.

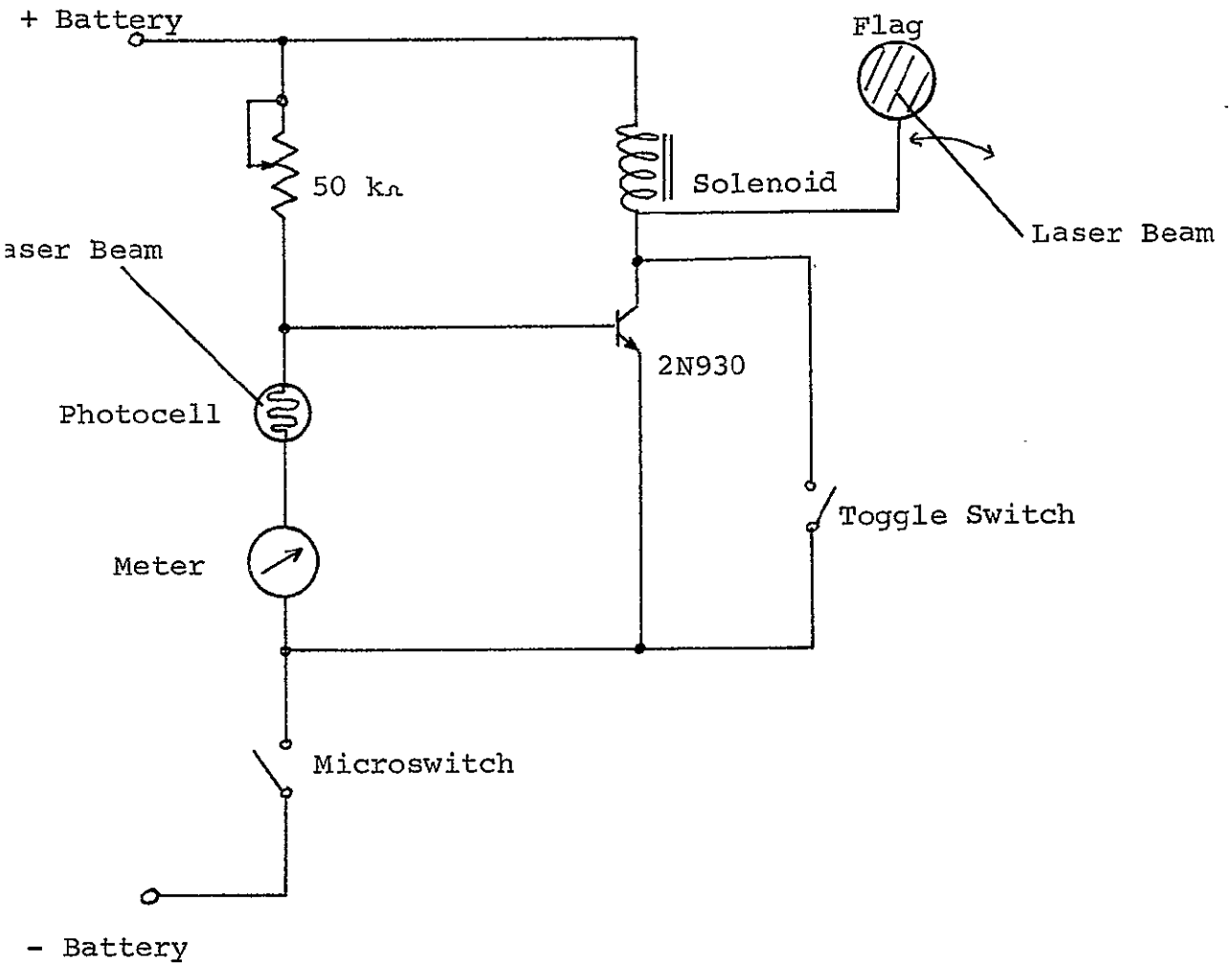

Figure 3-7. Eye Safety Circuit

The solenoid can also be energized through a toggle switch, which bypasses the light sensitive circuit. A milliampere meter is connected in series with the photocell to provide an indication of the light level independent of the solenoid.

The shutter closes if the photocell current exceeds 0.5 mA, an reopens if the current drops below 0.15 mA.

The following table gives typical circuit parameters.

LIGHT LEVEL	LOW	HIGH
Photocell Resistor	> 5.0 kΩ	1.0 kΩ
Base-Emitter Voltage	0.5 V	0.75 V
Photocell Current	< 0.1 mA	0.5 mA
Base Current	0.5 mA	< 0.1 mA
Collector Current	20.0 mA	< 4.0 mA
Solenoid	ON	OFF
Shutter	OPEN	CLOSED

The safety flag will not be activated to the "open" condition until the variable attenuator is adjusted to allow no more than the safe limit of energy density to fall on the eye. Thus, both the meter indicator and mechanical flag protects the untrained from using the alignment controls on the All Angle LDV unless the beams have been adequately attenuated by variable Glan- laser prism. The above calculation, as performed, is a worst-case analysis and, in addition, has a factor of safety larger than 10 due to the value of transmittances selected in the computations.

3.3 ALL ANGLE LASER DOPPLER OPTICAL RECEIVER

The All Angle Laser Doppler Optical Receiver as designed and fabricated is shown in its true, final form in Figure 3-8. The instrument is shown, on the photograph, in its vertical position, set on 0° on the front dial and at a 5° scattering angle. Figure 3-9 is a similar view of the Optical Receiver, set however, at the 12° scattering angle. Comparison with the design sketch shown in Figure 3-1 and reference to the description given in Section 3.2 will help identify all parts of the All Angle Laser Doppler Optical Receiver. On the front side of the instrument the handle protruding just below the "Raytheon" trademark is the iris adjustment of the scattered radiation receiving lens. Behind the dial, the protruding handle, is the iris adjustment on the LO lens. The instrument may be locked in position at the front, over a 260° range by rotating it on supporting journal bearings. The front bearing is split and an Allen screw at the upper right hand side of the front dial is used to permit free rotation and locking of the device. The front vertical adjustment is easily performed with the instrument locked in position, by moving the collar along the supporting threaded vertical shaft. A handle, as shown, is supplied for this purpose. Since the back of the receiver is not locked in position, a corresponding adjustment of the collar is performed by moving it up or down manually. The precision slides, as shown, move the receiver along a sideways traverse. The bottom plate of the instrument has been made to fit the present configuration of the 3-Dimensional Laser Doppler Velocimeter presently in use at NASA/MSFC. Hence back and forth motion is accomplished by means of the slide adjustments available on that set-up. The polarizer,

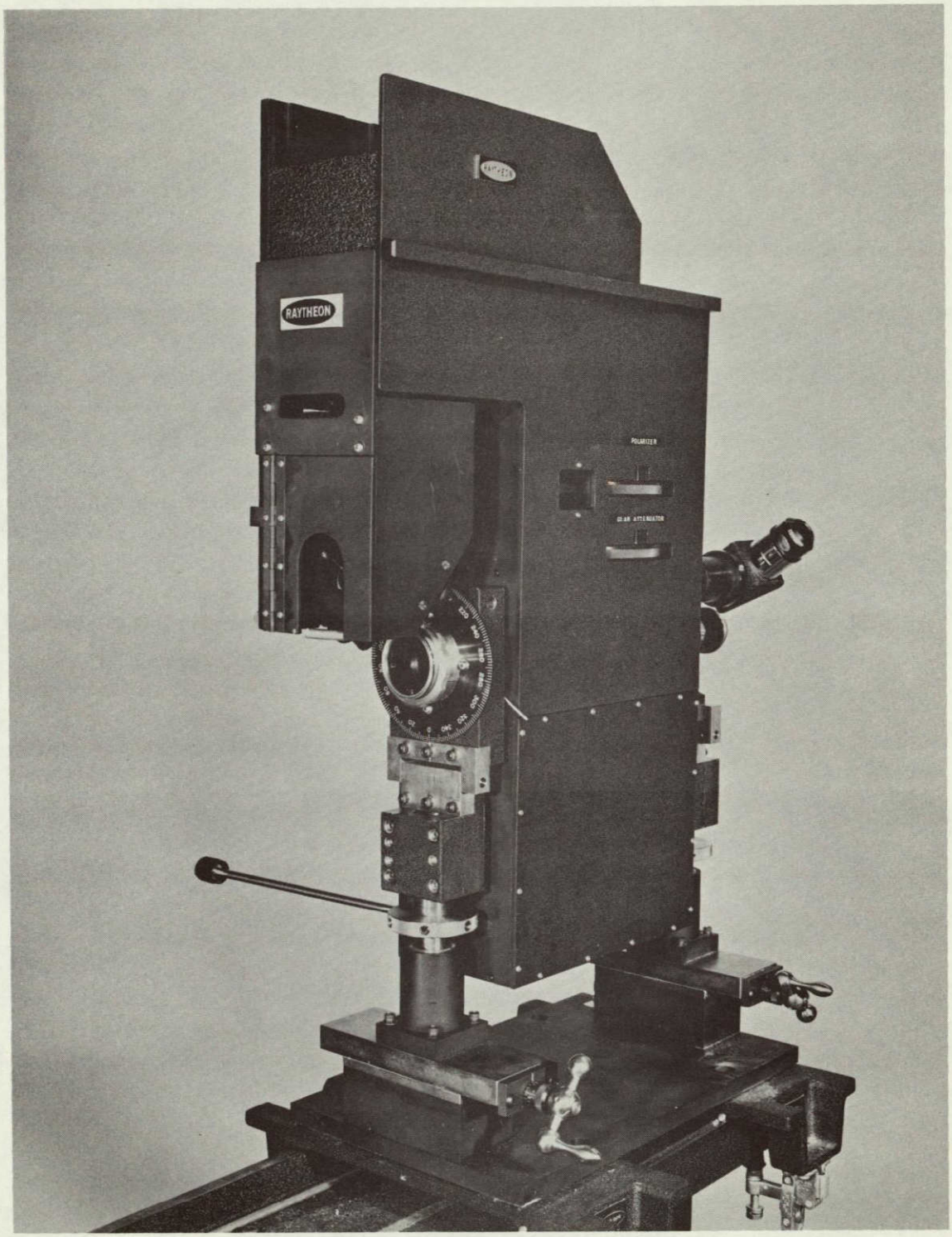

Figure 3-8 All Angle Laser Doppler Optical Receiver Set at 5^{o} Scattering Angle/Vertical

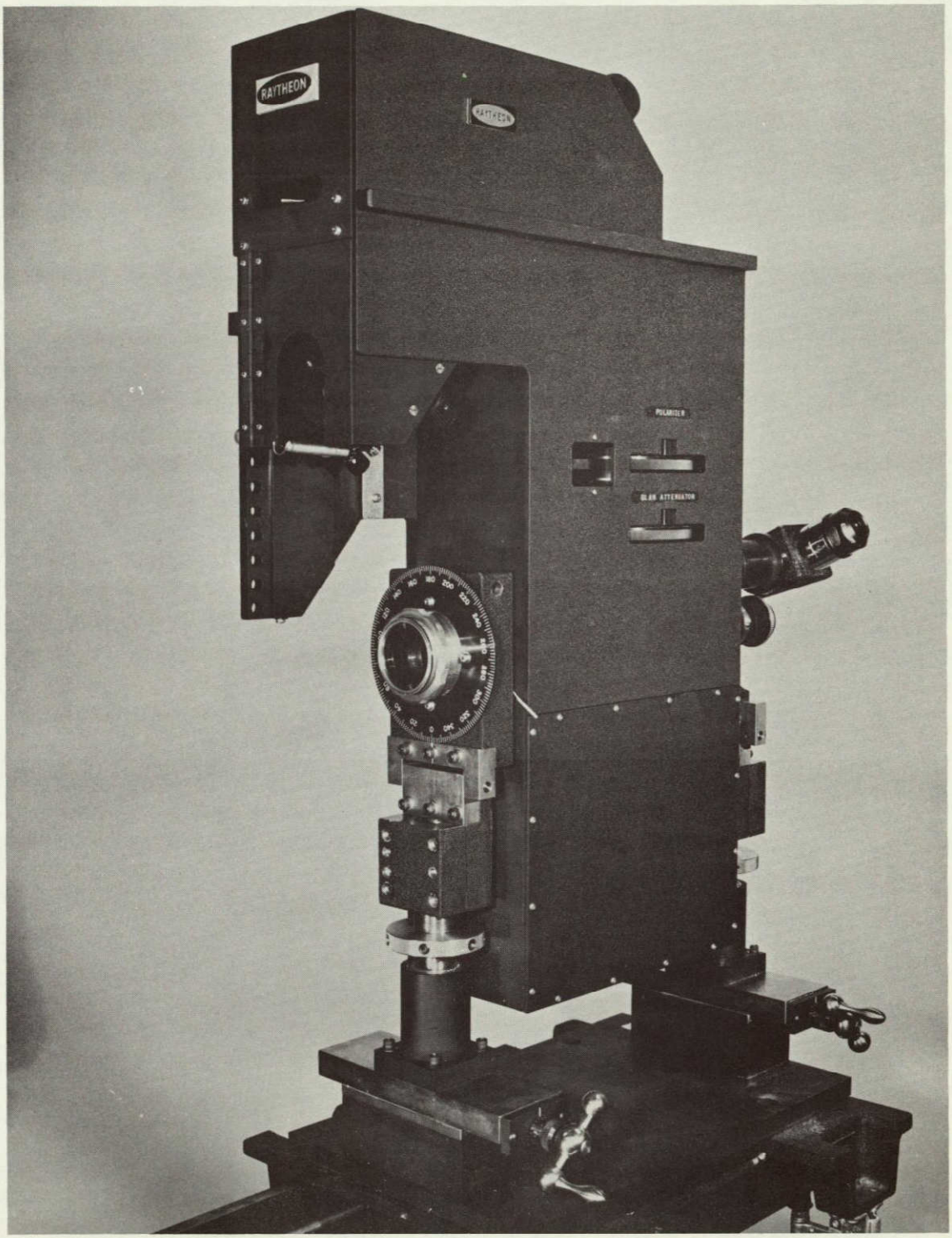

Figure 3-9 All Angle Laser Doppler Optical Receiver Set at 12° Scattering Angle/Vertical

Glan Laser prism attenuator and field stop window are all identified and can be seen on the right side of the picture, facing the instrument. The microscope that permits viewing the field stop for perfect alignment of the scatter and LO beams, as well as the boresight cross-hair alignment are seen protruding from the rear of the instrument.

Figure 3-10 is a photograph of the left side of the instrument. The receiver, as seen from the scattering angle adjustment pins, is at a 5^{o} scattering angle. Changing the scattering angle to any one of the desired positions over the 5^{o} to 12^{o} range is simply done. Three dowel pins are moved to the desired, marked holes, and the upper left bolt is loosened to slide in the slot. One degree changes are thus accomplished to an accuracy much better than 1 minute of arc, while preserving at all times, as described in Section 3.2, the equal path length feature of the device. For each change of scattering angle, a potentiometer adjustment, shown in Table XI of Section 3.3.1, must be reset to tilt the front mirror of the scattering lens to its proper vertical alignment position. The picture also shows the location of the variable field stop dial, and the switch for moving the viewing mirror V, Figure 3-2, in and out of the optical LO and scatter beams. The output signal BNC terminal, the photomultiplier high voltage input terminal and a bias meter switch which may be in or out of the photomultiplier signal circuit, Figure 3-17, are at the bottom left hand corner of the device.

Figure 3-11 is the back end view of the optical receiver. The upper knobs tilt mirror P5, Figure 3-2, up and down and sideways. They are marked "A" and "B" and correspond to similar

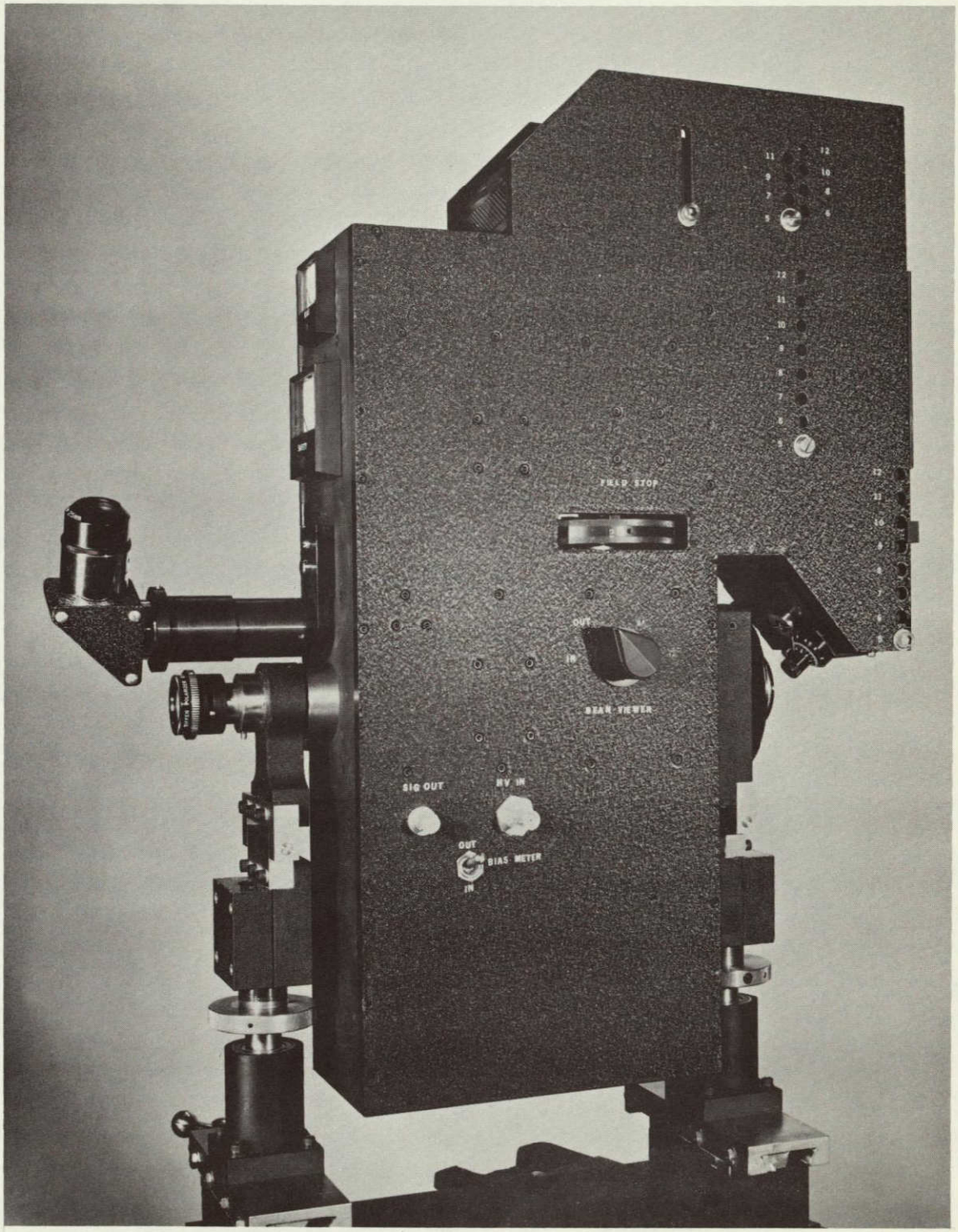

Figure 3-10 Left Side View of All Angle Laser Doppler Optical Receiver

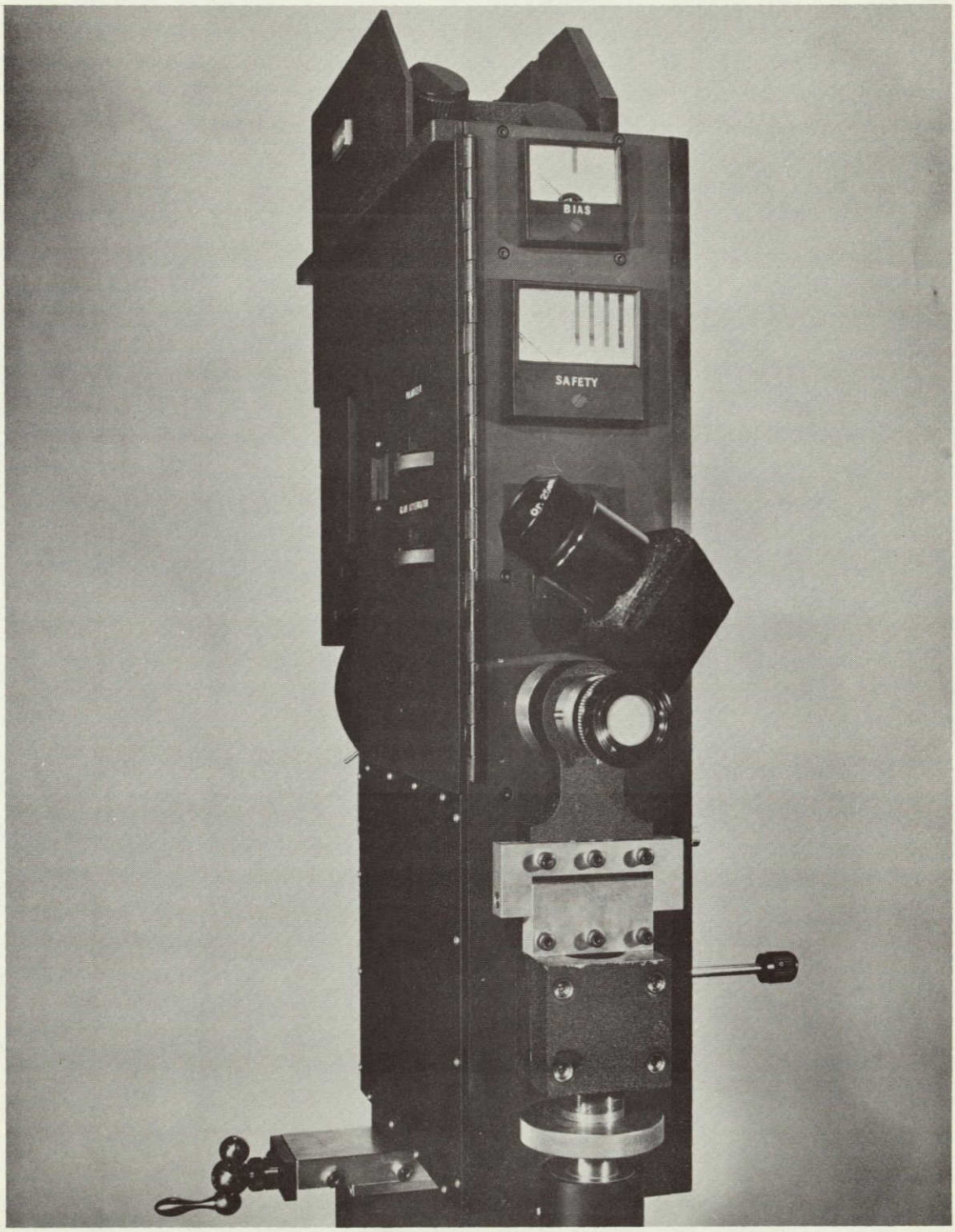

Figure 3-11 Back-end View of All Angle Laser Doppler Optical Receiver

markings on adjustments provided on scatter mirror L5. The "Bias" meter, which may be disconnected in the "Out" position of the bias meter switch on the left side of the instrument, measures the anode current in the photomultiplier circuit, Figure 3-17. The "Safety" meter, is a measure of the detector current, Figure 3-7, when the instrument alignment is performed with the field-stop viewing microscope. The markings on the safety meter indicate a limit for the safety detector current that must not be exceeded for the comfortable and safe viewing of the scatter and, in particular, the LO beam. When the pointer is in the right-half of the meter, the safety detector automatically blocks the microscope objective by activating the flag, as described in Section 3.2.4. The microscope mount and bore-sight alignment cross-hair optics, Figure 3-2, are also shown. Figures 3-12 and 3-13 show the instrument in the 7^{o} scattering angle/120^{o} rotation angle and 12^{o} scattering angle/220^{o} rotation angle position respectively. It is indeed very simple and straight forward to make such changes, accurately and within a matter of a few minutes, to accommodate any desired measurement position.

The front and side panels of the optical receiver can be swung open, as shown in Figure 3-14. This exposes the full optical homodyne optics and permits easy adjustment of critical components. Tracing of the LO or scatter beams is greatly facilitated if they have been inadvertently "lost" in the process of changing the scattering angle and rotational position of the instrument. The front open panel shows the location of the scatter mirror and scattering lens. Markers on the scattering lens indicate its respective position for each change of the scattering angle. Figure 3-15 is a close-up of the homodyne and eye-safety

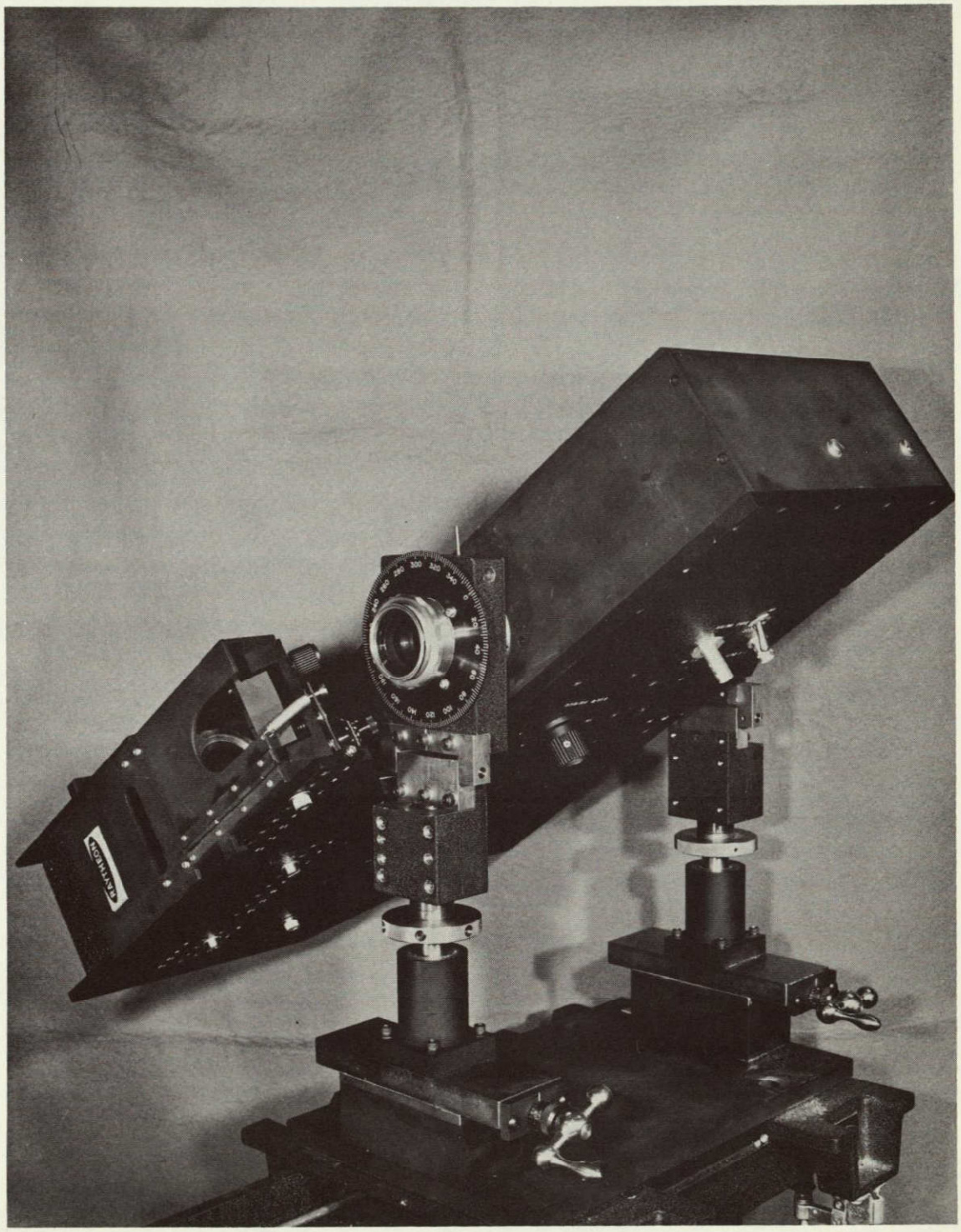

Figure 3-12 All Angle Laser Doppler Optical Receiver Set at 7° Scattering Angle/120° Rotational Position.

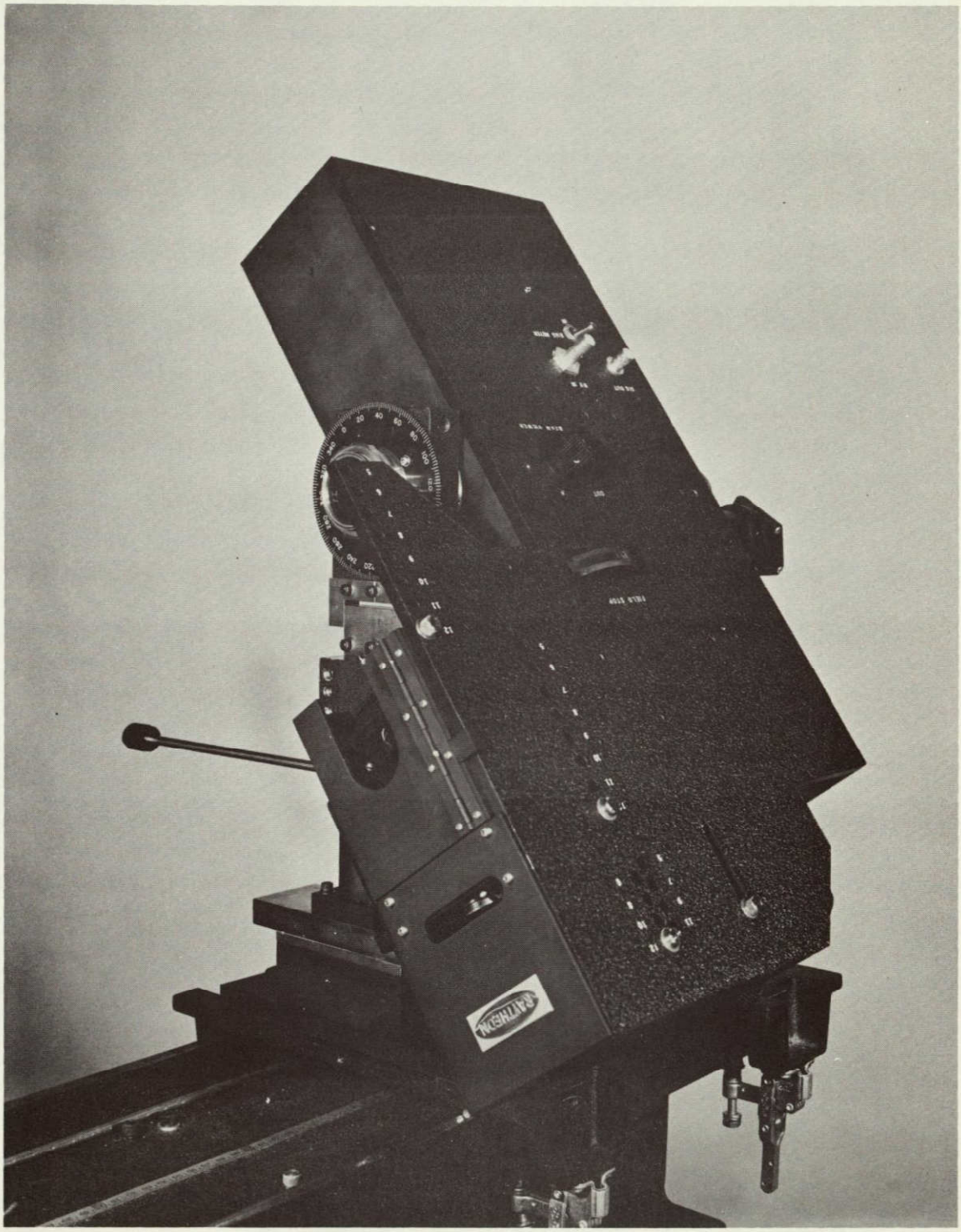

Figure 3-13 All Angle Laser Doppler Optical Receiver Set at 12° Scattering Angle/220° Rotational Position.

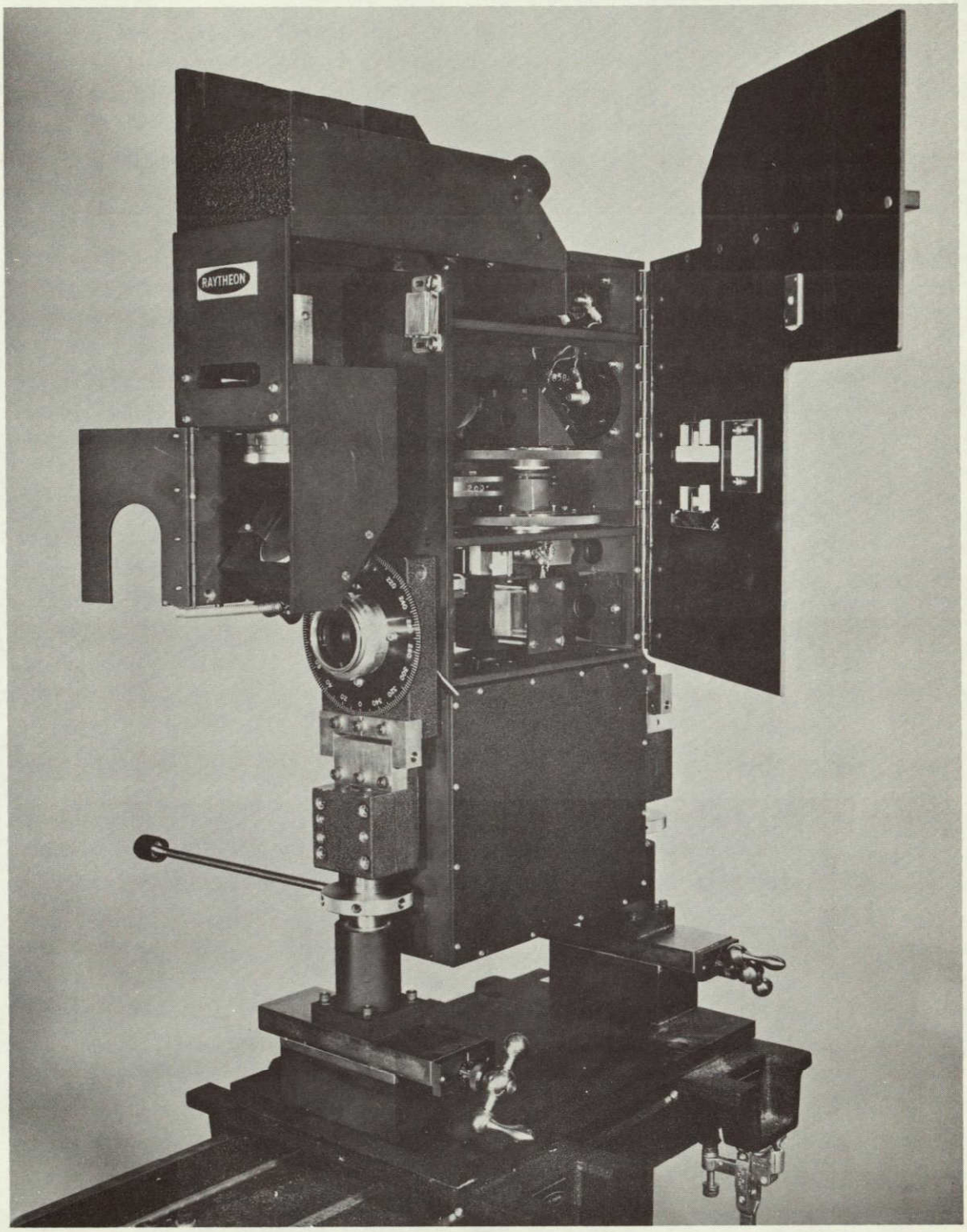

Figure 3-14 Open Front and Left Side Panels of All Angle Laser Doppler Optical Receiver

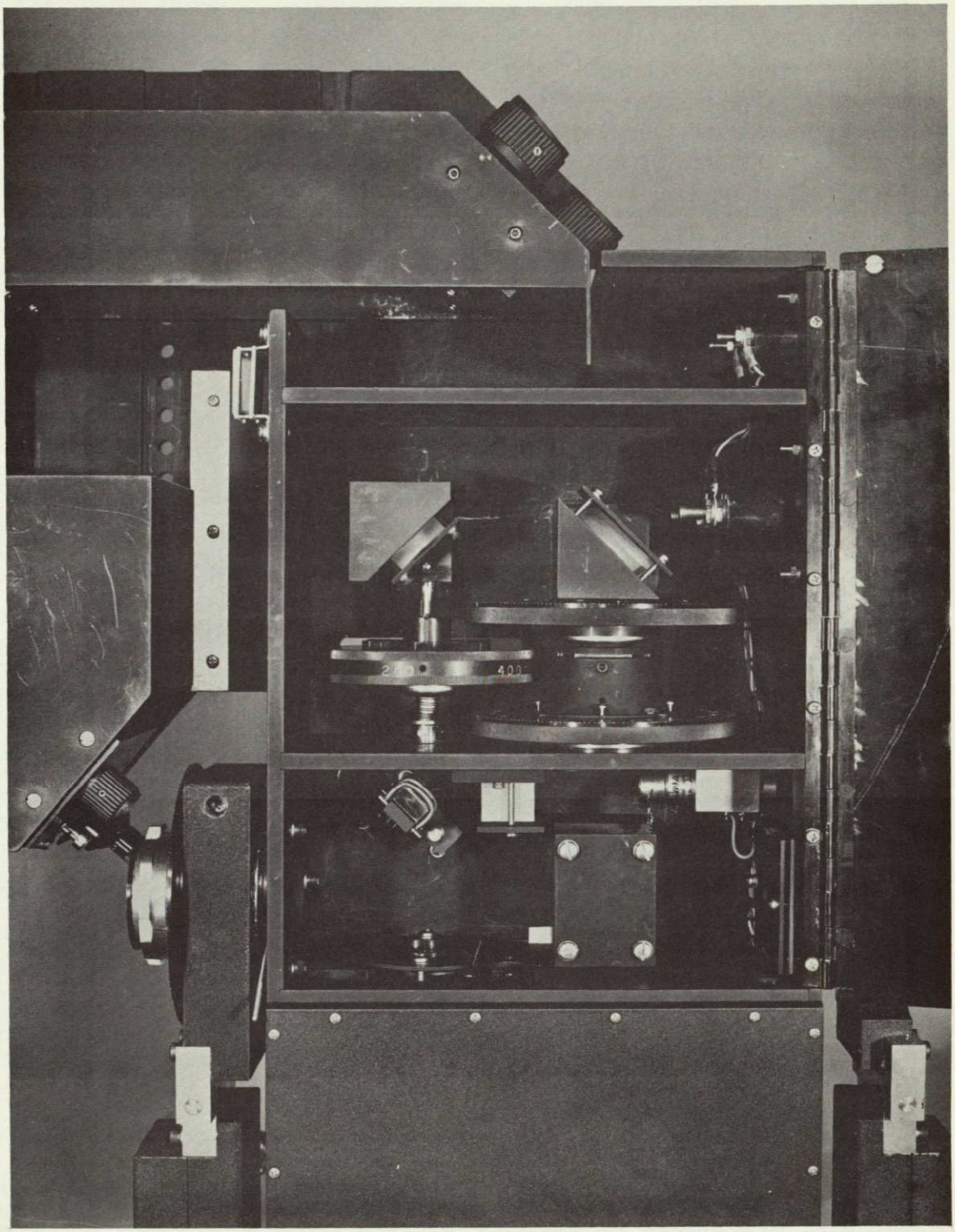

Figure 3-15 Local Oscillator, Homodyne and Alignment Optics

optics. Reference to Figure 3-2 will help in identifying all parts. The LO lens, backed by its iris, focuses the beam directly on the field stop. A cubic beam splitter, C, directs the beam onto the boresight optics horizontally on one side, and the Glan-Laser prism-Polarizer combination on its other vertical side. The Glan prism and Polarizer are installed on fully rotatable mounts. Mirror F, deflects the LO beam onto the photomixing beam splitter G. The scatter beam contribution, in turn is focused onto the field stop. The alignment mirror V is shown in its active position, diverting the LO and scatter beams onto the viewing microscope. The eye-safety level detection beam splitter and solenoid driven metallic flag indicator are shown to the right of the mirror. Figure 3-16 is the full view of the homodyne and safety optics as well as the photomultiplier and eye-safety control electronics. The alignment mirror V is now in the off position, permitting the LO and scatter beams directly to illuminate the RCA 8645 photomultiplier. An additional iris in front of the photomultiplier permits adjustment of the size of the photo cathode as desired. It is best to operate at the position of the iris corresponding to full photocathode illumination. The photomultiplier circuit is shown in Figure 3-17 and the eye-safety level control electronics is shown in Figure 3-7. At the bottom of the case lead blocks, bolted down into the frame, counterbalance the static torque of the instrument for ease of rotation over its full 260^{o} swing. Thus, the journal bearings are not subject to any loading that may distort the alignment of the device.

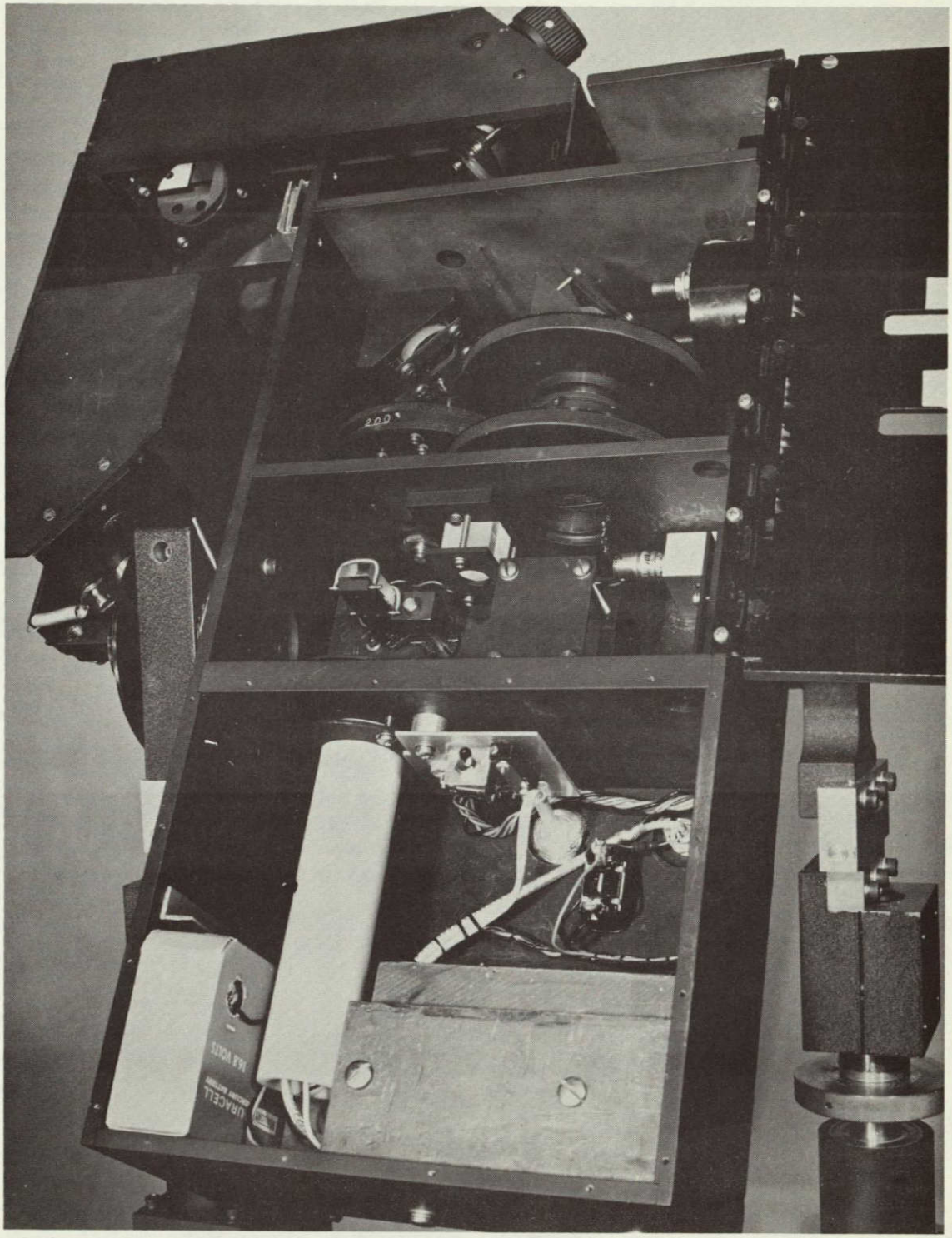

Figure 3-16 Full View of Scatter, LO, Alignment, Photomultiplier Optics and Eye-Safety Control Electronics.

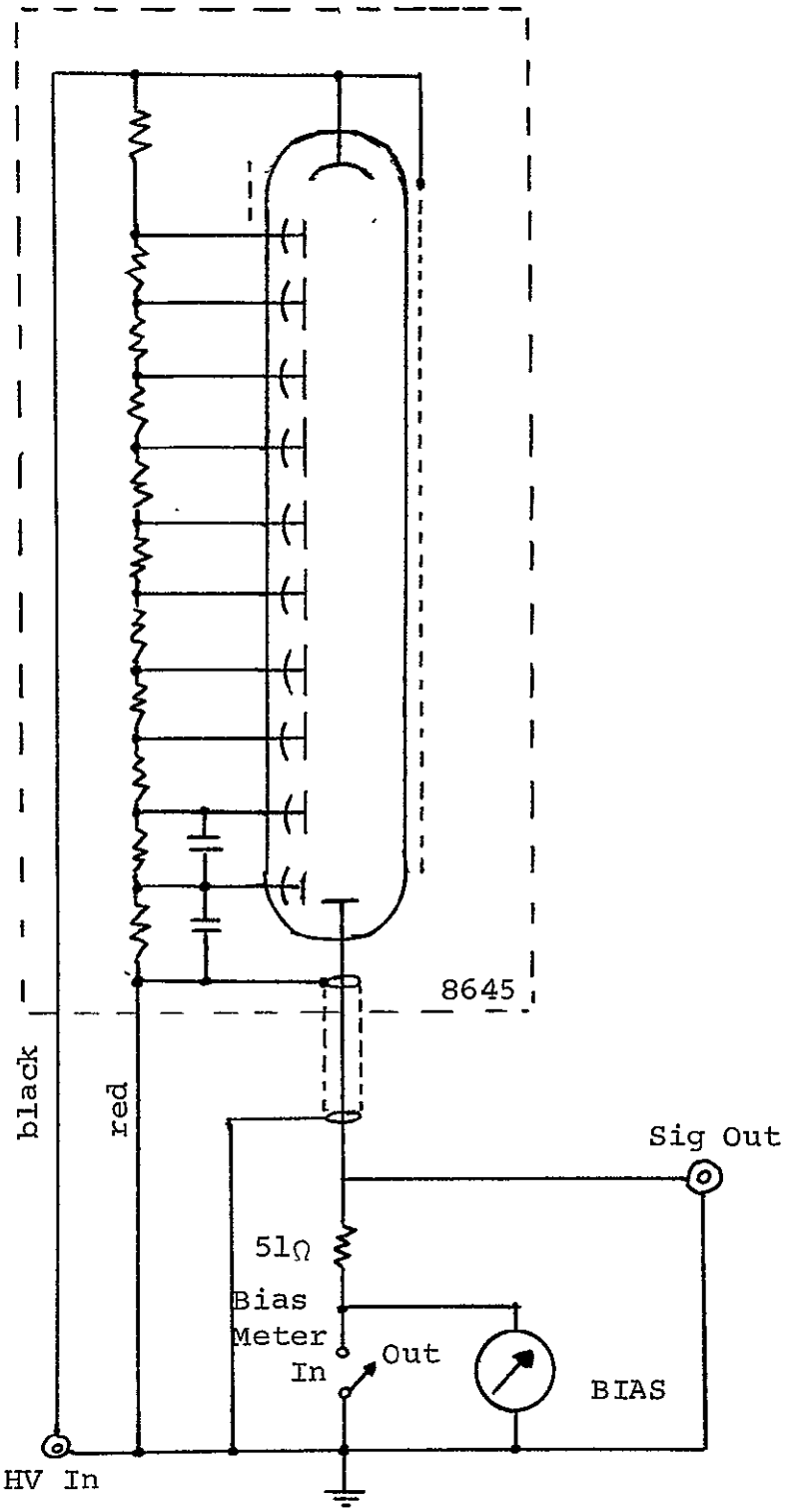

Figure 3-17 Photomultiplier Circuit

3.3.1 Operational Alignment Procedures

The desired scattering angle is set by the location of the front and top slides. Each slide is held in position by a dowel pin screw and a socket head screw. The case holes are numbered in degrees of scattering angle so it is only necessary to put the screws in the desired hole and move the slide until the screws drop in place. The scattering lens and the mirror tilt, using the turns counting dial, are also set for the angle desired. Only minor adjustment of the other mirror controls may be required. Following is a table of dial settings vs. angle of scatter:

Angle	Setting
5^{o}	870
6^{o}	769
7^{o}	667
8^{o}	566
9^{o}	464
10^{o}	362
11^{o}	260
12^{o}	160

TABLE XI. Settings vs. Angle of Scatter for Scatter Path Mirror

It has been found that the setting can vary by as much as 25 from these figures depending on the accuracy of setting of the focal distance and boresighting.

The velocity vector is selected by rotating the instrument, using the dial to set the desired angle. The instrument is then

boresighted as described in Section 3.2.1. It is necessary to keep the two friction screws of each vertical adjustment locked tight to give maximum instrument stability while operating. When making adjustments, it will be necessary to loosen these screws to allow rotation. A rod is supplied which can be inserted in the front vertical adjustment knob to add a mechanical advantage to this adjustment.

By opening the door or looking through the window, the scatter beam can be observed at the field stop. One can then quickly determine the adjustments necessary to direct the beam through the field stop. Once the beam is through the field stop, one can view the beam through the eyepiece while adjusting the mirrors to quickly optimize the setting. If the input irises are reduced on both beams, a small spot can be seen on the eyepiece view screen. Then, by adjusting the first and third scatter mirrors, the scatter beam can be made coincident and parallel to the L. O. beam. The first mirror moves the spot in relation to the L. O. beam. The third mirror optimizes it. The knobs on each mirror are labeled A and B. When knob A on the first mirror is moved, a compensating motion of knob A on the third mirror will bring the signal through the field stop and correspondingly with the B knobs. When the scatter spot on the view screen is at maximum intensity and concentric with the L. O. spot, the instrument will give a Doppler signal.

The bias meter is connected into the circuit by means of its switch. Voltage can be then applied to the P. M. tube while observing the bias meter. The bias should not exceed .4ma nor should more than 1750 volts be applied to the tube. The meter should be switched off when looking at signals as it adds noise to the output.

The polarity of the L. O. can be matched to the signal by rotating the polarizer. The L. O. can be attenuated to the desired ratio with the scatter signal by rotating the Glan prism. As all Glan prisms have some wedge built into them, the beam is diverted slightly. By rotating the prism, the beam may move enough to go out of the field stop hole, particularly on the small size holes. In this case, it will be necessary to use the rear boresighting adjustments to bring the beam back through the hole. This adjustment may also require slight readjustment of the scatter mirrors.

The instrument is capable of being rotated about the laser axis to allow readings of different direction velocity vectors. The speed with which this can be done depends upon the accuracy of boresighting and the field stop being used. We have been able to keep the L. O. in the 200μ field stop while rotating the instrument throughout its range.

There are two contributors to beam wander during rotation. They are misalignment of the lens optical axis with the instrument axis of rotation, and misalignment between the laser beam and the axis of rotation. The lens has been adjusted so that its contribution at the field stop is a .002 inch circle. This was achieved by using a 44 foot long path to observe runout. As this is a focused beam, the edges are not distinct at this distance. It is estimated that the maximum runout is 1/16" at 44 feet or 0.0018" at the field stop.

If the instrument is boresighted so that there is a .001 inch misalignment between the laser beam and the axis of rotation at the cube beamsplitter, there will be a 0.005 inch circle described at the field stop during rotation. Therefore, with the lens error

and only a 0.001 inch boresight error, the beam will wander 0.007 inch or just about stay in the 200M hole during rotation. The method of boresighting does not allow this accuracy on the initial set up. It has been found necessary to rotate the instrument and observe the beam wander. Then, by very slight adjustment of the boresight, (principally the front adjustments) this wander can be reduced. After rotating and adjusting several times, a setting can be achieved that will allow continuous readings to be taken during rotation while using the 200μ field stop.

3.4 REFERENCES

(1) Born & Wolf: Principles of Optics, The MacMillan Co., New York, 1964

(2) Eberhardt, E.H.: "Source Detector Spectral Matching Factors", Techn. Note No. 100, ITT Industrial Labs., Ind.